ASSESSMENT OF SIMULATING UNDERWATER IMPACT USING THE ICFD SOLVER IN LS-DYNA

by

© Xiaoli Gao

A thesis submitted to the School of Graduate Studies

in partial fulfilment of the requirements for the degree of

Master of Engineering

Faculty of Engineering and Applied Science

Memorial University of Newfoundland

October 2016

St. John's Newfoundland Canada

Abstract

This thesis demonstrates that although the ICFD solver of LS-DYNA is a practical tool that can precisely model fluid and structure interaction, it is not effective for simulating the underwater impact of two objects. A numerical model was developed using the ICFD solver to simulate the submerged impact of a structure and ice at model scale. The numerical results were compared with physical experiments conducted in the laboratory. This thesis reveals that a water mesh exists between the structure and the ice model on contact, which leads to the incorrect calculation of pressure at the ice-structure contact points and causes incorrect impact force.

This thesis also proposes a method to verify that the peak impact force of two objects in the water equals the peak impact force of the same objects in air with equivalent artificial added mass and velocity.

Acknowledgments

I would like to thank my supervisor, Dr. Claude Daley, a Professor in the Faculty of Engineering and Applied Science at Memorial University, and my co-supervisor, Dr. Jungyong Wang, a research officer of National Research Council Canada, for their patience, guidance, financial support, and encouragement throughout the Master program.

I would like to express my appreciation to Dr. Ayhan Akinturk who is a senior researcher of National Research Council Canada, for the guidance and help during the research.

I would also like to thank Dr. Bruce Colbourne and Dr. Bruce Quinton, who are professors at Memorial University, for their great help and patience.

I would like to state my greatest appreciation to Mr. Trevor Clark, lab technologist, and Mr. Subodh Chander, a fellow graduate student, for their great help during the physical experiments.

I would like to acknowledge STePS^2 for the generous financial support.

Lastly, I would like to thank my husband, Ken and daughter, Jiayi, for their unconditional support, love, and encouragement throughout the program. This thesis is dedicated to you.

Table of Contents

List of Figures

List of Tables

Nomenclature and Abbreviations

2D	Two Dimensional
3D	Three Dimensional
CAD	Computer-aided Design
ICFD	Incompressible Computational Fluid Dynamics
FEA	Finite Element Analysis
LS-DYNA	a FEA program
LSTC	Livermore Software Technology Corporation
LS-PrePost	an pre- and post-processor for LS-DYNA models

Chapter 1 Introduction

As there is growing interest in the Arctic area as well as in the availability of Arctic shipping routes. Ship operation in ice regimes is of increasing interest. Ships navigating in ice-infested areas can be characterized into two types: ice-breaking ships (or icebreakers) and ice-strengthened ships. Icebreakers have a strong steel hull that can sustain significant ice impacts and are able to navigate through different types of ice covered water to support ice-strengthened ships. Ice-strengthened ships are not as strong as icebreakers. These classifications play an important role in transportation, in that they are always accompanied by strong impacts with ice. The only areas of a polar class ship that are not ice-strengthened are well above the waterline, however, almost all ice load research has been focused on cases of ice load near the water surface.

This thesis contains six main chapters. This chapter defines the scope and objectives of this thesis and outlines the steps for approaching the objectives. Chapter Two contains the literature review for this thesis, discusses the added mass effect and introduces the finite element analysis program and the computer clusters that have been used in this research. Chapter Three outlines the capability of LS-DYNA in simulating the fluid and structure interaction while Chapter Four presents and compares the physical and numerical underwater tests. Chapter Five proposes and verifies a proposed method about the added mass effect on the impact force. Chapter Six presents the conclusion of this thesis and recommendations for future work.

1.1 Objectives

When an ice-strengthened ship encounters ice during navigation, some broken ice drifts to the sides of the hull, while some others may be drawn into the water under the hull and then flow

upwards due to water buoyancy. In the latter case, the ice might hit the hull under the water surface before it slides away to the sides. To date, however, the underwater impact of the ship's structure from submerged ice has not yet been studied. Hence, there are some questions that may arise during ship design scenarios: Is the structure under the water line overdesigned from ice impact? What is the optimal design load associated with underwater ice impact?

When a ship is maneuvering in the ice field, in reality, the ship's movement and surrounding fluid flow have significant effects on the motion of nearby ice. However, the research presented in this thesis neglects the ship's movement and fluid flow effect and focuses only on one scenario: the impacted structure stays stationary and the water domain is still.

During the impact process, the kinetic energy of the submerged ice is normally equated to the energy dissipated by ice crushing while neglecting any hydrodynamics; then the maximum ship and ice contact force can be solved using the energy method (Popov et al., 1967). This research will focus on the ice loads caused by submerged ice and its added mass. The contact by ice crushing is not the interest of this study. In summary, there are two purposes of this study: the first is to develop a numerical model to simulate the kinematics of the submerged ice and local impact force on the ship structure from the submerged ice; the second is to verify a proposed method. This thesis proposes that the local peak impact force on the structure from submerged ice and its added mass equals to the impact force from ice in the air with prescribed added masses at prescribed velocities. The added masses and velocities here are obtained from the hydrodynamic study of the submerged ice during impact.

1.2 Test Plan

In order to achieve these two purposes, a series of model scale experiments were planned. The impacting object, an ice model, was released from different water depths. The ice model floated

up due to the buoyancy force and hit the model ship's bottom structure, which was stationary. Various submergence depths resulted in different velocities at impact and further generated different local impact forces on the structure. A numerical model was developed using the commercial finite element analysis (FEA) program LS-DYNA to duplicate these tests. The final numerical model should have been capable of modelling not only the kinematic behavior of ice in water, but also the impact force of the ice with the structure under the water surface. It was expected that LS-DYNA could perfectly combine its solid mechanics solver and Incompressible Computational Fluid Dynamics (ICFD) solver to simulate this scenario. This work hoped to show that ICFD of LS-DYNA was fully capable of producing useful results for practical assessment. There was no evidence in the literature that such a capability had been previously demonstrated. In addition, the computing environment for the software can be one of the effects that influence the simulation results. Hence, an extension work of a verification study of drag coefficients of a 2D cylinder, which was initiated by LSTC, was performed before the final numerical model was developed.

The numerical model of the free falling ice model test in air were developed and verified with physical experiments. Furthermore, this numerical model were used to verify the proposed method.

Chapter 2 Literature Review and Some Background Information of LS-DYNA

This literature review includes some past studies on the coefficient of restitution, and added mass, in addition to the introduction of LS-DYNA, which was the finite element software used in this study.

2.1 Coefficient of Restitution

There were limited studies about underwater impact and most of them focused on the movement of the impacting object. Zhang et al. developed a mechanistic model using the Lattice-Boltzmann method and simulated the dynamic motion of the collision of two spheres for the low Reynolds number range (Zhang et al., 1999). The simulation results were then compared with the experimental results. They pointed out that accurately predicting the particle velocity upon contact is the key to proper quantification of the particle collision characteristics.

The coefficient of restitution (COR) is expressed in an equation below. It is the ratio of relative velocity after the impact to the relative velocity upon the impact, and it is very important in terms of modeling impact.

$$COR = \frac{\text{Relative velocity after impact}}{\text{Relative velocity upon impact}}$$

COR was introduced by Sir Isaac Newton in 1687 and it is another interpretation of conservation of energy and momentum. When two objects impact, how the energy is transferred depends on the material, and the value of the COR is usually between zero and one. A COR of 0 corresponds to an inelastic impact, while a COR of 1 corresponds to a perfectly elastic impact.

Ardekani and Rangel numerically investigated the collisions and the bouncing motion of a spherical particle colliding with a wall along with the effect of the coefficient of restitution

(Ardekani and Rangel, 2008). When a sphere hits a plate in the air it can exert a force on the plate greater than its weight, and the plate exerts a force on the sphere of the same magnitude. This force along with gravitational force acting on the sphere compresses the ball. As the sphere is compressed, its kinetic energy is converted into elastic potential energy and thermal energy. When rebound happens, the elastic potential energy is converted back into kinetic energy. If this impact happens in the water, the hydrodynamic effect would make the problem more complicated.

The coefficient of restitution is a measure of the amount of kinetic energy that has been dissipated in the impacted structure and in the fluid. Correctly modeling the coefficient of restitution is the key to model impact force. In other words, in order to correctly model the impact force on the structure in the water, the kinematics of the impacting object is an important aspects.

2.2 Added Mass

When ice travels in water with a certain speed, a certain amount of water is accelerated along with the ice. The inertia caused by the water due to an acceleration or deceleration is so-called "added mass". As the ice is decelerated when it approaches a boundary or structure, its added mass would resist the decelerating process but eventually would move along with the ice. The impact force that the structure encounters is heavier than can be accounted for by the ice mass alone because of the added mass effect.

Studies show that the added mass coefficient is around 0.5 when a sphere is moving in an unbounded ideal incompressible fluid or far from the boundary. For example, Stokes posits that "when a solid sphere moves in any manner in an infinite fluid, the only effect of the motion of the fluid is to increase the mass of the sphere by half that of the fluid displaced" (1880).

Pantaleone and Messer conducted experiments with different types of balls in various sizes and showed that the added mass coefficient were all around 0.5 (2011).

When the sphere travels perpendicular towards a wall, the added mass increases. Hicks (1880) analyzed the kinetic energy of the fluid in the form of an infinite series due to the motion of two spheres along the line connecting their centers. He introduced the method of successive images where the added mass coefficient increases as the sphere approaches the wall. The added mass coefficient is 0.803085 for a sphere approaching a wall at the instance of contact. The added mass coefficients were later calculated by Kharlamov as well (2007), where they used the method of successive images to approximate the fluid velocity potential as a sum of the images consisting of dipoles. For the case of a sphere moving perpendicular to the wall, each image consists of one dipole and the kinetic energy of the fluid was determined based from the formulae of Hicks (1880). The added mass coefficient of the sphere moving perpendicular to the wall was obtained from the kinetic energy of the fluid. To verify that the added mass coefficient is 0.803085 at the point of contact, Kharlamov (2007) calculated two hundred sphere positions with dimensionless distances of the sphere center to the wall, $\frac{h}{r}$, from 15 to 1 with increasing position density close to the point of contact. The full expression is shown in Equation 2.1.

$$C_o = 0.5 + 0.19222\left(\frac{h}{r}\right)^{-3.019} + 0.06214\left(\frac{h}{r}\right)^{-8.331} + 0.0348\left(\frac{h}{r}\right)^{-24.65} + 0.0139\left(\frac{h}{r}\right)^{-120.7} \quad \text{Equation 2.1}$$

Where: h is the distance from wall to the center of the sphere

r is the radius of the sphere

That study compared the prediction with those of Stokes and Yang and showed that their prediction agreed with each other for $h/a \geq 2$, as shown in Figure 2.1 (Kharlamov et al., 2007).

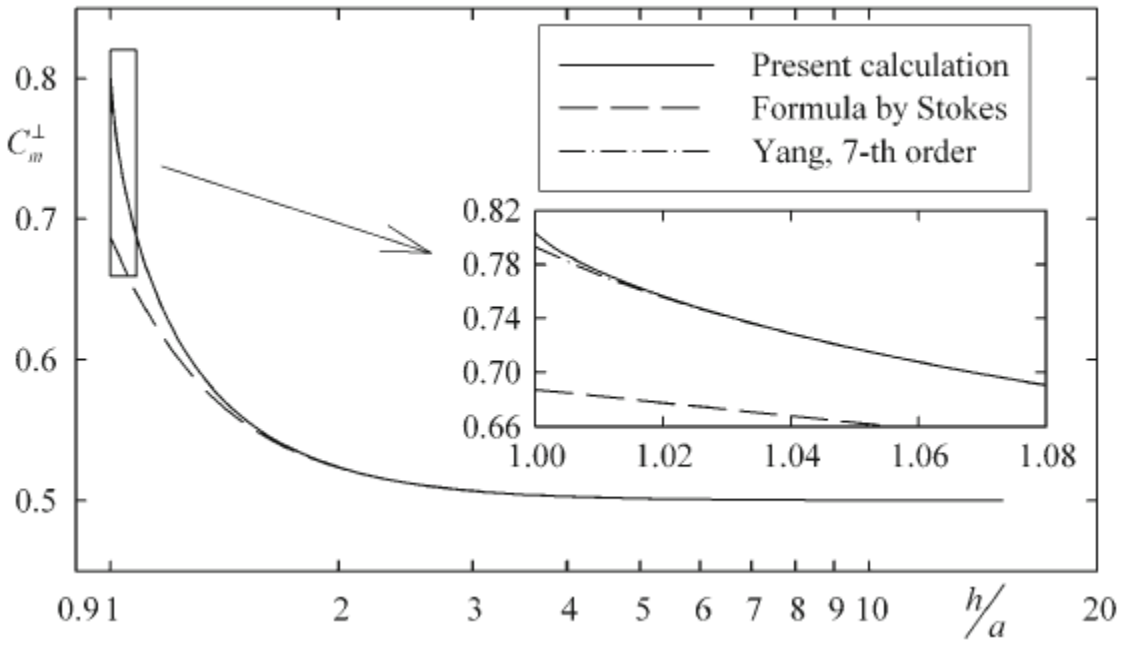

Figure 2.1: Add mass coefficient of a sphere travels perpendicular to the wall (Kharlamov et al., 2007)

2.3 LS-DYNA

This section introduces the finite element analysis program LS-DYNA, which was used through the whole research. The general characteristics of the program and some typical features that are beneficial to the model development are outlined in this section.

2.3.1 General information

LS-DYNA is a finite element program developed by Livermore Software Technology Corporation (LSTC), which is broadly used in different areas (e.g., construction, manufacturing, bioengineering, automobile and marine industries). Its main attraction is a highly nonlinear

transient dynamic finite element analysis using explicit time integration. LSTC briefly explains "nonlinear" as characterised by at least one of the following complications:

- Nonlinear boundary conditions – contact between parts that changes over time
- Nonlinear geometry – parts geometry changes during the simulation
- Nonlinear materials – materials that do not exhibit linear elastic behavior (LSTC, 2011)

Underwater impact of ice and structure involves the change of contact over time. This activity starts with the fluid and ice interaction first, and then the ice and structure contact is involved. The contact between parts changes over time, which meets the first criteria of nonlinearity.

"Transient dynamic" refers to the cases which happen with high speed or in short duration. The underwater impact of ice and structure may happen in a very short time period.

"Explicit" is one of two numerical methods to solve a dynamic equilibrium equation at each time step. The difference of explicit and implicit will be introduced later in this section.

A typical LS-DYNA model consists of different keyword cards that provide input to different solvers. Most of the keyword cards can be modified either through LS-PrePost or keyword files directly. LS-PrePost, literally, is a pre- and post-processor for LS-DYNA. The keyword files contain all the inputs which can be arranged according to various purposes into the following categories:

- Geometry - This part includes the detailed geometric information of model, for example, shapes and dimensions. The geometric models can be generated by LS-DYNA's pre and post-processor, LS-PrePost, or other CAD programs. All of the 2D and 3D geometric models involved in this thesis are generated using LS-PrePost.

- Parts information - This category consists of all the cards for defining parts, element types, element parameters, and material types. Material properties and element types can be applied to the respective parts by specifying the keywords in the various cards.
- Execution - This category consists of all the execution cards for the simulation, for example, the starting time, termination time, and the time step.
- Contact - The contact cards are for user to define the contact types. Contact types can be varied for different scenarios. By changing the parameters, different types of methods can be chosen to calculate the contact stiffness or to improve the convergence.
- Boundary conditions - In LS-DYNA, user can set the boundary conditions by defining point, line, or surface constraint on the parts. Prescribed motions can be also applied. Moreover, it allows a user to set the initial conditions for both the structure and fluid, such as initial velocities, initial strains, fluid boundaries, and free surface.
- Output - This category includes the output cards that start with DATABASE for the desired output for the simulations; for example, displacement, velocity, acceleration, and force can all be recorded with a pre-set time step.

2.3.2 Incompressible Computational Fluid Dynamics (ICFD)

LS-DYNA version 971 released the ICFD solver which is capable of working alone to study fluid dynamic effects, and also can be coupled with the solid mechanics or thermal solvers to simulate more complicated problems. With the ICFD solver, a large number of fluids and gases can be easily represented in a simple way, as there is no need to define an equation of state to close the system (LSTC – Class Notes, 2013). This thesis has made use of the ICFD solver with the solid mechanics solver. The information about the thermal solvers is not included in this thesis as it is not relevant.

The ICFD solver was developed by LSTC for solving incompressible Navier-Stokes equations. Normally, a fluid can be assumed to be incompressible when the Mach number is lower than 0.3. Mach number is the ratio of velocity of flow (V) to the velocity of sound (a), and can be expressed below as:

$$M = \frac{V}{a} \leq 0.3 \qquad \text{Equation 2.2}$$

The main features of the ICFD solver are well explained in the ICFD theory manual (LSTC–ICFD theory, 2013). This section only introduces the features that are involved in this research: automatic volume meshing, adaptive meshing, free surface flow, and fluid structure interaction (FSI). The numerical models, which are presented in Chapter Four and Five, benefitted from all these features.

The automatic volume mesher can simply create the fluid or air domain. The ICFD solver reads the surface nodes and elements defined by the user, and then joins the surface nodes to build an initial volume mesh satisfying the Delaunay criterion. The Delaunay criterion is fundamental in the construction of the volume mesh in ICFD solver. To satisfy the Delaunay triangulation, in mathematics and computational geometry of ICFD, no node should be inside the circumcircle of any triangular plan formed by a set of nodes. In Figure 2.2, the Delaunay criterion is satisfied in (a), and violated in (b) as P_4 is inside the circumcircle of the triangle comprised of P_1, P_2 and P_3. After the initial volume mesh has been built, the solver will progressively add nodes to create the volume mesh in the fluid or air domain based on the Delaunay criterion. It is very important that the surface be non-overlapping and there should not be any open gaps or duplicate nodes.

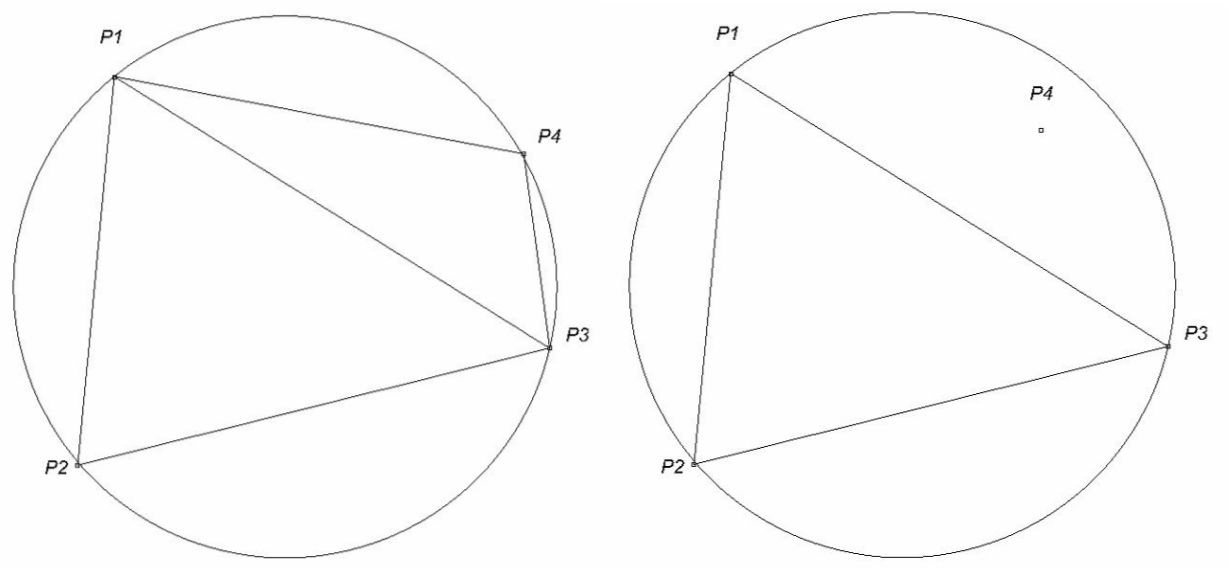

(a) (b)

Figure 2.2: Satisfaction and violation of Delaunay Criterion

After the fluid/air had been created, it may be changed due to the movement of fluid/air themselves or the structure. The fluid/air domain can be automatically re-meshed to keep good mesh quality when large displacements happen in FSI simulations. It also allows a user to define the minimum and maximum mesh size by using the *ICFD_CONTROL_ADAPT card, for example, the mesher can re-mesh and make sure that mesh size of fluid/air mesh elements satisfy both the Delaunay criterion and user's setting. Furthermore, a user can use *MESH_SIZE_SHAPE to impose the local mesh size in the specific zones which can be defined as a box, sphere, and cylinder shapes. Figure 2.3 is a 2D LS-DYNA mesh profile of a cylinder in water stream. There were two *MESH_SIZE_SHAPE cards that were applied to this model. This resulted in two different mesh size regimes namely, Box1 and Box 2, which surrounded the

cylinder. By doing so, fewer elements are involved to achieve more precise results, in addition, less time and storage space are required for the simulations.

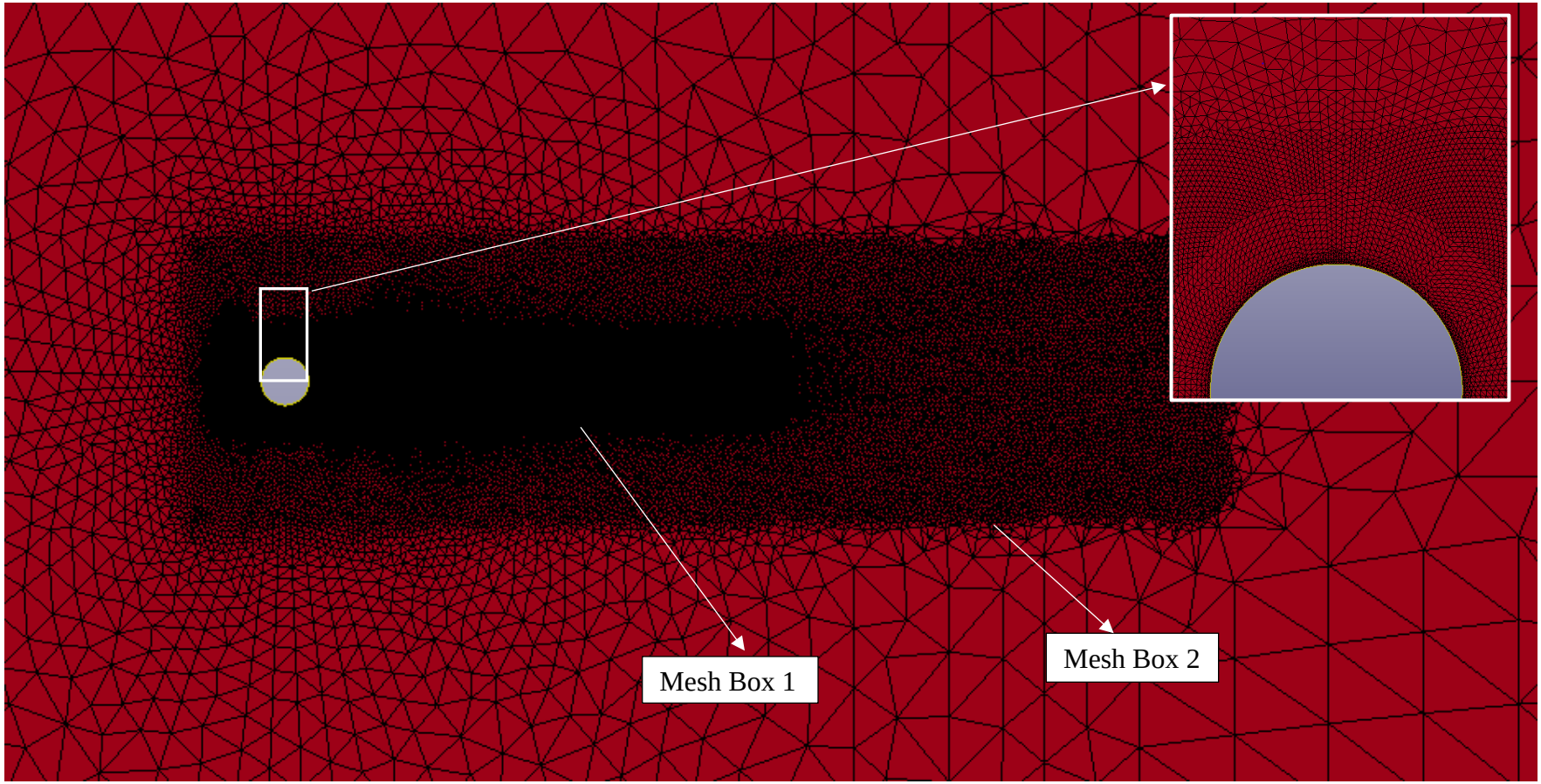

Figure 2.3: 2D Profile of a cylinder in water stream

Pin and Çaldichoury (2012) have introduced the traditional method and the level set method for handling the interface problems. The interface problems includes air and water dynamics, waves, and solid objects penetrating in fluids. The differences of these two methods are shown in Figure 2.4. A traditional way of defining an interface between different domains is by assigning some nodes to exist on the interface. The nodes' movement would be based on the fluid velocity values through the grid. This is based on a Lagrangian formulation, which is hard to accomplish if the interface element mesh are changed or distorted too much. Hence, a frequent and regular re-meshing is required to apply to the distorted domain, which implies a high computational time cost. The ICFD solver uses a level set method to track and represent the moving/changing interfaces. The level set function φ is an implicit distance function with a convection equation applied to it. The absolute value of φ is the distance to the interface and $\varphi = 0$ at the interface. Different signs indicate two different sides of the interface. The level set method can more accurately simulate interface dynamics, breaking surface waves and structure penetrating in fluids.

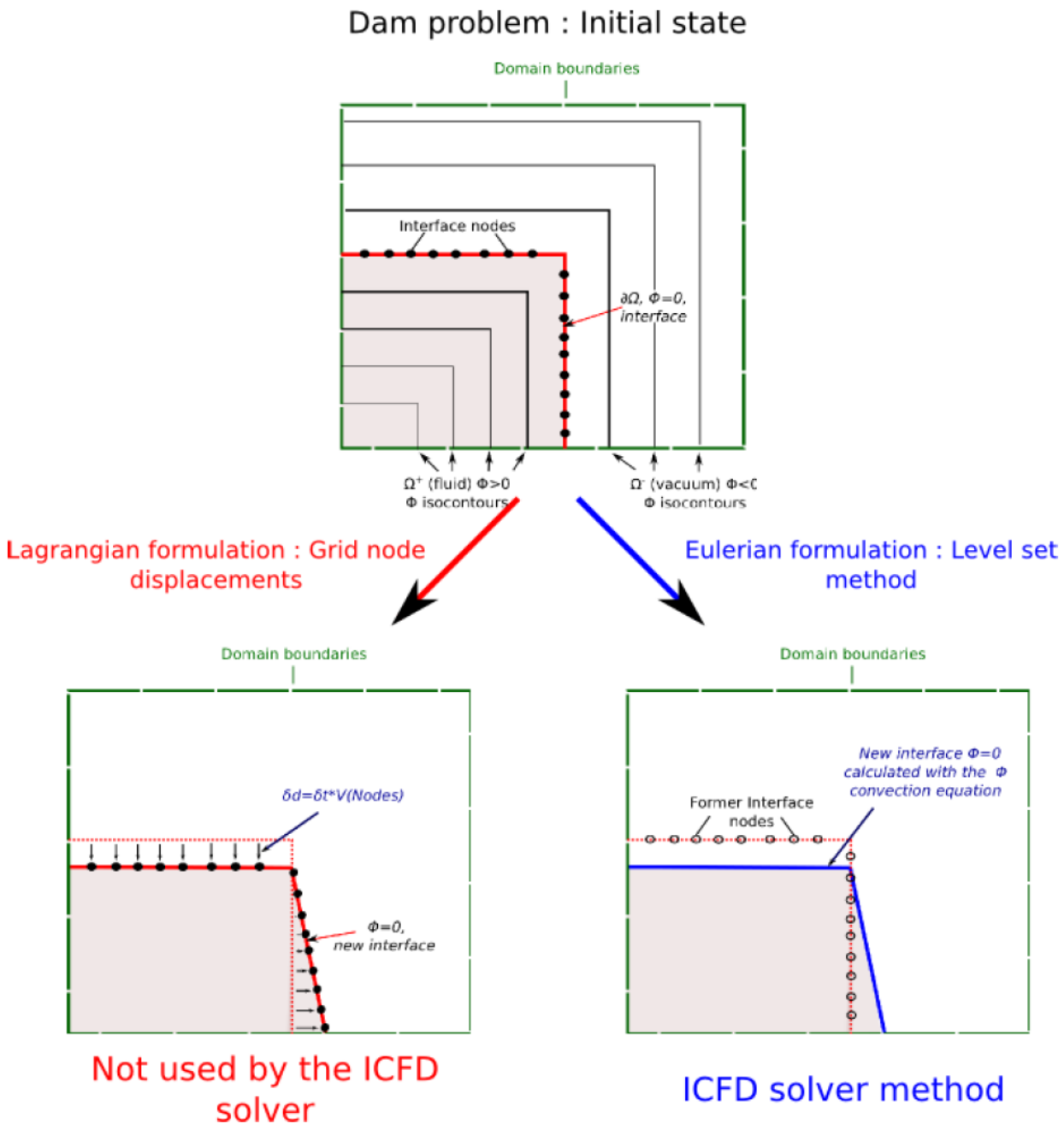

Figure 2. 4: Different interface handling methods for free surface dam breaking problem (Pin and Çaldichoury, 2012)

Another one of the ICFD solver's key benefits is to solve fully coupled FSI problems. FSI is the non-linear interaction of a structure and an adjacent incompressible viscous fluid. In the past FSI

problems had been solved using a couple of different methods. The monolithic approach treats the coupled problem (the fluid and the structure) as a single domain and the equations of the fluid and structure are solved simultaneously (Michler et al., 2003). However, the computational cost is too high when solving the pressure along with the other unknowns. The second approach would be to separate the pressure from the other unknowns in the monolithic approach while keeping the computing cost low. However, the fluid and structure are still solved in the same domain and require solving the structure equations in ICFD solver directly, which is not a practical solution. On the other hand, the third approach, the partitioned approach, considers the equations of fluid and structure separately. The system is broken into partitions based on functional, physical, or computational considerations and with communication of interface data in between, to link the partitions. The partitioned approach includes three directions on how to couple the interaction simulation programs (LSTC – ICFD theory, 2013):

- One-way coupling: the fluid solver transfers stresses or loads to the solid solver only
- One-way coupling: the solid solver transfers displacement to the fluid solver only
- Two-way coupling: the loads and displacements are transferred across the FSI interface and the full non-linear problem is solved.

The advantage of one-way coupling simulations is that the computational time is lower than two-way coupling simulations; however, the former does not guarantee energy conservation at the interface (Benra et al., 2011). The numerical model presented in this thesis uses two-way coupling.

The two-way coupling can be further divided into a strongly coupled scheme (implicit) and a loosely coupled scheme (implicit-explicit). These two schemes are available when using the ICFD solver in LS-DYNA. The explicit solver is usually used for dynamic analysis, while the

implicit solver can be used for both static and dynamic analysis. The explicit scheme is also called the central difference method and is well explained by Bathe (1996). For this method, the solution at time $t + \Delta t$ is calculated based on the solution at time *t*. On the other hand, the implicit method can solve a dynamic equilibrium equation at time $t + \Delta t$ based on itself and as well as the fluid solver's solution at time *t*. The explicit solver requires only one solution of either field for each time step and does not require to inverse the stiffness matrix so it is computationally fast. The implicit solver requires to inverse the stiffness matrix once or more during one load/time step.

One of the great advantages of LS-DYNA is that the program would calculate the critical time step internally according to the mesh size. It is very close to the highest natural frequency of the model. The critical time step is the well-known ratio of characteristic length and the speed of sound or flow which is usually used to determine the proper time step to avoid contact instabilities. The critical time step for explicit simulation with solid or shell elements is calculated as:

$$\Delta t_c = \frac{l_e}{c_e} \qquad \text{Equation 2.3}$$

$$l_e = \frac{V_e}{A_{e_{\max}}} \quad \text{for 8-node solid element} \qquad \text{Equation 2.4}$$

Where: c_e is the speed of sound travels across an element

l_e is the characteristic mesh size and equals to minimum altitude for 4-node tetrahedral

V_e is the element volume

$A_{e_{max}}$ is the area of the largest side of the solid elements

For the explicit simulation, the simulation might run with the suggested time step and output in the time frequency chosen by user. However, for the implicit simulation, the model would be simulated with the time step chosen by user. The time step should be carefully determined to ensure that the time-dependent phenomena are captured appropriately. The initial guess of time step for the implicit simulation can refer to Equation 2.5 (LSTC – Class Notes, 2013):

$$\Delta t_c = \frac{l_e}{u_e} \qquad \text{Equation 2.5}$$

Where: u_e is the speed of flow

Normally the impact scenario would be better simulated using explicit time integration. However, the strongly coupled scheme (implicit) is more appropriate for the study in this thesis. It is because the instabilities generated when the density of the fluid and the density of the solid are comparable is easier to deal with in a strongly coupled simulation.

2.3.3 Contact modeling of implicit analyses of LS-DYNA

LS-DYNA offers a large number of contact treatments and parameters that control different aspects of the contact treatment. They can be grouped into three main algorithms: one-way contact, two-way contact, and tied contact.

One-way contact treatments only check the user-specified slave nodes for penetration against the master segments. Then it transfers the compression loads between the slave nodes and the master segments, as well as the tangential loads when relative sliding occurs and contact friction is active. The transition from static to dynamic friction requires a decay coefficient be defined

and also the static friction coefficient must be greater than the dynamic friction coefficient. This transition is done by a Coulomb friction formulation with an exponential interpolation function (LSTC, 2011). Since the master segments do not undergo any checking, it is possible that it might penetrate the slave segments without the application of contact forces to prevent the penetration. Accordingly, the one-way contact treatments are appropriate when the master side is a rigid body, or when the slave part has a fine mesh and the master part has a coarse mesh to delimit the chance of master node penetrating the slave part.

Two-way contact treatments work basically the same way as the one-way contact treatments, except that the penetration direction is symmetric. Firstly, the slave nodes are checked for penetration through the master segments and then the master segments are checked for possible penetration. This dual treatment is highly recommended when the master segments and slave segments have a similar mesh. As a matter of course, the computational time for two-way contact treatments is higher than the one-way contact treatment.

For tied contact treatments, the slave nodes are constrained to move with the closest master surface when certain criteria, for example, the normal projected distance, is satisfied. It is recommended by LS-DYNA that the tied contacts be defined by node/segment sets instead of part ids for a better control.

The AUTOMATIC contact types are strongly recommended for the impact analysis. *CONTACT_AUTOMATIC_SINGLE_SURFACE is a two-way contact treatment and has been chosen for all the simulation in this study. It is represented by linear springs between the slave nodes and closest master segments. LS-DYNA offers SOFT options (0, 1, and 2) to determine the contact spring stiffness differently. SOFT = 0 is the default method of LS-DYNA. It is based on the contact segment size and the material properties to calculate the contact spring

stiffness. It works more effectively when the two contacting materials have the same order of magnitude of stiffness parameters. Hence this option is suitable when the contacting objects have similar material properties. SOFT = 1 is very similar to SOFT = 0 except that the SOFT = 1 calculates the contact spring stiffness differently. SOFT = 1 option calculates the contact stiffness based on the contacted nodal masses and global time step size. The SOFT = 2 option determines the contact stiffness using the similar method as the SOFT = 1 option. The difference is that the former option invokes a segment-based contact algorithm which is more suitable for contact surfaces with sharp corners.

For contacts using the implicit solver of LS-DYNA, the gap flag IGAP is used to improve convergence behavior. IGAP is the default active, i.e., IGAP = 1 for the implicit solver. For the contact where the gap exists the contact force is transferred when the gap is still open, hence, a certain amount of negative contact pressure can be transferred between contact surfaces. In addition, this option, IGAP = 1, can produce "sticky" interfaces that prevent surfaces from being separated.

2.3.4 Boundary conditions

The boundary conditions of the models can be simply defined using LS-PrePost. The two most common boundary conditions for the structures are the single point constraints (SPC) and prescribed motions. A user can either apply the constraints to nodes by visually selecting nodes or by entering the node's number. Prescribed motions can be defined by firstly choosing the nodes, parts set or rigid bodies that need to be defined. Then user can describe the curve for the motion including the starting and termination time.

There are a number of ICFD cards available to define the fluid's boundary conditions, which include temperature, velocity, hydrostatic pressure, and viscosity of fluid. The fluid free surface

and the interface of the fluid and structure interaction can be defined by ICFD solver cards, *ICFD_MESH_INTERF and *ICFD_BOUNDARY_FSI, respectively.

The plane boundary is another common boundary in the fluid dynamic problem. The velocity boundary condition of the fluid flowing over a wall can be divided into two categories: non-slip condition and free slip condition. This is due to the friction of the plane surface. The non-slip condition is the state in which the flow velocity at the plane surface is zero and increases within the boundary layer. On the other hand, the free slip condition is when the plane surface is frictionless or when the fluid flows outside of the boundary layer, where the viscosity is neglected. The velocity profile of non-slip and free slip conditions are shown in Figure 2.5. *ICFD_BOUNDARY_NONSLIP and *ICFD_BOUNDARY_FREESLIP cards are available in ICFD solver for user to define these two boundary conditions.

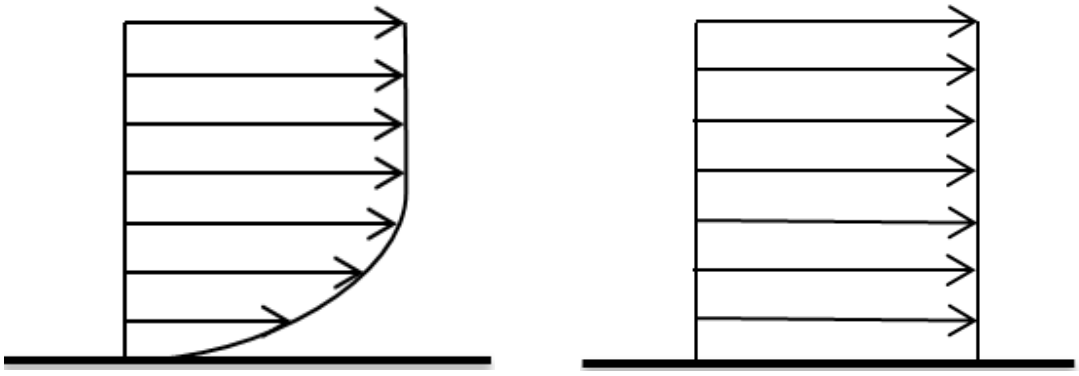

(a) (b)

Figure 2.5: (a) Non-slip boundary (b) Free Slip boundary

2.4 The Hardware for the Simulation

ICFD solver was initially developed and tested in Linux. Hence, in order to obtain more accurate results and also to save the computing time cost, this study used only one version of LS-DYNA which is Massively Parallel Processing (MPP). MPP is a type of implementation that

runs on a computer cluster. It is powerful and efficient in solving large models that contain a large amount of elements or long simulation time. A server cluster consists of many servers. The servers are also called nodes. Each node analyses a part of a model and communicates with each other simultaneously. The cluster used in this research is manufactured by IBM and consists of many processors running in parallel with their own memory. It contains one head node and twenty-four compute nodes which supports up to 400 parallel processes. The model types for these nodes are listed in Table 2.1(Quinton and Kearsey, 2011).

Table 2.1: Simple description for servers of cluster

Node	Model	Description
Head Node	x3650M3	12GB RAM, a single Xeon E5620 quad-core processor at 2.4 GHz with a 12MB cache, and 1.7TB storage capacity
1 Compute Node	x3650M2	32GB RAM and dual Xeon(R) E5520 quad-core processor 2.27GHz with a 8 MB cache, and a 15K rpm 600GB SAS hard drive
16 Compute Node	x3550M2	24GB RAM and dual Xeon(R) E5520 quad-core processor 2.27GHz with a 8 MB cache, and a 15K rpm 600GB SAS hard drive
7 Compute Node	x3550M4	64GB RAM and dual Xeon 8-core processors operating at 2.4GHz with a 20MB cache, and a 15K rpm 146GB SAS hard drive

Chapter 3 Fluid Structure Interaction Test with Incompressible CFD Solver

LS-DYNA has become a well-known finite element analysis tool in the past decade. Besides its capability of problems regarding automobile, manufacturing, construction, the ICFD solver was developed and apply the state of art Finite Element technology to fluid mechanics. The ICFD solver provides the ability for simulations of heat transfer, free surface flow and fluid-structure interaction.

This chapter extends one of the validation cases that had been done by LSTC to show the ICFD solver's capability to correctly reproduce the flow around a stationary 2D cylinder and the drag coefficient for a Reynolds number up to 50,000. This Reynolds number range covers the tests' range for the final numerical model that is presented in Chapter Four.

3.1 Fluid and Structure Interaction Test Setup

When dealing with the fluid and structure interaction, the ICFD solver employs a partitioned method and considers the fluid and structure in different domains. It allows a user to apply specifically designed codes to the different domains. Therefore, different characteristics of fluid and structure could be included into corresponding domains which significantly increases the solvers' efficiency.

Considering uniform flow with velocity V_o passing over an infinite long circular cylinder that is aligned perpendicular to the flow direction. The flow velocity around the cylinder is shown in Figure 3.1. This can be separated into different regions. The sidewise regions are on both sides of the cylinder, where the flow velocity is higher than V_0. The wake region is located behind the cylinder and the velocity is lower than V_0. The free shear layer region develops at the border of the near wake region.

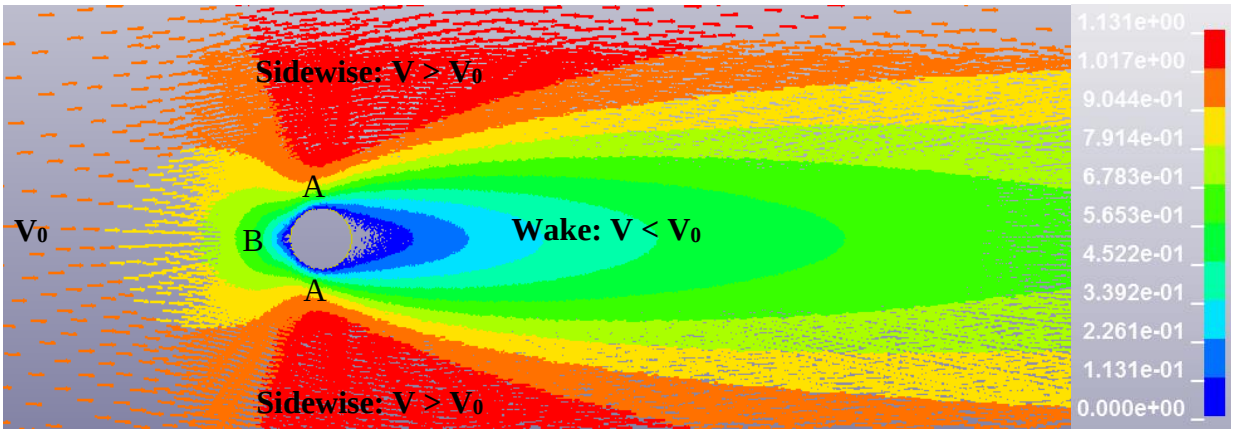

Figure 3.1: Flow passes a stationary circular cylinder

The pressure distribution over the cylinder is also varying around the circumference. The point B is the stagnation point, where the velocity is zero. The pressure at this point is the maximum and decreases from point B to the minimum at points A, where the maximum velocity is reached. The point A is called the separation point because separation of the fluid occurs at this point. The net force caused by the pressure differences between the front and rear surface of cylinder is called form drag. The pressure drag is the main part of the total drag on the cylinder. The other small part is the skin friction drag, which is due to the interaction between the fluid and the wetted skin surface. The drag force (F_D) can be quantified by the drag coefficient (C_d), fluid density (ρ), reference area (A) and velocity of the fluid relative to the object (V). This is expressed in Equation 3.1. The drag coefficient is not a constant. It is varies base on fluid density, fluid viscosity, flow velocity, flow direction, object shape and object position in the fluid. The Reynolds number is the ratio of inertial effects and viscous effects. Its equation, shown in Equation 3.2, comprises the flow velocity, kinematic viscosity (υ) and the characteristic linear dimension (D). Therefore, for the incompressible flow, the drag coefficient can be treated as a function of the Reynolds number (Re).

$$F_D = \frac{1}{2} C_d \rho A V^2 \qquad \text{Equation 3.1}$$

$$\mathrm{Re} = \frac{VD}{\upsilon} \qquad \text{Equation 3.2}$$

The Reynolds number is usually used to delimit different fluid flow patterns in the wake, for example, laminar flow, transient flow and turbulent flow. Lienhard has classified the flow phenomenon into seven flow regimes based on the Reynold number (Lienhard, 1966). In this study, only the first few regimes designated by Lienhard are simulated and compared: (1) unseparated flow regime when Re < 5, (2) a fixed pair of "Föppl" vortices in the wake when $5 \sim 15 \le \mathrm{Re} \le 40$, (3) vortex street is laminar when $40 \le \mathrm{Re} \le 150$, (4) transition range to turbulent in vortex when $150 \le \mathrm{Re} \le 300$, (5) vortex street is fully turbulent when $300 \le \mathrm{Re} \le 3 \times 10^5$. "Föppl" vortices refer to the pairs of vortex placed symmetrically above / blow the flow centerline and behind the obstacle (Föppl, 1913). Recently Zdravkovich has systematically categorized almost all of the experimental, analytical and numerical simulation data about flow past cylinders (since 1936), into different flow regimes based on the different Reynolds number, shown in Table 3.1, which is very similar to Lienhard's study.

Table 3.1: Flow regimes for flow pass a circular cylinder (Zdravkovich, 1997)

Corresponding to Lienhard's	**Reynolds number**	**Flow regimes**
(1)	$0 < \mathrm{Re} < 4 \sim 5$	Non-separation regime
(2)	$4 \sim 5 < \mathrm{Re} < 30 \sim 48$	Steady separation
(3)	$30 \sim 48 < \mathrm{Re} < 180 \sim 200$	Periodic laminar regime

(4)	$180 \sim 200 < Re < 220 \sim 250$	Transition of laminar eddies in the wake
	$220 \sim 250 < Re < 350 \sim 400$	Transition of an irregular eddy
(5)	$350 \sim 400 < Re < 1000 \sim 2000$	Transition waves developed at the shear layer
	$1000 \sim 2000 < Re < 2\times10^4 \sim 4\times10^4$	Transition eddies formed at the shear layer
	$2\times10^4 \sim 4\times10^4 < Re < 1\times10^5 \sim 2\times10^5$	Turbulence appears at the shear layer

LSTC had developed a numerical model to test the flow around a two-dimensional cylinder for the Reynolds number from 2 to 160 (LSTC, 2012). This thesis used the same numerical model layout and extends the test range up to Re = 50,000. In this case, the element size convergence study was not included because it had been tested by LSTC and the result agreed with the reference included in the Test Case Documentation and Testing Results (LSTC, 2012).

Figure 3.2 is the test layout with dimensions. In the simulation, the flow with a velocity 1 m/s came from the left of a cylinder and passed a stationary cylinder. The diameter of the cylinder is 1 m. For all the simulations, the drag coefficients were compared with available data from the literature. Five 2D simulations were chosen to represent each corresponding regimes and compared with the available literature.

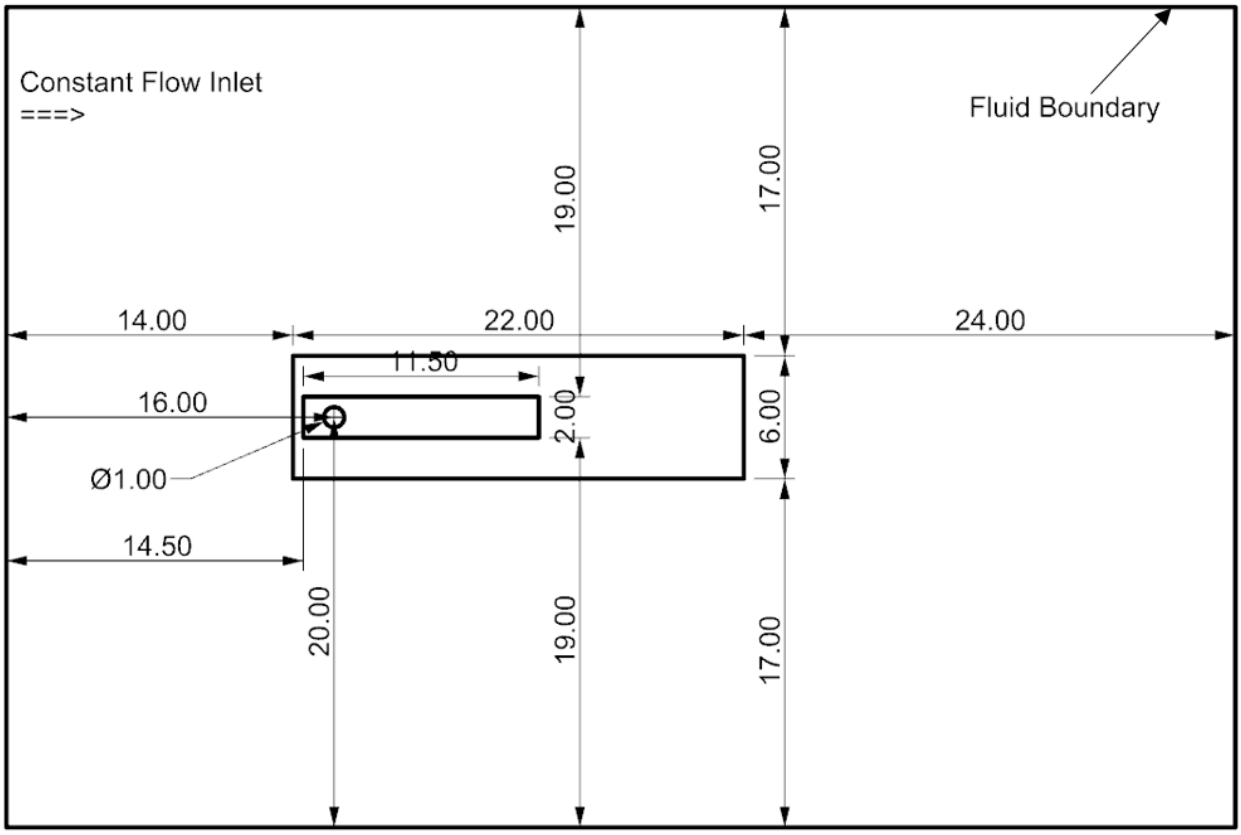

Figure 3.2: Layout of the fluid structure interaction test model

3.1.1 Mesh development

LS-DYNA can automatically generate the mesh within the domain between the fluid boundary and cylinder boundary by two steps. The first step is to define the number of nodes for the fluid boundary and cylinder boundary. The nodes divide the boundary into a number of segments. This can be done by inputting the desired amount of nodes or desired segment size. The second step is to define the fluid volume which includes all the boundaries. The nodes of the fluid boundary will connect to the nodes of the cylinder. The triangular mesh will then be formed to satisfy Delaunay Criterion.

The preliminary mesh shown in Figure 3.3 is coarse. Normally, in order to refine the mesh size, a smaller size is needed to apply to the whole fluid domain, which requires more storage space for the test result and more computation time cost. LS-DYNA's *MESH_SIZE_SHAPE card can refine the mesh size locally in different shapes. In this mode, two mesh boxes were included to surround the cylinder and to create finer meshes gradually. The dimension of the two mesh boxes is indicated in Figure 3.2. Figure 3.4 shows a finer layout with *MESH_SIZE_SHAPE card. The other mesh information is listed in Table 3.2.

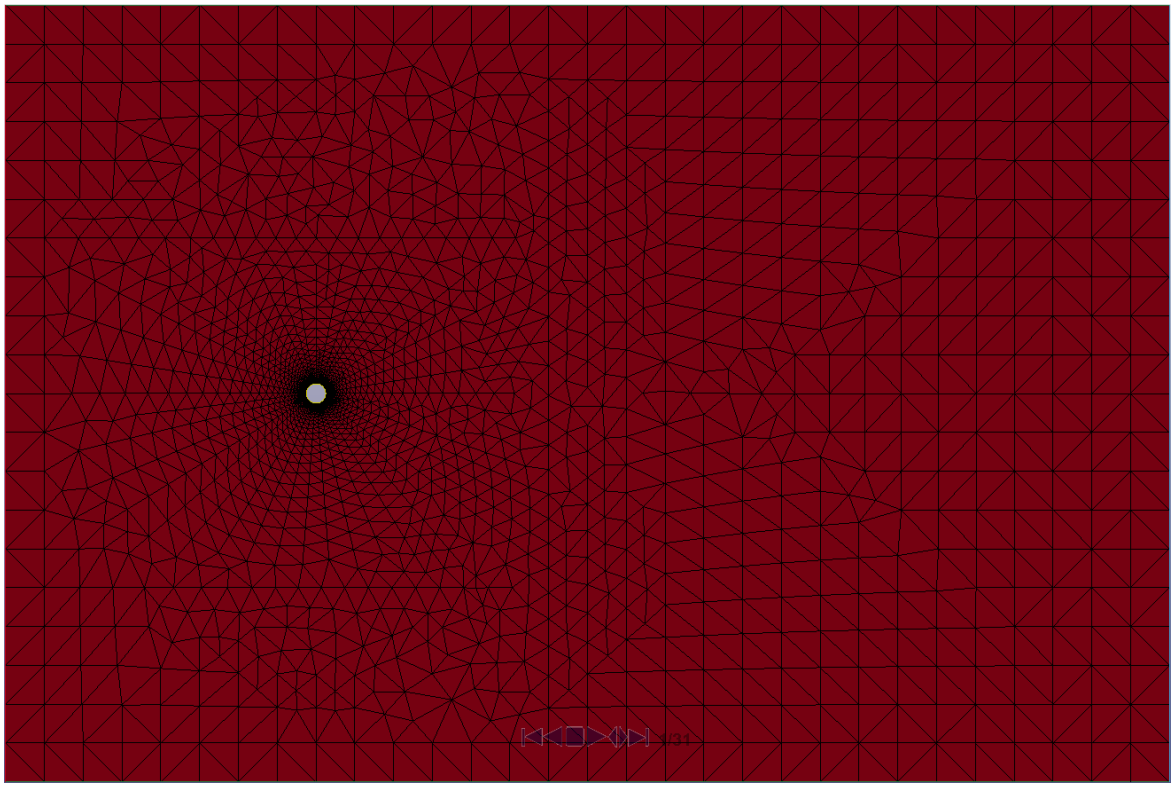

Figure 3.3: Mesh layout

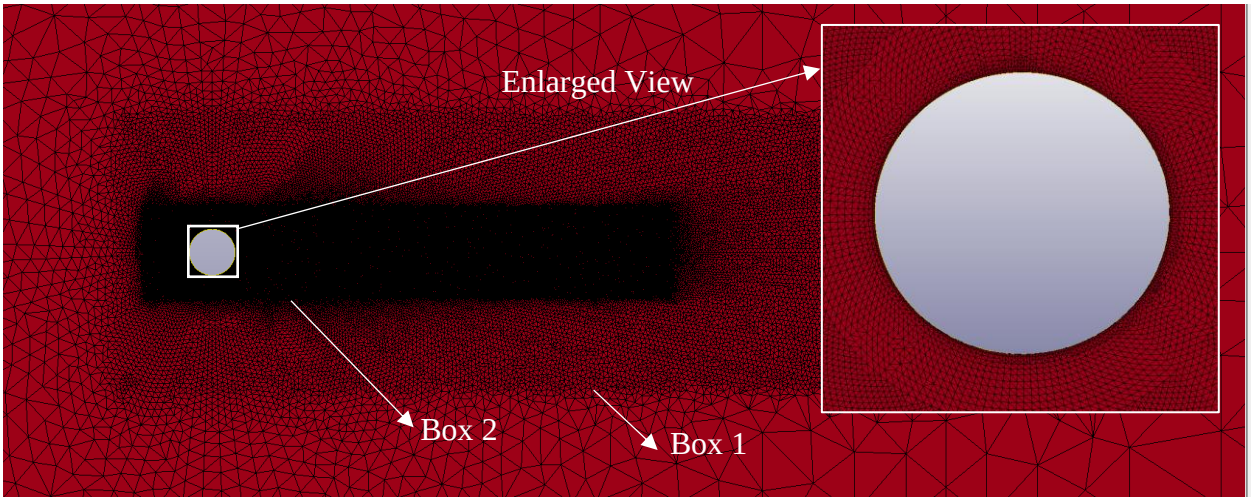

Figure 3.4: Revised mesh layout

Table 3.2: Model information

Number of nodes	63,394
Number of elements	126,368
Element size of fluid boundaries	2.00m
Element size of cylinder	0.01m
Element size of meshing box 1	0.10m
Element size of meshing box 2	0.025m

3.1.2 Boundary condition

In the fluid domain, a uniform fluid stream comes into the inlet from the left with a flow velocity of 1 *m/s*. It passes the stationary cylinder and exits to the outlet on the right. The whole model consists of four parts, and their boundary conditions are tabulated in Table 3.3.

Table 3.3: Boundary conditions

Part	Name	Boundary condition
1	Inlet	Prescribed velocity of 1 *m/s*
2	Outlet	Prescribed pressure of 0 *Pa*
3	Two walls	Free slip
4	Cylinder	Non-slip

The fluid density is set to 1 kg/m^3 for ease of calculation. The fluid viscosity is varied from 0.5 to 2E-5 m^2/s in order to reach the Reynold number from 2 to 50,000.

The main k-file is list in Appendix A.

3.1.3 Time step convergence study

The critical time step for the fluid and structure interaction test was 0.01s. Since the simulation ran in implicit, the solver can use the time step values a few times higher than the critical time step. The time steps from 0.01s to 0.06s with the increment of 0.01s are chosen into the convergence study. The time step convergence plot is shown in Figure 3.5. The simulation time is 200 seconds. At the beginning of the simulation, the drag force is not stable and shows extreme high values. It settles down after t = 100 s. Figure 3.5 shows that convergence occurs after 100 s for the time step that equals or less than 0.06 s. As a result, the critical time step 0.01s is chosen for all the subsequent simulations.

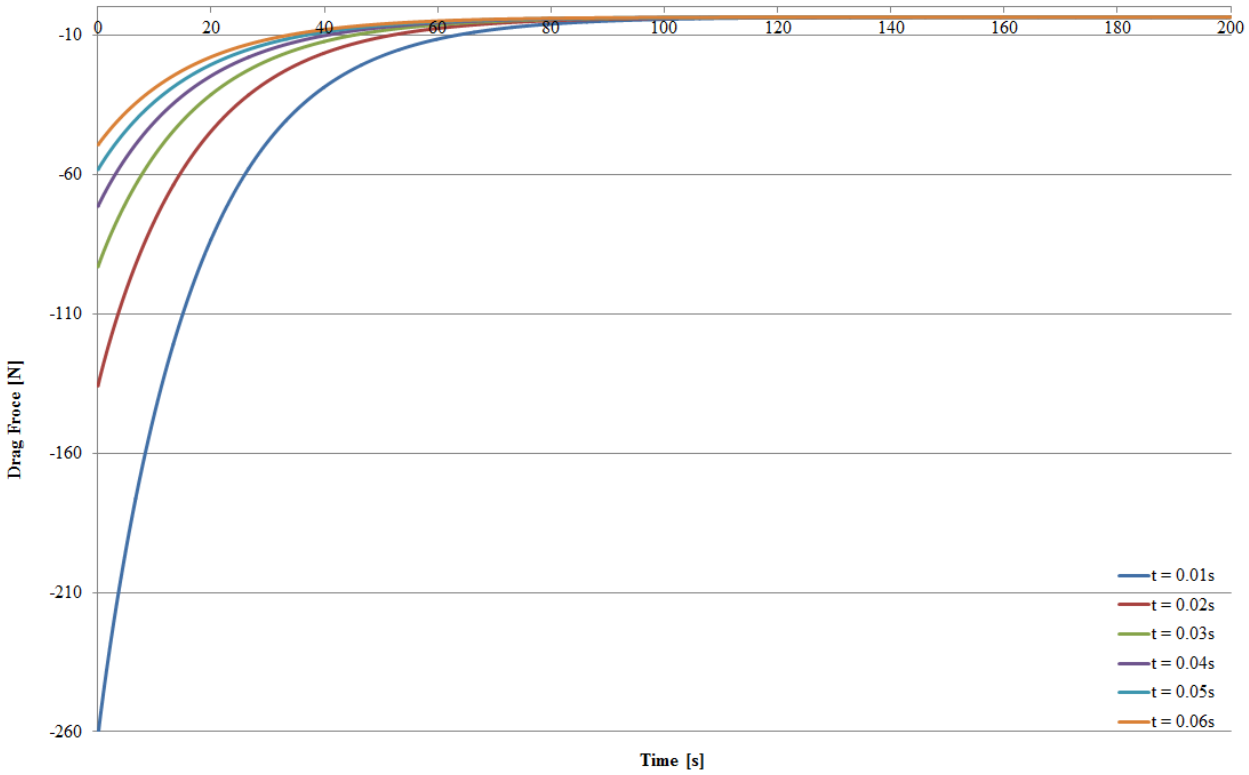

Figure 3.5: Time step convergence study

3.2 Test Results

At the beginning of each simulation, the drag force was extremely high and then gradually settled down at around t = 100s. For each of the simulations, the drag force was produced and output in a data format. By using Equation 3.1, drag coefficients were calculated. The drag coefficients for the Reynolds number from 2 ~ 50,000 are compared with available literature and tabulated in Table 3.4 and plotted in Figure 3.6. For the Reynolds number 2 ~ 160, the drag coefficient obtained from LS-DYNA is very close to Park et al's (1998). The result for $\mathrm{Re} \leq 40$ is similar to the results from Dennis et al (1970) and Fornberg (1979). For the range of $300 \leq \mathrm{Re} \leq 700$, the simulation result is closer with Schlichting's (1979) than Fornberg's (1984).

However, in Schlichting's study the drag coefficient reaches a minimum value of 1 at Re = 2,000, while LS-DYNA's model in this study has a minimum drag coefficient at Re = 50,000.

Table 3.4: Drag coefficient comparison

Re	$Cd_{[LS\text{-}DYNA]}$	$Cd_{[Park\ et\ al.,\ 1998]}$	$Cd_{[Dennis\ et\ al.,\ 1970]}$	$Cd_{[Fornberg,\ 1979]}$	$Cd_{[Fornberg,\ 1984]}$	$Cd_{[Schlichting,\ 1979]}$
2	7.34	6.85				6.38
4	4.78	4.53				4.49
5	4.20					4.16
8	3.32					3.52
9	3.04					3.39
10	2.91	2.78	2.846			3.26
20	2.09	2.01	2.045	2.0001		2.70
40	1.56	1.51	1.522	1.498		2.45
50	1.44					2.36
60	1.42	1.39				2.29
80	1.38	1.35				2.18
100	1.36	1.33	1.056	1.058	1.06	2.09
120	1.34	1.32				2.01
140	1.34	1.32				1.93
160	1.34	1.32				1.87
180	1.34					1.84
200	1.35			0.829	0.833	1.79
300	1.38			0.722	0.729	1.56
400	1.41				0.645	1.42
500	1.43				0.528	1.32
600	1.44				0.433	1.24
700	1.45					1.20
800	1.46					1.14
900	1.48					1.12
1,000	1.50					1.08
2,000	1.60					1.00
3,000	1.59					1.03
4,000	1.57					1.08
5,000	1.52					1.14
6,000	1.53					1.18
7,000	1.49					1.22
8,000	1.45					1.24
9,000	1.33					1.26
10,000	1.51					1.30

20,000	1.36					1.34
30,000	1.35					1.34
40,000	1.37					1.36
50,000	1.26					1.36

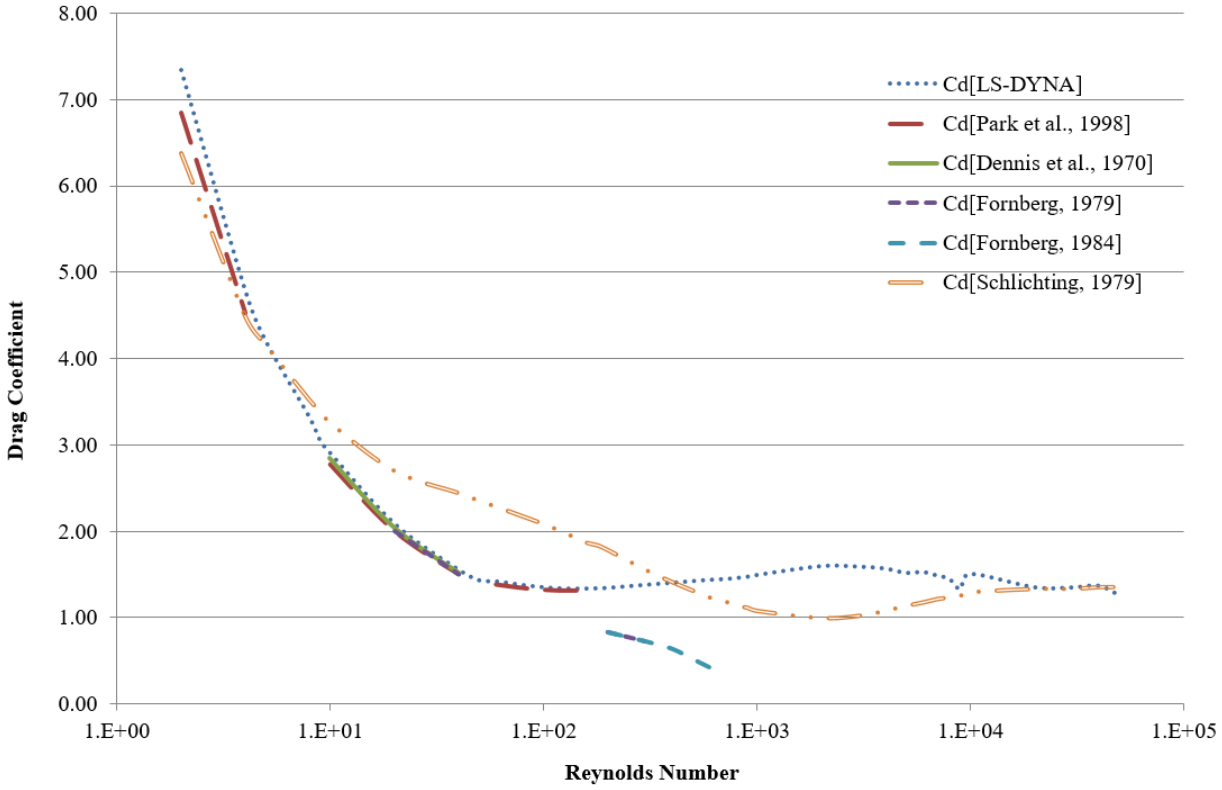

Figure 3.6: Drag coefficients comparisons

The disturbed flow around the cylinder changes as the Reynolds number changes. Observation of the fluid stream for each simulation was recorded in LS-DYNA's d3plot file. For Re < 9, the streamline was firmly attached to the surface of the cylinder and came together behind the cylinder as shown in Figure 3.7. The stream velocity appeared in oval shape. The oval became narrower and longer as the Reynolds number increased. As the Reynolds number reached 9, a

pair of “Föppl” vortices were formed right behind the cylinder (Figure 3.8). The “Föppl” vortices become bigger and appear further from the cylinder as the Reynolds number increases.

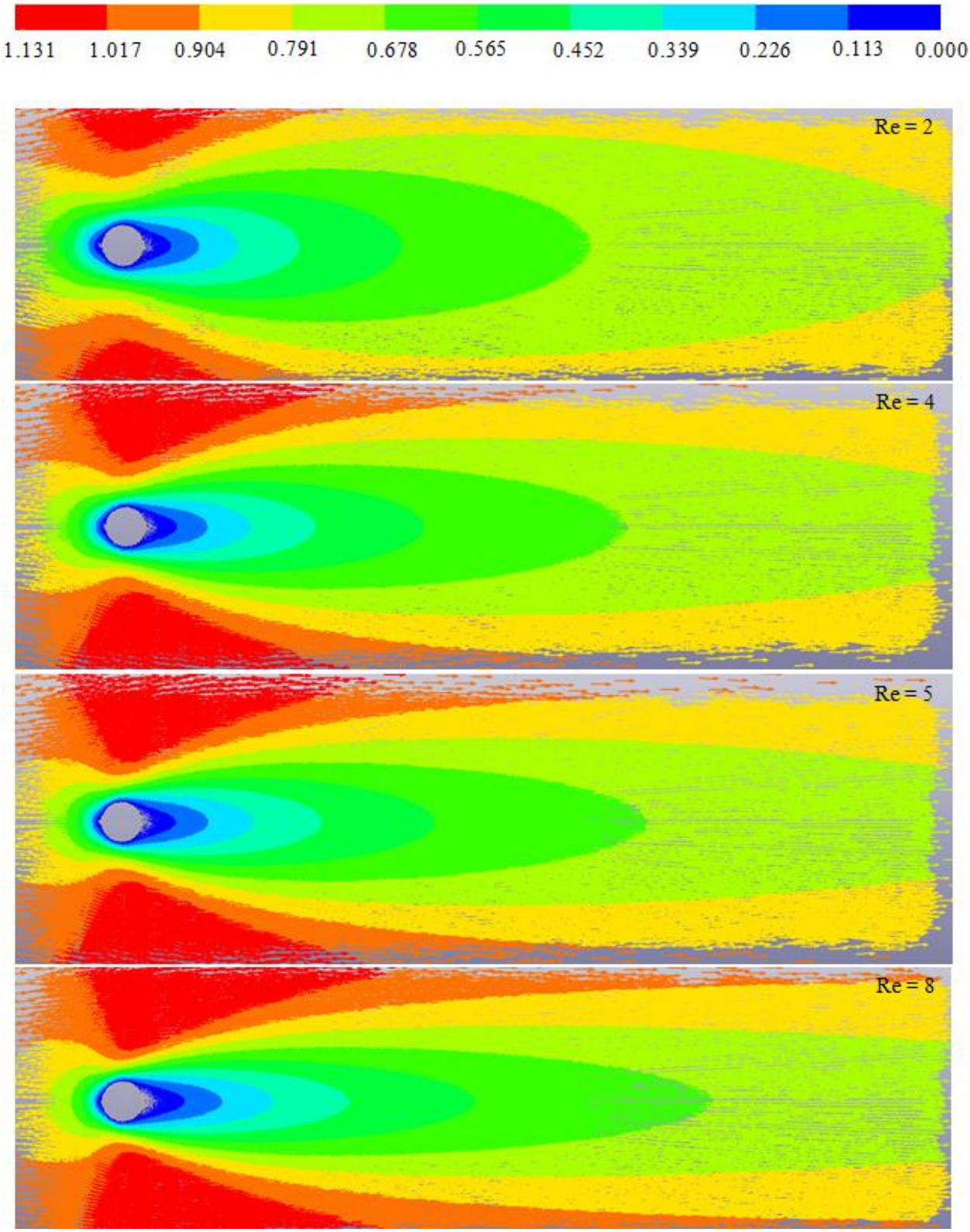

Figure 3.7: Velocity of streamline for Re = 2, 4, 5, 8

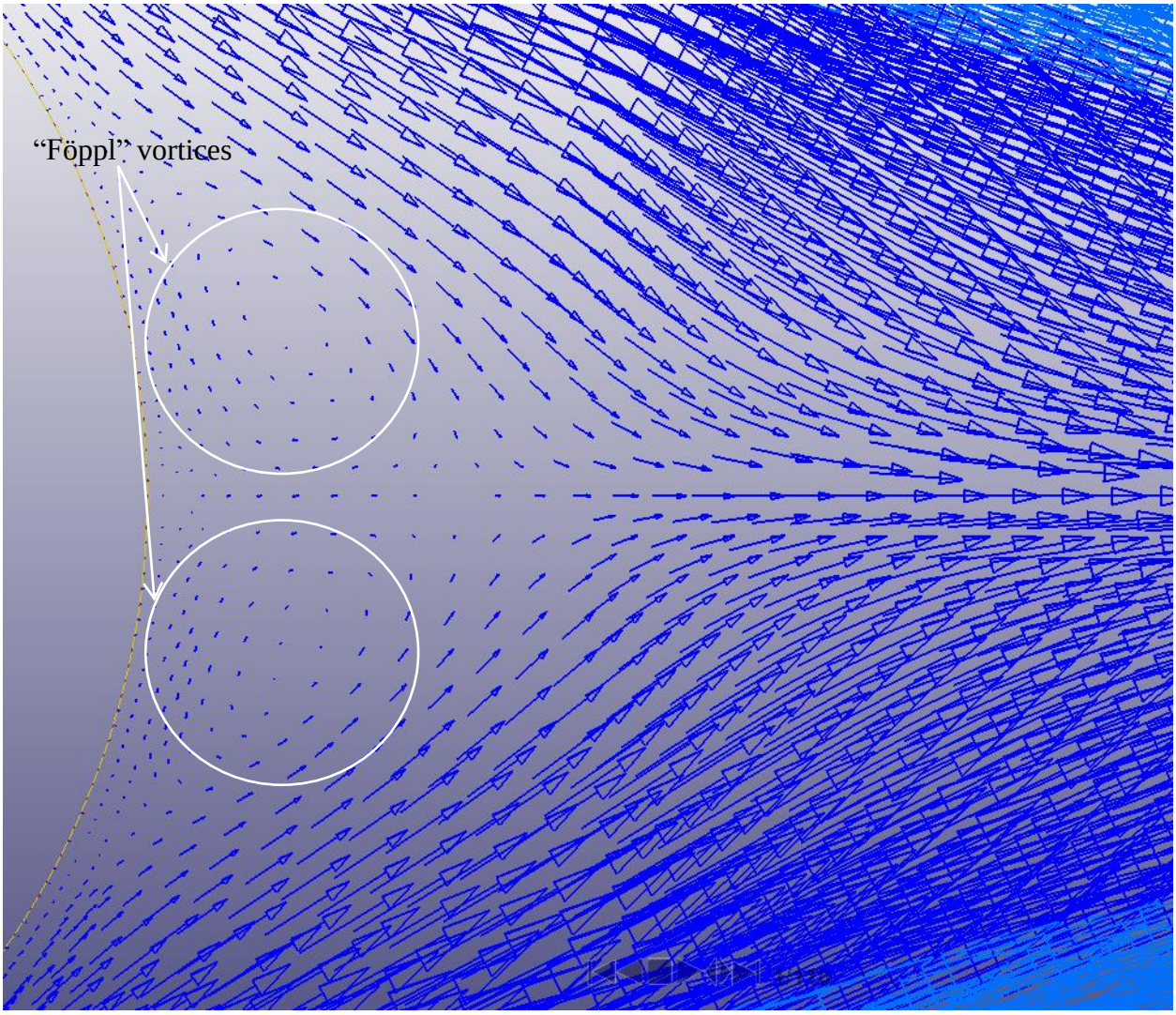

Figure 3.8: Föppl vortices appear when Re = 9

As the Reynolds number approached 50, the “Föppl” vortices became unstable. The shear layers of stream initiated at the confluence point oscillated sinusoidally (Figure 3.9). As a result, two rows of “Föppl” vortices were formed, one vortex in one row located opposite the midpoint of two nearby vortices in the opposite row, as shown in Figure 3.9, this arrangement of vortices is called Kármán Vortex Street (Massey, 2006).

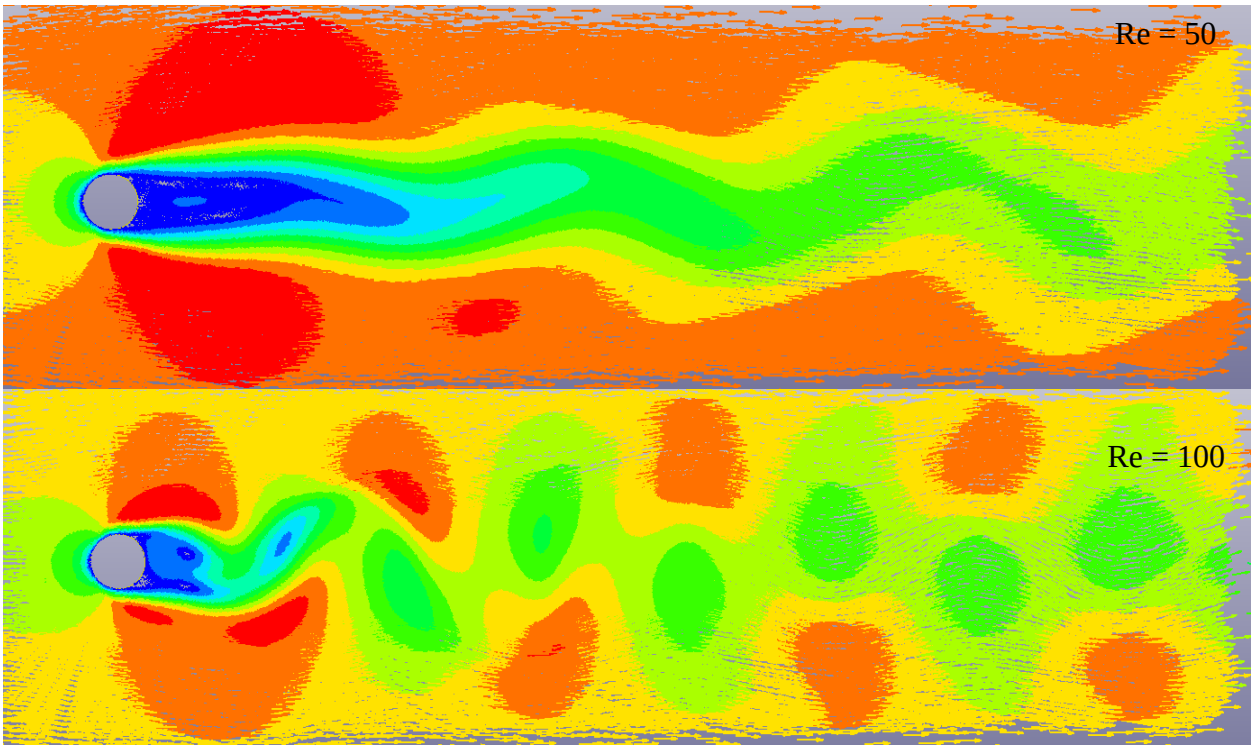

Figure 3.9: Re = 50, Re = 100

As the Reynolds number increased, the transition from laminar regime to turbulent regime began from the wake region. The vortices street became irregular. Lienhard has observed that the vortex periodicity has vanished completely at a distance of about 48 diameters downstream from the cylinder when Re = 300 (Lienhard, 1966). In order to observe this phenomenon, finer mesh was required for the downstream. As a result, the dimension of the mesh box 1 has been extended from $6 \times 22m$ to $12 \times 41m$. The mesh size was kept the same as the original size. The simulation result had corroborated Linhard's. As shown in Figure 3.10, the vortex vanished at the lower end of the stream far from the cylinder.

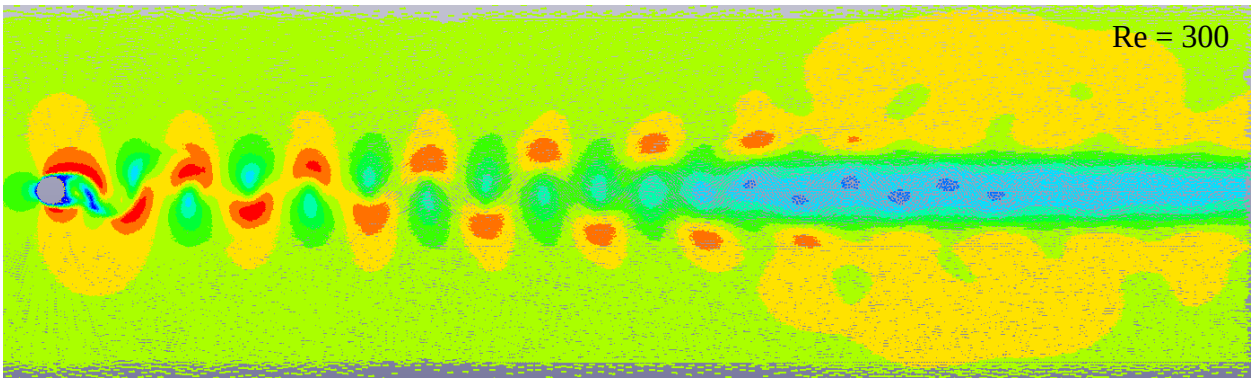

Figure 3.10: Re = 300

Along with the increase of the Reynolds number, the vortex periodicity vanished at the regimes that became closer to the cylinder and the free shear layers started to undulate, as shown in Figure 3.11 (a). When the Reynolds number increased to around 1,000 ~ 2,000, the transition waves rolled up to the sides and turned into discrete eddies, shown in Figure 3.11 (b). As the Reynolds number increased up to 20,000, shown in Figure 3.11 (c), turbulence formed in the free shear layers near the side of the cylinder.

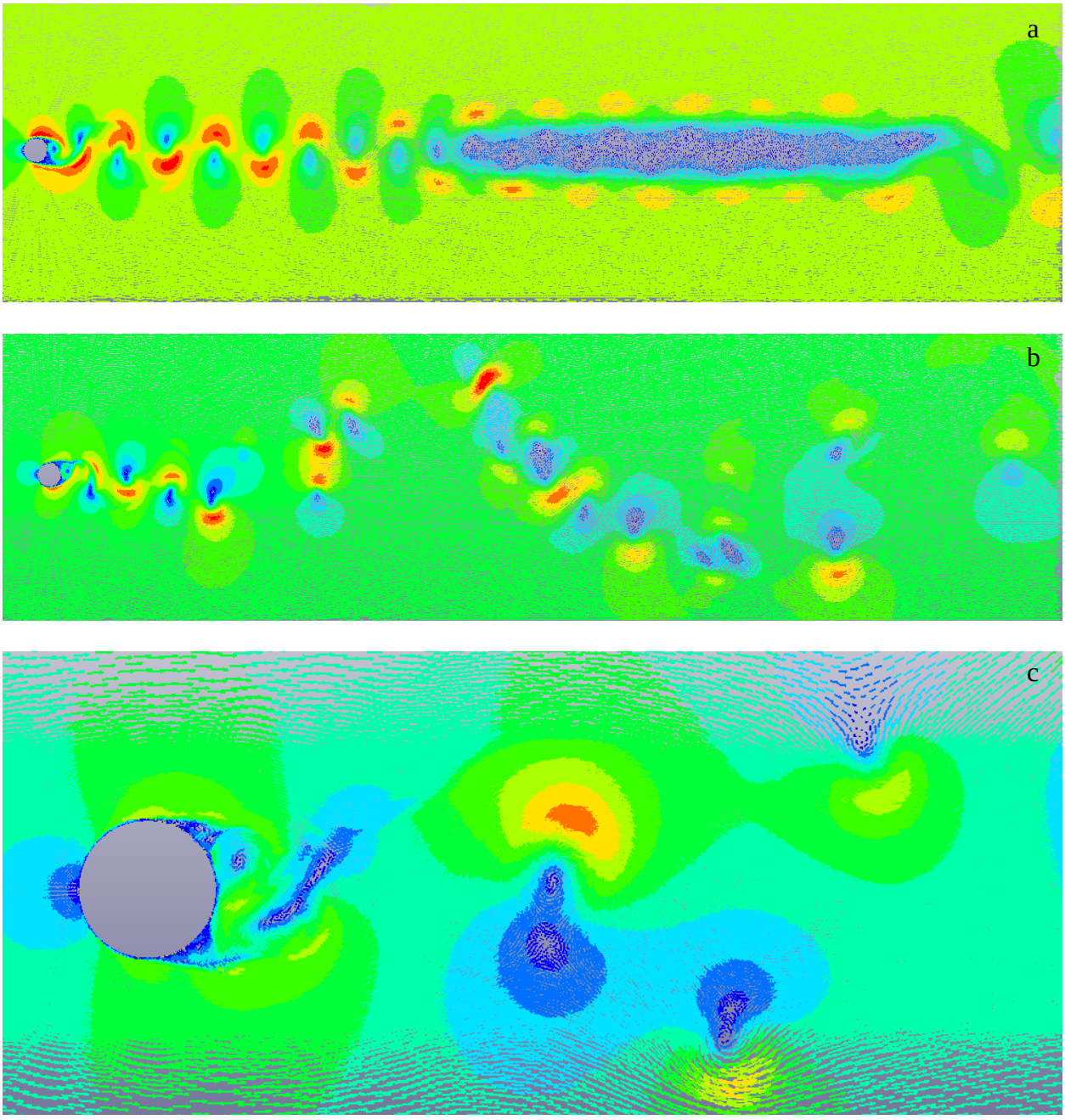

Figure 3.11: (a) Re = 500, (b) Re = 1000, (c) Re = 20,000

3.3 Summary

This chapter validates the ability of ICFD solver of LS-DYNA in dealing of fluid and structure interaction. A numerical model had been built in 2D. For the model, a uniform fluid was

applied from the left of a stationary cylinder and exited to the right in a rectangular fluid domain. The flow direction was perpendicular to the axis of the cylinder. The viscosity of the fluid varied from 2×10^{-5} to 0.5 in order to reach the range of the Reynolds number from 2 to 50,000. In each simulation, the drag forces over the simulation time were directly given by LS-DYNA. The simulation time for each was 200 seconds. The drag forces obtained from the simulations were not stable for the first 100 seconds. It gave an unexpected high value for the drag force at the beginning of each simulation, then settled down to a constant value.

The drag coefficient was calculated based on the average drag force when the result was settling. From the simulation, the drag coefficient decreased as the Reynolds number decreases when $\mathrm{Re}<180$. It rose slightly when $180<\mathrm{Re}<2,000$ and dropped again when the Reynolds number is greater than 2000. Compared to some of the available literature, the simulation results agree with others when the Reynolds number is small. The result generated from LS-DYNA is very close to Park et al's study at $0<\mathrm{Re}<160$ (1998). The result at $100<\mathrm{Re}<600$ generated from the simulation is not very close to Fornberg in his study (Fornberg, 1984). It agrees with Schlichting for most of the time. The only difference is that in Schlichting's study the drag coefficient decreases to the minimum value of 1 as the Reynolds number decreases to 1000, and then increases slowly after.

The disturbed flow around the cylinder appeared differently as the Reynolds number changed. The detailed description is summarized in Table 3.5.

Table 3.5: Flow regimes for different ranges of the Reynolds number

Reynolds Number	**Flow Regimes**
$2 \leq Re < 9$	Non-separated fluid stream, the velocity gradient appears in an oval shape
$9 \leq Re < 50$	A pair of "Föppl" vortices is formed behind the cylinder and become bigger and narrower as the Reynolds number increases.
$50 \leq Re < 180$	The vortices street is formed.
$180 \leq Re < 400$	The vortex street has vanished at the lower end of the stream.
$400 \leq Re < 1000 \sim 2000$	The shear layer starts to undulate
$1000 \sim 2000 \leq Re < 20000$	The fluid undulation turns into discrete eddies
$20000 \leq Re < 50000$	Turbulence forms in the free shear layers near the side of cylinder

The change of the flow regimes was compared with Lienhard's and Zdravkovich's studies. All the important transitions as the Reynolds Number changes were simulated. It shows that the ICFD solver has the ability to correctly simulate the flow around a structure and the drag coefficient for a Reynolds number up to 50,000.

Chapter 4 Impact Test in Water

This chapter discusses modeling the impact of ice model and structure in the water. The impact tests were implemented physically and numerically. The scenario under discussion assumes that the impacting object (ice model) is initially floating up naturally, while the impacted object (structure) is stationary. The behaviour of an ice model in water when it floats up is not only the result of gravity force, buoyancy force and drag force, the surrounding fluid affects the ice's behaviour. The ice model floats up with a certain speed, the fluid affect the motion of the ice model through its inertia due to an acceleration or deceleration is so-called "added mass". When the ice model floats close to the structure, the existence of structure affects the movement of the ice model and further causes the change of the added mass. At the same time, the added mass resists the change of movement of the ice model. Consequently, when the impact happens, the structure should receive the force results based on both the ice model and its added mass effects.

A series of experiments were conducted to study the kinematic behavior of the submerged ice model during impact. The experiments were used to verify the numerical model that was developed to simulate the underwater impact. Only the kinematic behavior from both aspects were compared. If a numerical model is able to correctly simulate the movement of the ice model under the interreaction with ambient fluid and the structure, it is believed that any energy transferred by water from the ice and added mass to the structure can be duplicated as well.

4.1 Test Plan

When a ship travels in an ice field, some ice might be submerged by the streamflow around the hull. Due to the buoyancy force, the ice pieces might flow upward and impact with the hull. The impact might be classified into different scenarios: (1) impact at the bow area when both ship and ice are moving, (2) impact at the bow area when ice is moving and the ship is at rest, (3)

impact at the bottom of hull when ice is moving and the ship is at rest, (4) impact at the bottom of hull when both the ship and ice are moving (Figure 4.1). The impacts that happen when both ship and ice are in motion are more complicated than other scenarios. In addition, as in reality, the moving water stream around the ice and ship makes this case more complicated. In order to simplify the problem, the experiments were carried out in a still water domain. The ice model was naturally released from certain distances below the impacted structure, which was stationary.

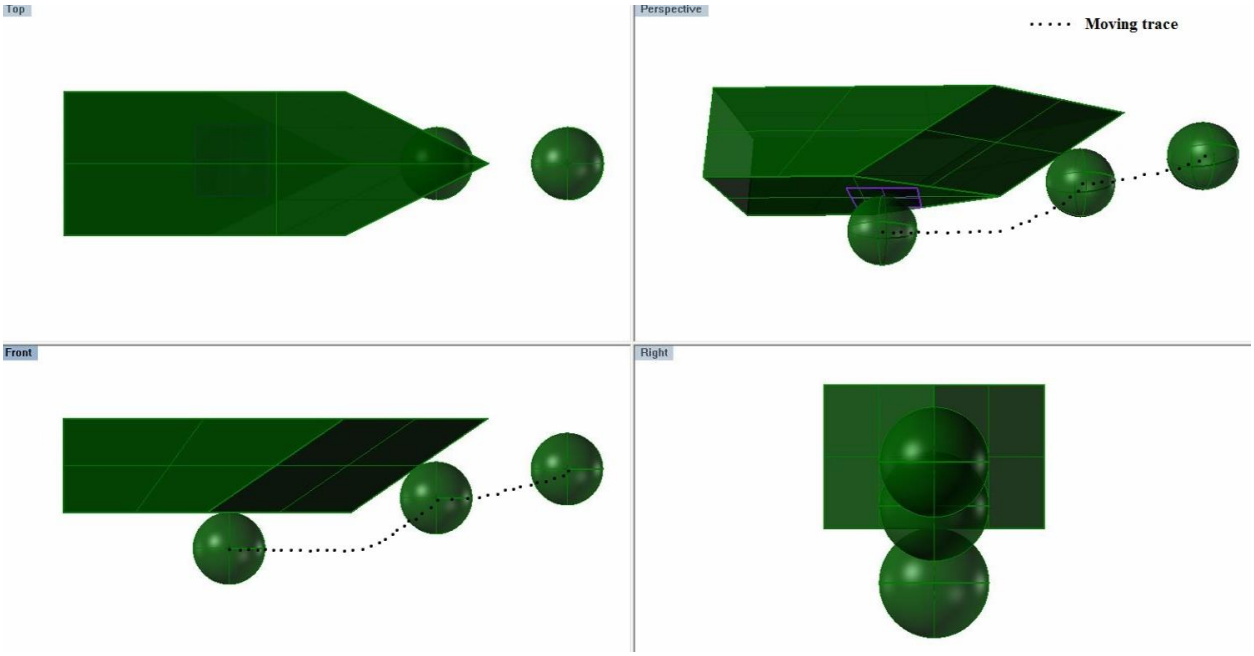

Figure 4.1: Impacts of ship and ice floes

A series of underwater impact tests with the submergence of the ice model varying from 0.01m to 0.34m under the structure were planned. There were five data points generated from this travelling distance range. They are tabulated in Table 4.1. Each travel distance was tested repeatedly.

Table 4.1: Planed travel distance of Ice model

NO.	1	2	3	4	5

Travel Distance [m]	0.01	0.10	0.2	0.30	0.34

4.2 Physical Experiments

4.2.1 Substitution of ice material

The physical experiments took place in Memorial University's S. J. Carew Building. Real ice was not used because of a number of reasons. In room temperature, the ice would melt during the test and cause instable physical properties. In addition, using the real ice would increase the degree of difficulty for the release mechanism during the physical tests. Furthermore, the ice crushing mechanism is not the main goal for this study. So the artificial and non-crushable material was used as ice in this study. Polyethylene was chosen for all the tests in this study because it has a similar density as ice. Its density is around 930 kg/m^3 and ice density is around 916 kg/m^3.

The shape of model ice feature was chosen to be as a sphere for two reasons. First, the contacts involving sharp edges might introduce negative volume problems in LS-DYNA, which would cause the simulation to be terminated automatically. The contact edge is better rounded. The second reason is because the submerged object might rotate as it floats upward in the later tests, which would increase the difficulty of image analysis. The sphere has a symmetrical shape that would disturb the fluid domain less than other unsymmetrical objects. The choice of ice and structure model was limited by the laboratory and the LS-DYNA model.

The ice model has a diameter of 0.1m, mass of 0.459kg, and density of 930 kg/m^3. At one end of the polyethylene sphere, a screw was built in and flushed with the surrounding surface. A thin fishing line was tied to the screw, as shown in Figure 4.2. A strip of thin foil was attached around the sphere in order to detect any rotation during the test. In the center of the sphere, a slot with a dimension of $0.021 \times 0.021 \times 0.070$ m was used to house an accelerometer.

Figure 4.2: Polyethylene ice model

4.2.2 Release mechanism of the sphere

In the process of the experiments, the ice model was released from different water depths. A simple release mechanism was designed and shown in Figure 4.3. Two pieces of aluminium L-bar were welded into an L-shape release mechanism. Two eye bolts were screwed at both open ends of the L-bar. They are marked as A and B in Figure 4.3. For each of the tests, the release mechanism was placed in the tank with eye bolt A lining up with the center of the tank, as shown in Figure 4.4. The center of the tank bottom was marked to ensure that eye bolt A was located at the same position for each test. One end of a thin fishing line was tied to the built-in screw in the sphere while the other end went through eye bolts A and B sequentially and then was fixed by a heavy weight on the edge of the tank. With this design, the sphere could be located at any desired depth by adjusting the fishing line. When the tests started, the heavy weight was removed rapidly so that the sphere could float upward freely. The fishing line was very thin and light hence there was negligible disturbance to the water domain.

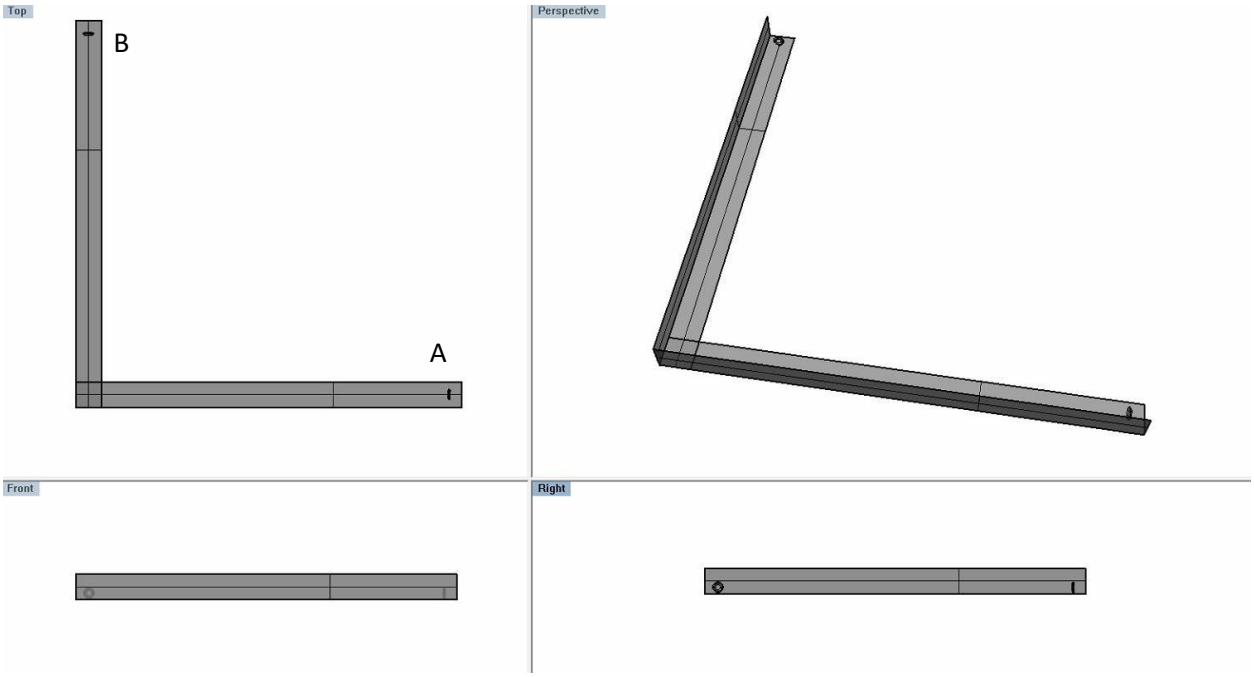

Figure 4.3: Drawing of release mechanism

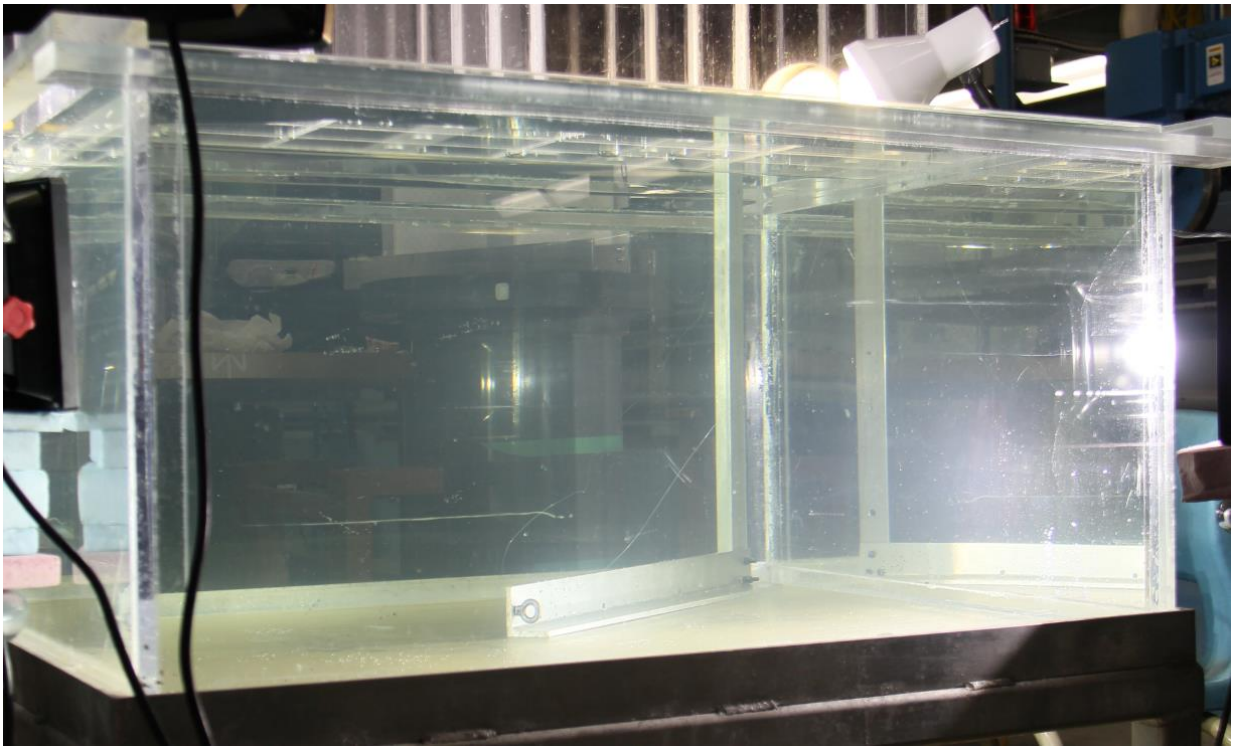

Figure 4.4: Release mechanism in the water tank

4.2.3 Other preparations

In order to observe the sphere's movement in water, the physical impact tests were conducted in a transparent water tank. The dimension of the tank is $0.49 \times 0.96 \times 0.96$ m. The impacted structure used in the physical experiment was the main body of a ship model that was made of Lexan. It was laid on the edge of the tank during the test as shown in Figure 4.5. Its dimension and the spacing of transverse and longitudinal compartments are tabulated in Table 4.2. In the process of the test, the fresh tap water was filled up to the tank edge so that the bottom surface of the ship model was fully immersed in water. All the air bubbles between the bottom surface and water surface were removed to ensure that the impact would happen completely in the water.

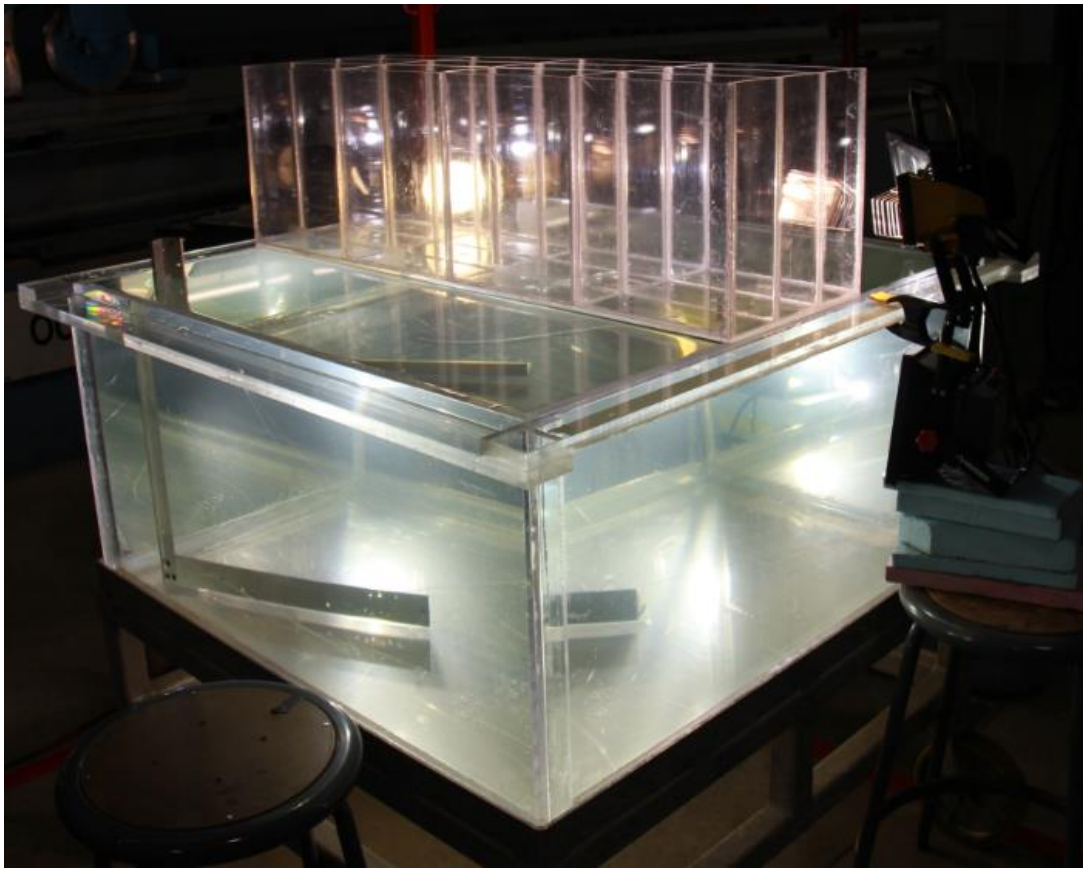

Figure 4.5: Clear water tank

Table 4.2: Dimension of the main section of a ship model

Length	Width	Height	Longitudinal Spacing	Transverse Spacing	Plate Thickness
0.99m	0.3m	0.3m	0.1m	0.25m	0.005m

4.2.4 Calibration

The experiments were recorded using a high speed camera for the purpose of image analysis. The recording resolution was 1028×800 and could not be any smaller because of the large recording range. The recording frequency was 400 Hz. The camera was placed outside of the water tank to record the test. Depending on the angle of view, the water and the tank surface might distort the scene through reflections differently. Therefore, calibration was very important.

Calibration had been completed twice prior to the experiments. A chess board print with waterproof coating was placed in the center of the tank where the ice model would be released from, shown in Figure 4.6. The length of the grid was measured. The high speed camera was placed at the same location throughout the entire experiment process. The chess board print in the water was recorded as a video and then converted into pictures. The number of pixels within each grid length was obtained. With the known dimension of the grids, the length of a pixel within the image was then determined. It was found that the grid at the bottom of the picture is slightly different from the upper grid, however, the differences were less than 0.01 mm hence they could be negligible. Hence, one pixel length was used for the image analysis regardless of the location of the ice model.

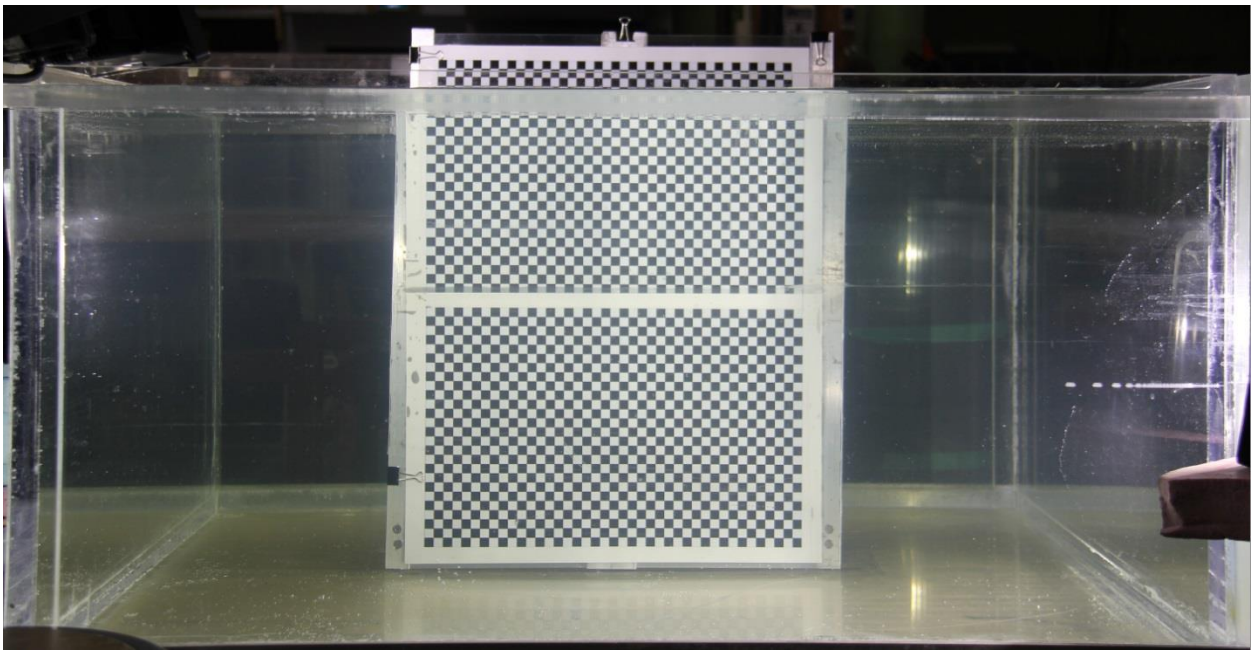

Figure 4.6: Chess board print for calibration

4.2.5 Test results

Before the ice model was released at the planned position, it was very important to wait for few minutes for the water to calm down. Any oscillation of the sphere due to unsettled water would increase the difficulty of image analysis. Figure 4.7 shows that the sphere stayed still in the water. The high speed camera started to record a few seconds before the sphere was released. As soon as the heavy weight was removed from the fishing line, the sphere floated upward without any rotation. It bounced downward right after it hit the bottom surface of the ship model. The video of each test was converted into picture frames. The center of the sphere in each picture was determined by reading the pixel coordinate. There were over thousand of pictures for each test. In order to minimize the human error and also to speed up the analysis, a Matlab program was developed by Dr. Ayhan Akinturk was used to determine the boundary box of the sphere. Figure 4.8 shows the sphere moving in water in a high contrast mode, which was

generated by Matlab. By running the program, the dimension of the boundary box and pixel coordinate of the top left point were output.

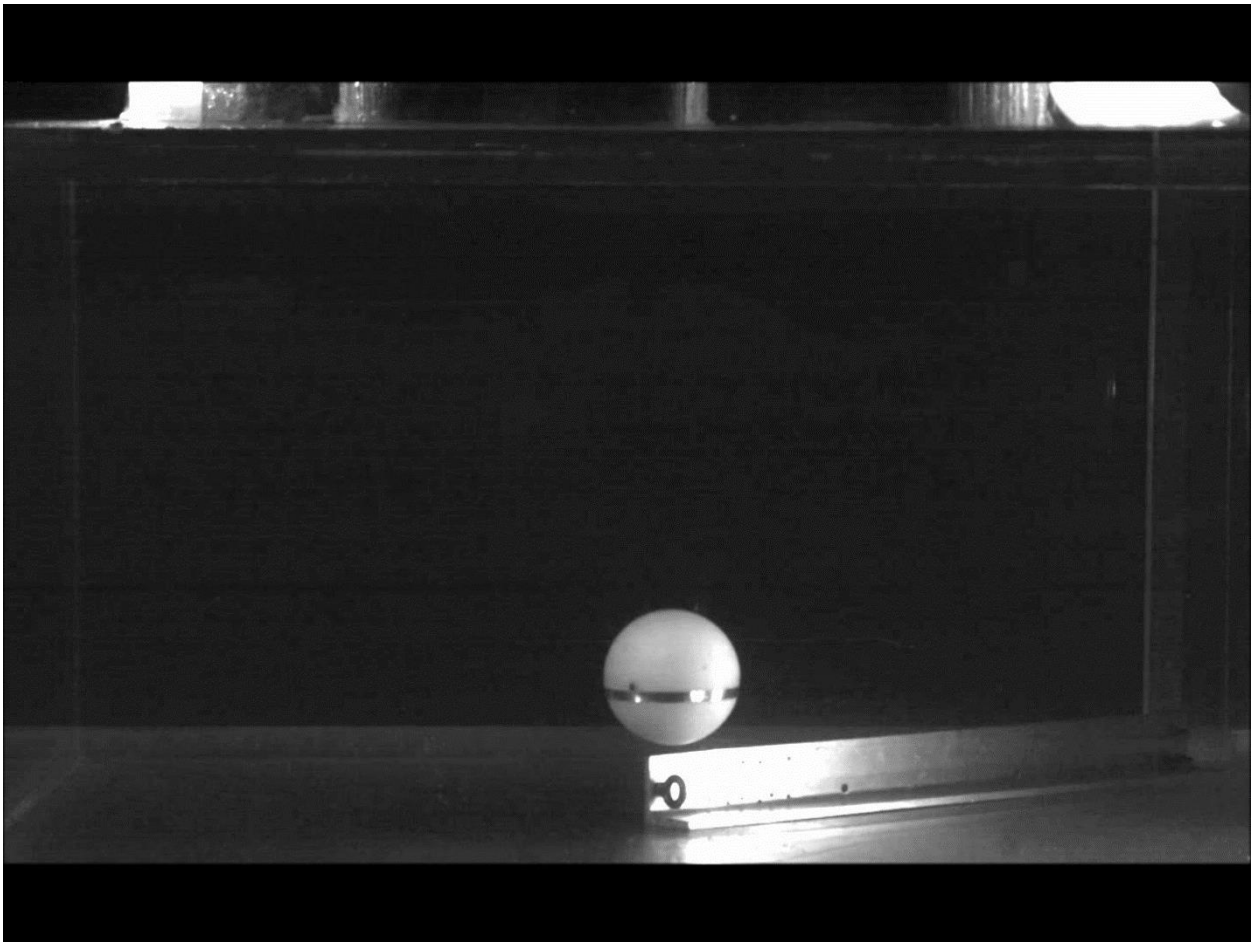

Figure 4.7: Ready for the Test

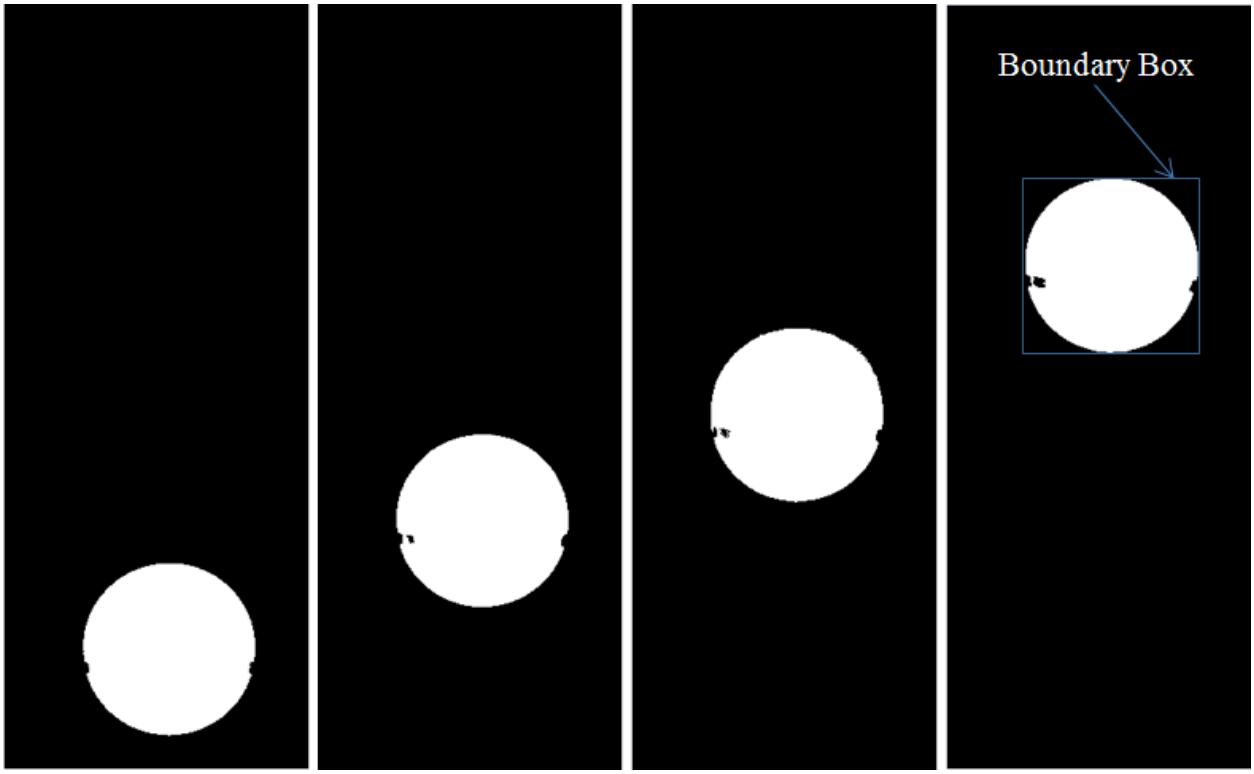

Figure 4.8: Contrast image of the sphere during movement

The displacement of the ice model was then determined based on the pixel coordinate and pixel length. The real traveled distances, tabulated in Table 4.3, were not exactly the same length as the test plan. Then the displacement was differentiated to obtain velocity. The moving average method was used to remove the noise. Figure 4.9 shows before and after the moving average method was applied for one of the tests with a maximum traveled distance (y) of 0.335m.

Table 4.3: Traveled distance of the sphere

NO.	1	2	3	4	5
Traveled Distance [m]	0.011	0.10	0.192	0.283	0.335

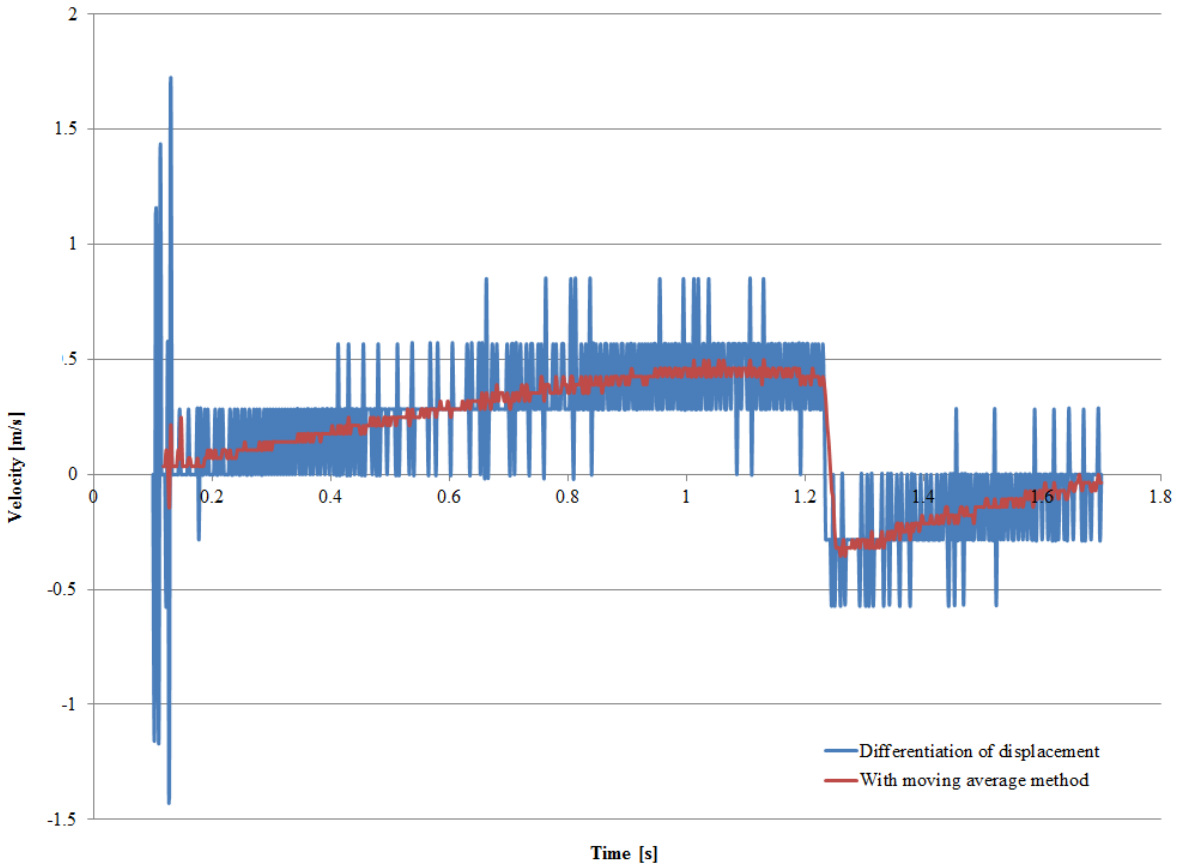

Figure 4.9: Displacement of ice with and without moving average method

Figure 4.10 shows the travel trace and velocity for the same case. It took about 1.2 seconds for the sphere to float up to the plate and then bounce downward. When the ice model was approaching the structure, it accelerated firstly and then decelerated when it went near the structure. The deceleration was due to the resistance from the structure. Figure 4.11 and 4.12 show the displacement and velocity for five different submergences.

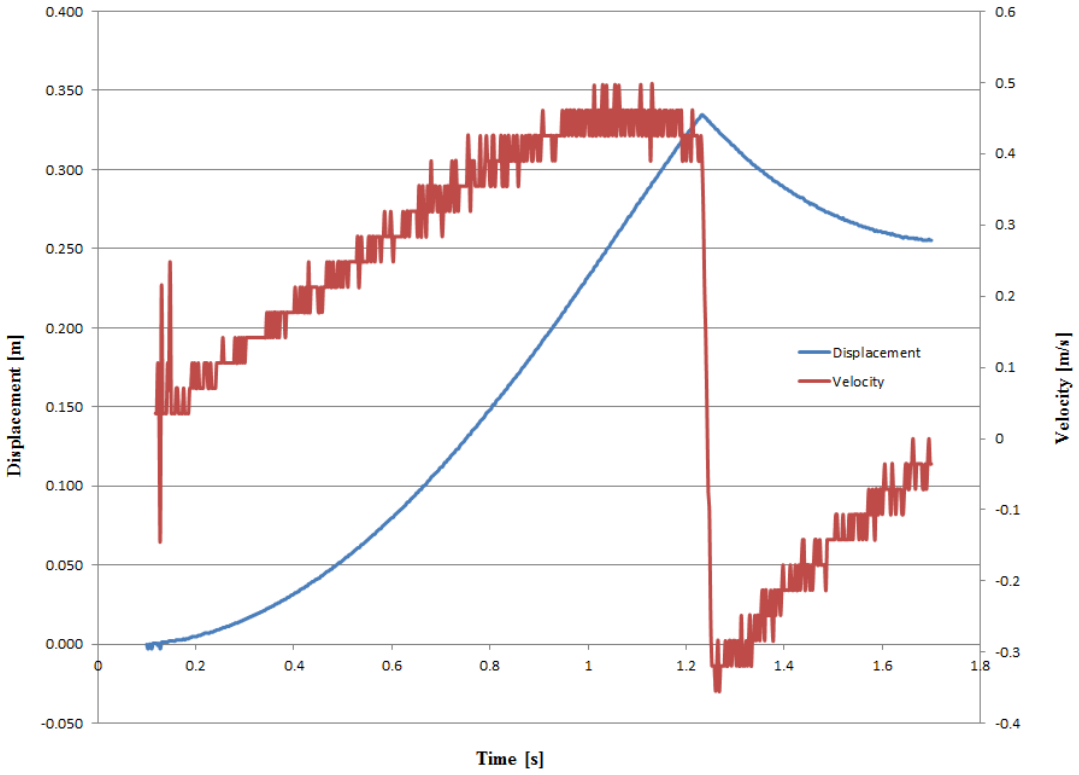

Figure 4.10: Displacement and velocity (y = 0.335m)

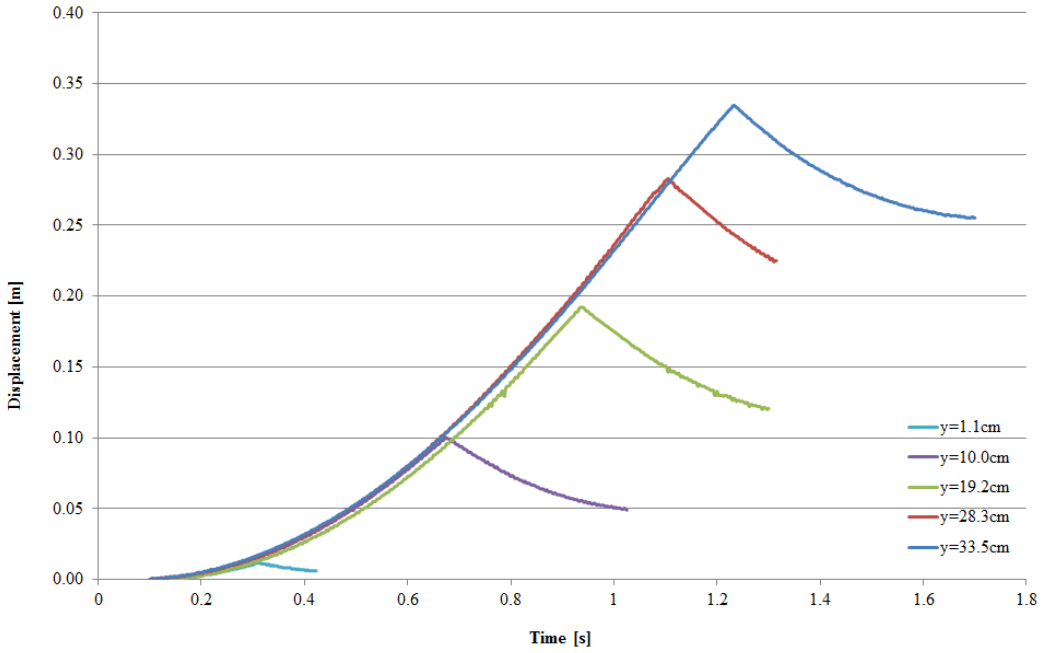

Figure 4.11: Displacement verse time

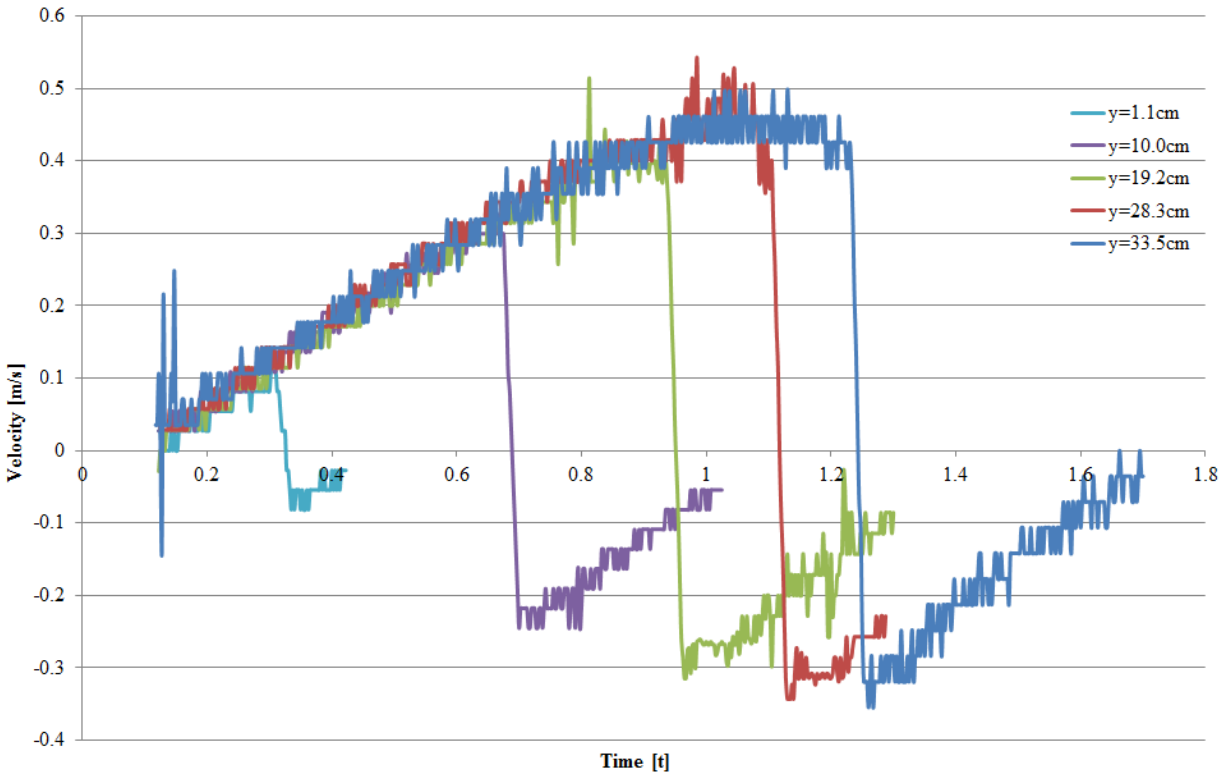

Figure 4.12: Velocity verse time

4.3 Numerical Model of Impact Tests

The physical experiments only studied the kinematics of the submerged ice model. They didn't measure the impact forces. As mentioned, the author believes that the impact force that is transferred to the structure could be duplicated when the kinematics of ice model under the interreaction of ambient water and structure are simulated well.

This section presents the numerical model of the physical experiment that was introduced in the previous section. The numerical model was built using the coupled ICFD and implicit structural solvers of LS-DYNA. It includes the impacted structure, ice model, air, water, and the interface of air and water. The keywords files include three parts: the structure mesh file, the fluid/air mesh file and the command file. The structure mesh was developed based on the section

property of plate and ice sphere. The fluid/air mesh was generated based on the boundary shell for water, air, and submerged objects. The command part comprised all the necessary commands that make the model functional (Appendix B). These will be explained in the remaining part of this section.

4.3.1 Numerical model of the impacted structure

The impacted structure, which represented a hull, was laid on the water surface for the whole time of the physical test. The impacted structure in the numerical model was originally located at the same position, however, the simulation terminated automatically with a non-detailed error message as shown:

```
*** Error 120003 (ICFD+3)
    I 3
```

The error was guessed as the overlapping of the surfaces or nodes for the boundaries. Hence, the structure was simplified from a ship model to the bottom plate of the hull. The plate was placed at a certain distance below the water surface to avoid the overlapping. In the process of volume mesh development, the automatic volume mesher detects the surface nodes and elements first, and then connects the nodes by building an initial volume mesh base on the Delaunay criterion. When the structure stays too close to or right on the air-water interface, the automatic volume mesher might fail to build the volume mesh respecting the Delaunay criterion. Consequently, the plate was placed at 7mm below the water surface.

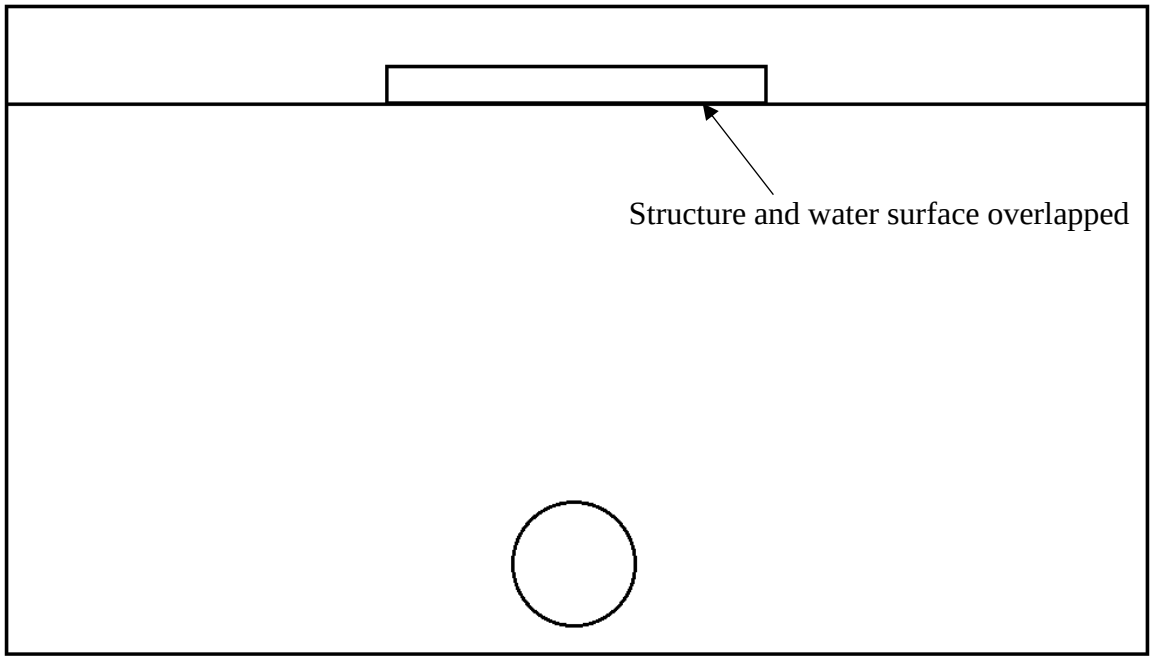

Figure 4.13: Original layout of numerical model

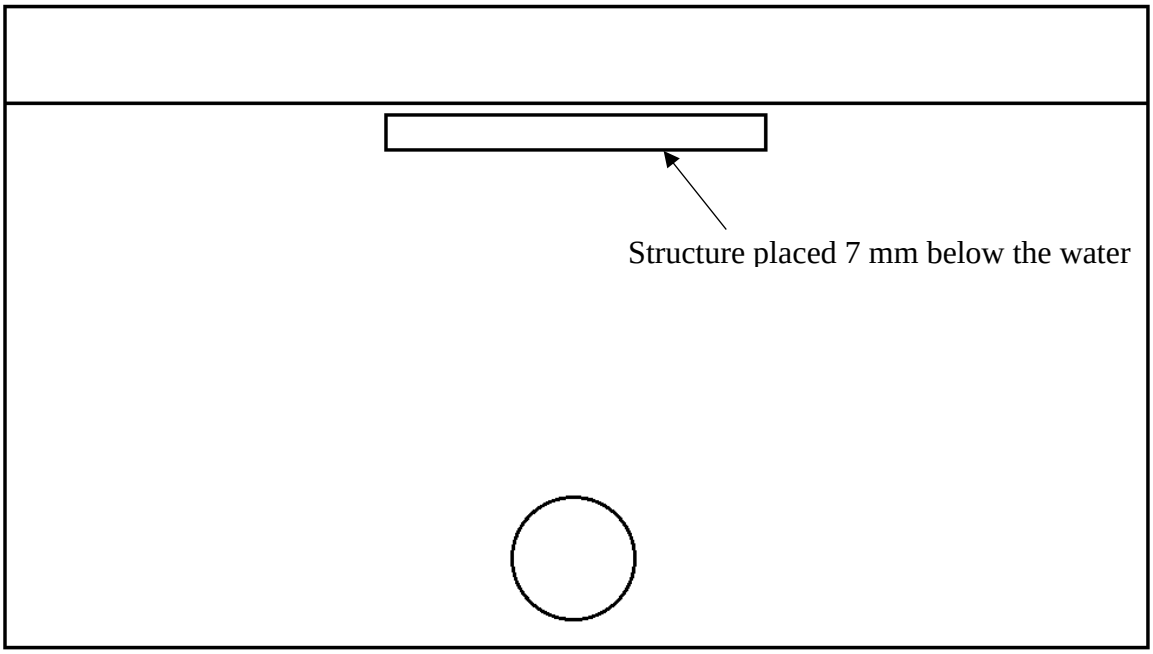

Figure 4.14: Revised layout of numerical model

The dimension of the plate is $0.2 \times 0.2 \times 0.02$ m. Solid elements were used for the plate structure. Instead of Lexan, the material of the plate in the numerical model was steel which ice would encounter in reality. Its material is defined in Table 4.4.

Table 4.4: Material property for the plate

Card ID	**MAT_PLASTIC_KINEMATIC (003)**			
Density	Young's Modulus	Poisson's Ratio	Yield Stress	Tangent Modulus
7850 kg/m^3	207 GPa	0.4	0.3 GPa	1E+9

4.3.2 Numerical ice model

As mentioned, the ice shape was spherical in order to avoid the sharp edge contact and also to reduce the degree of difficulty for analysis. The ice model has a diameter of 0.1m and is analyzed using rigidshell elements. Its material is defined in Table 4.5.

Table 4.5: Material property for the ice model

Card ID	**MAT_RIGID (020)**	
Density	Young's Modulus	Poisson's Ratio
920 kg/m^3	5 GPa	0.3

With the ice density of 920 kg/m^3, the weight is less than the sphere from physical experiments. In order to match the same weight, the desired weight is approached using the Mass_Trimming function in the pre-processing stage. The weight difference is evenly distributed to all the nodes on the sphere. By doing so, not only are the mass of the sphere of physical model and numerical model matched, but also the difference of density of both models are minimum. Figure 4.15 shows the original ice model and the ice model with added weight.

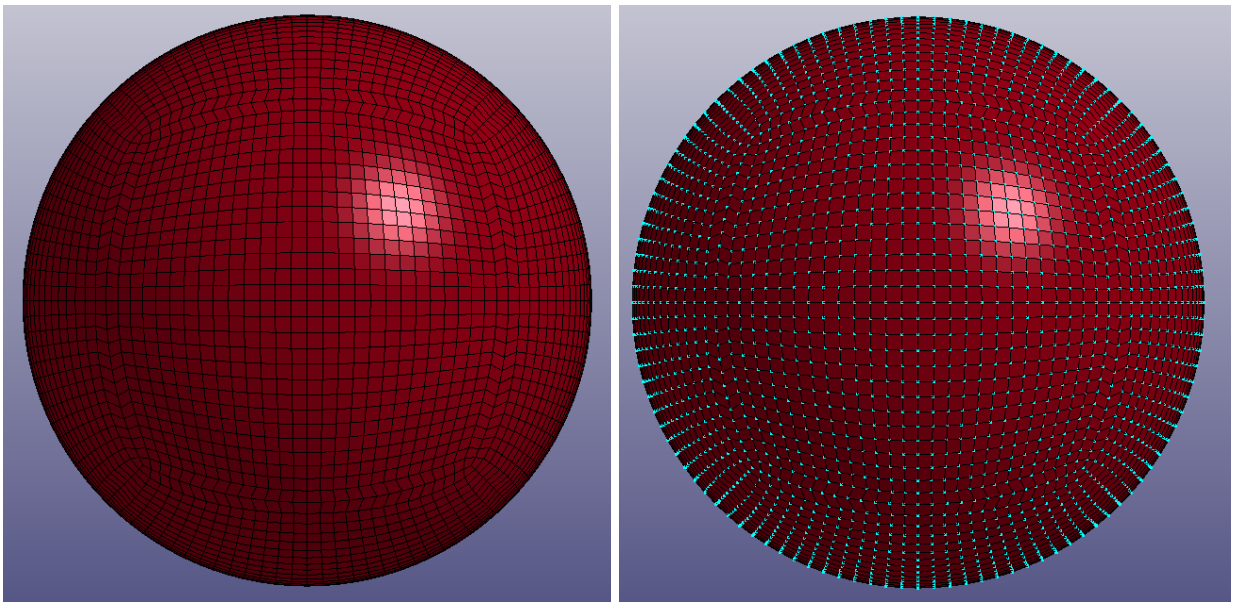

Figure 4.15: Before and after added weight of the ice model

4.3.3 Contact modeling in implicit analyses using LS-DYNA

For the shell or beams elements, the contact thickness can be defined through modifying Optional contact thickness (OPTT) of PART_CONTACT card. OPTT = 0 m was applied to the model with the intention of avoiding the gap; however, a 0.5 mm gap still existed when contact happened.

The two-way contact card CONTACT_AUTOMATIC_SINGLE_SURFACE was used for the numerical model. LS-DYNA offers different options for user to optimize the contact for different situations. The different SOFT options (0, 1, and 2) determine the contact spring stiffness differently and the gap flag IGAP is used to improve convergence behavior.

As mentioned in Chapter One, SOFT = 0 is more suitable when the contact objects have similar material properties. SOFT = 1 is more recommended for explicit simulation, especially when the contact parts have dissimilar material properties or mesh densities. For a better comparison,

SOFT = 0, 1 & 2 were all applied to the simulations with s = 0.011 m individually. This travel distance is the shortest traveled distance of the physical experiments. The resultant displacements are compared in Figure 4.16. The distance between the ice model and structure is marked as a purple line in the figure. The result shows that the ice traveled a certain distance and bounced back when it hit the plate. It can be seen that a gap exists when contact happens. The simulations with different SOFT options show that the SOFT = 0, in which the gap is closer to the defined contact thickness. Later the physical tests will show that the movement of the sphere was similar to the simulations with SOFT = 1 and 2 (Figure 4.21), however, the similar bouncing track only last for a very short period. With SOFT 1 or 2, the sphere bounced downward far below the initial released depth and even touched the bottom of the water tank, which is not realistic in water. This is because the contact was not detected properly due to the large time step with the implicit structure solver. SOFT = 0 was chosen for the final numerical model because the contact spring stiffness is lower due to the dissimilarity in Young's modulus, which is more suitable for this case.

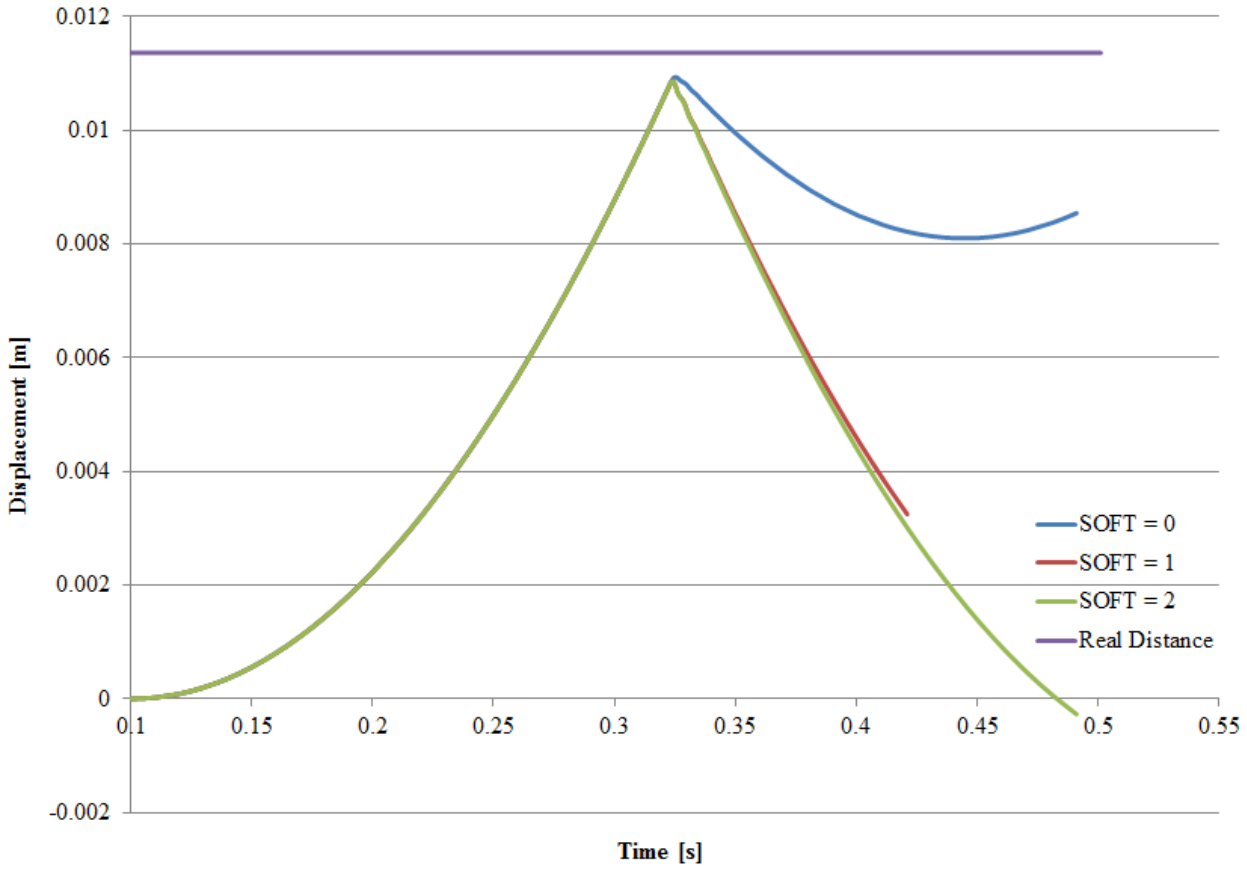

Figure 4.16: Comparison of SOFT = 0, 1 & 2

In the contact card, IGAP = 1 is the default option for implicit structural analyses, which allows a certain amount of negative contact pressure transfer between contact surfaces. It produces "sticky" interfaces that prevent surfaces from separating. This phenomenon was very obvious when comparing the resultant displacement of simulations with IGAP = 1 & 2, which is showing Figure 4.17. In the case of IGAP = 2, the ice model bounced downward to the opposite direction of the plate when it hit the plate. On the other hand, in the case with the option IGAP = 1, the ice stuck to the plate instead of bouncing back. Therefore, the IGAP option was turned off, i.e., IGAP = 2, for the final numerical model.

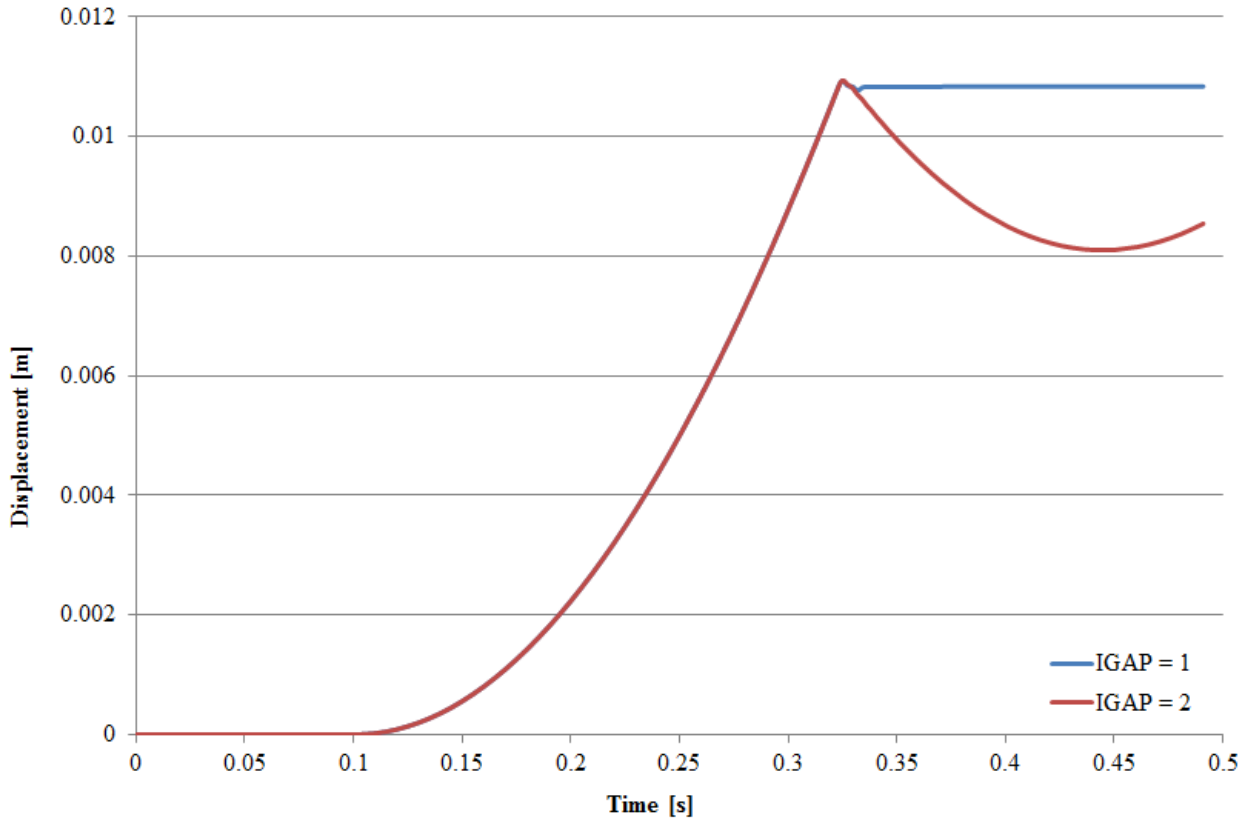

Figure 4.17: Comparison of IGAP = 1 & 2

4.3.4 Fluid/Air domain and boundary conditions

The numerical environment included two domains: air and water. The dimension of the water domain was the same as the tank used in the physical experiment. The air domain was right above the water domain and its dimension was $0.1 \times 1 \times 1$ m. Their properties are listed in Table 4.6.

Table 4.6: Property of air and water domains

	Density [kg/m^3]	**Dynamic Viscosity [kg/(m·s)]**
Air	1.225	1.81E-5
Water	1000	8.94E-4

In each of the simulations, four sides of the plate were fixed (see Figure 4.18). The gravity force was applied to the whole system. The ice model was constrained in all six degrees of freedom

for the first 0.1 second. Starting from 0.1 second, the ice model was released and no constraint was applied.

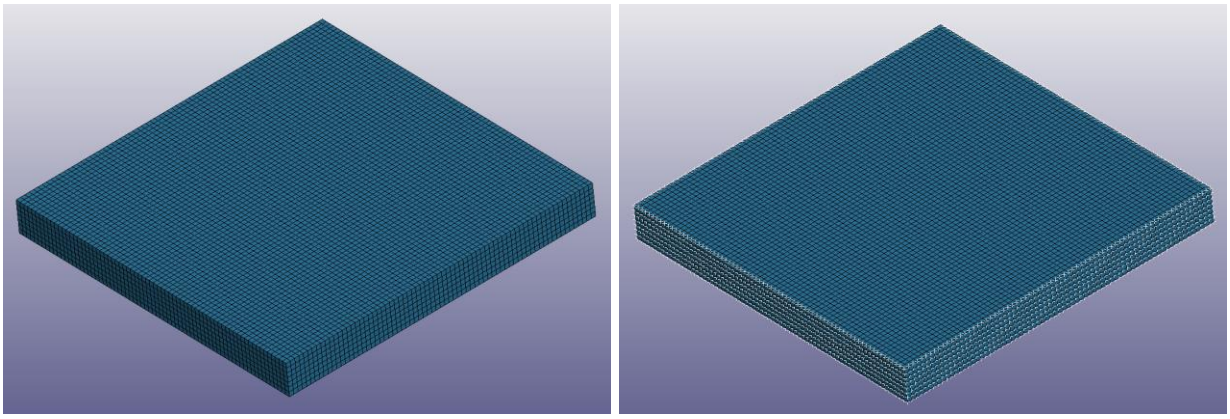

Figure 4.18: Plate with and without fixed the boundary condition

Not only do the boundary conditions of the plate and sphere need to be defined, but also the boundary conditions for the corresponding fluid mesh. Other boundary conditions are listed in Table 4.7.

Table 4.7: Boundary conditions

Part	Boundary Condition
Water Domain	Free Slip
Water Surface	Interface
Air Domain	Non-slip
Fluid Mesh for Plate	Non-slip
Fluid Mesh for Sphere	Non-slip

4.3.5 Mesh convergence study

The numerical model contained the ice model, plate structure, water and air. The plate structure's mesh only included solid elements. A shell mesh was used for the ice model. As

mentioned above, the fluid mesh was generated based on the boundary shell of water, air, the plate, and ice sphere. The role of the boundary shell of water and air here was to encircle the water and air domains. The boundary shell for the plate and ice sphere is like their jacket, which has the identical dimension and mesh size as the structure mesh. It is the communication medium between fluid and structure. After the boundary shell had been developed, it was then converted to a multi-solver mesh in order for the automatic volume mesher to detect the nodes on the mesh and further develop the initial volume mesh in respect to the Delaunay criterion. The solver then adds nodes progressively to create the volume mesh between the boundaries of structure and air/fluid. Hence, the structure and fluid geometry were matched at the interface.

As long as the structure and fluid geometry are matched at the interface, the meshes for the structure and fluid do not necessarily have to match to each other. The structure in this study contains more than one object: ice model and plate. Hence, it was necessary to conduct a mesh convergence study only on the ice model and the plate first. The mesh convergence study regarding fluid/air mesh would be followed after that. In addition, the quality of the mesh could also be checked by LS-DYNA. When the simulation starts, an *icfd_mstats* file is generated. It contains the overall mesh information at the initial stage, i.e., minimum/maximum angle, average minimum/maximum angle, and George Quality index. The George Quality (Q) is the standard determining the mesh quality. It can be calculated using Equation 4.1.

$$Q = \frac{L \times S}{V} \qquad \text{Equation 4.1}$$

Where: L is the longest edge length of the mesh element

S is the surface area of the mesh element

V is the total volume of the mesh element

High Q value means that the element mesh might be distorted and could lead to divergence issues. The higher the Q value is, the more deformed the mesh could be. Q values less than 10 are perfect. For some cases, high Q values can be acceptable if the percentage of element with high Q values is low.

Along with the movement of structure, the mesh changes as well. It could be stretched or compressed and no longer respect the initial mesh condition. Normally, re-meshing would happen when it is necessary in order to respect the Delaunay criterion. The alternate is the ICFD_CONTROL_ADAPT_SIZE card which can trigger a re-meshing when the mesh is over distorted, or when defined minimum or maximum mesh sizes are reached. ICFD_CONTROL_ADAPT is for defining the minimum and maximum mesh size for the fluid mesh. A new *icfd_mstats* file would be generated whenever a re-meshing happens.

The mesh convergence study was conducted by comparing the time histories of the velocity of the ice model. The test mesh sizes were 5.61 mm, 3.57 mm, 2.81 mm, and 2.62 mm. Figure 4.19 shows that convergence was reached when the mesh size was smaller than 2.81 mm. In this figure, the velocity trends were smooth except at around 0.85 s and 1.18 s, which is because of the re-meshing takes place. Furthermore, *icfd_mstats* files were checked for Q values. Table 4.8 shows that the maximum Q value for the mesh size of 2.81 mm was 9.30, which means that the percentage of element with high Q values is 0%. The maximum Q value for mesh size of 2.62 mm was 10^6 and the high Q value happens to 0.0058% of elements. Therefore, the mesh size of 2.81 mm was chosen for the ice model and plate.

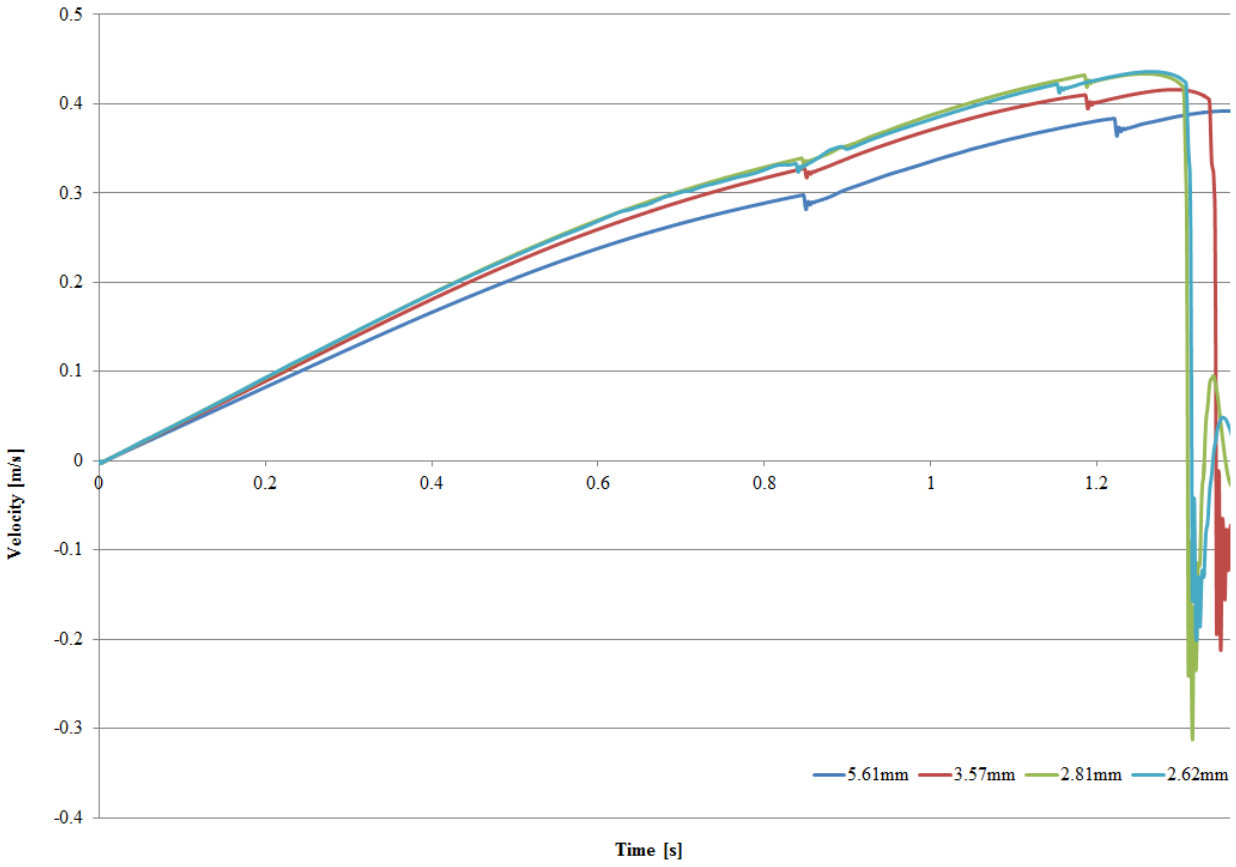

Figure 4.19: Mesh convergence study for the ice model and plate

Table 4.8: Q Values for different mesh sizes of the ice model and plate

Mesh Size [mm]	Minimum Q	Maximum Q	Average Q	Percentage of Element with High Q
5.61	1.00	9.68	1.65	0.00%
3.57	1.01	9.11	1.65	0.00%
2.81	**1.00**	**9.30**	**1.65**	**0.00%**
2.62	1.00	10^6	2.23	0.0058%

A mesh convergence study was conducted for the water mesh. In the convergence study, the mesh size for the ice model and plate was 2.81 mm and the mesh size for the water was varied from 15.6 mm and 31.3 mm. The mesh size of air is close to water's. The time histories of velocity of the ice sphere for different mesh sizes for water are compared in Figure 4.20. The

results shows that 20.8 mm mesh is odd but the rest four mesh sizes are converged. The *icfd_mstats* files give the Q values in Table 4.9 and indicate that 31.3 mm mesh is disqualified due to the high percentage of elements with high Q values. As the result the smallest mesh size (15.6 mm) was chosen for increased accuracy and based on the low Q criterion.

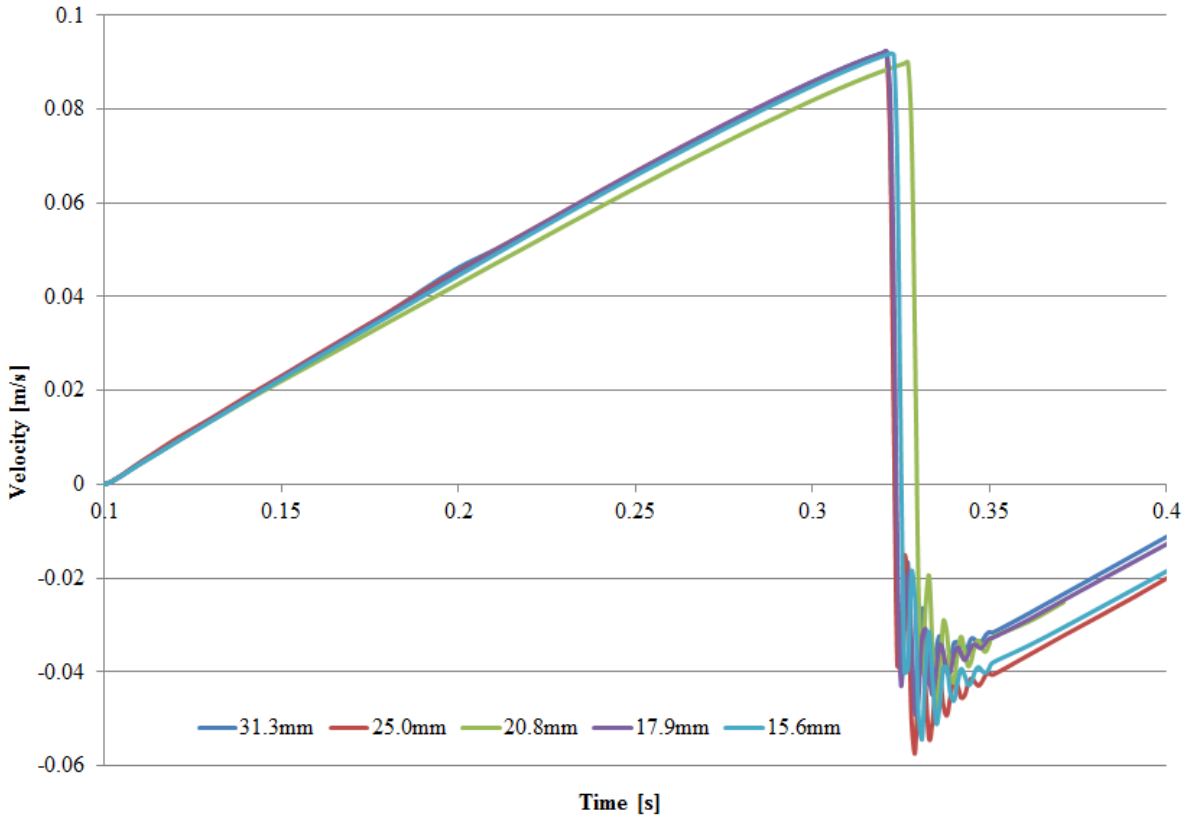

Figure 4.20: Mesh convergence study for fluid

Table 4.9: Q Values for different mesh sizes of water

Mesh Size [mm]	Minimum Q	Maximum Q	Average Q	Percentage of Element with High Q
31.3	1.01	10^6	16.25	39.51%
25.0	1.00	10^6	4.06	4.58%
20.8	1.00	9.83	1.73	0.00%
17.9	1.01	10^6	3.21	0.02%
15.6	**1.01**	**9.44**	**1.69**	**0.00%**

As a result, the mesh size of each part of the numerical model is shown in Table 4.10 and Figure 4.21.

Table 4.10: Model information

Number of nodes	44,697
Number of elements	46,178
Mesh Size for the Ice Sphere	2.8 mm
Mesh Size for the Plate	2.8 mm
Mesh Size for Water	15.6 mm
Mesh Size for Air	14.3 mm

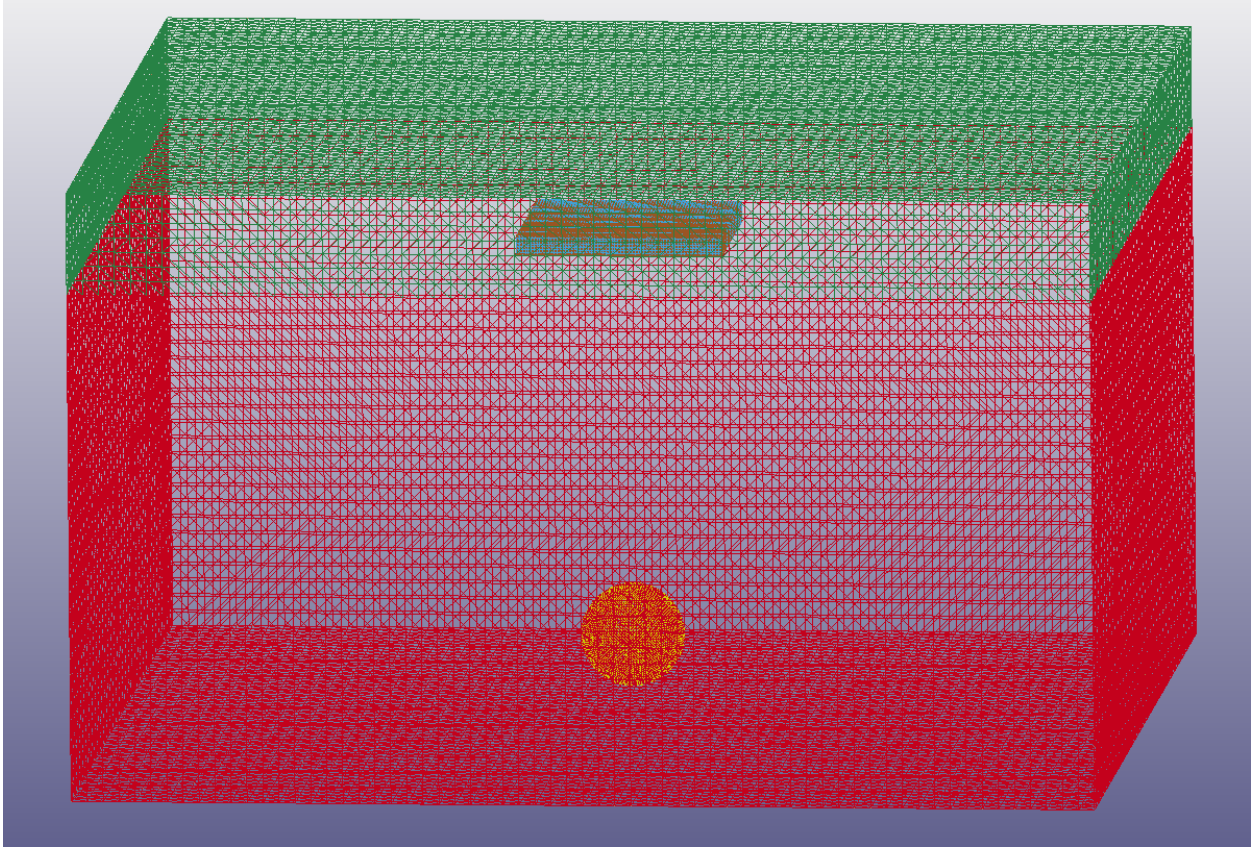

Figure 4.21: Numerical model layout

4.3.6 Time step control

The time step for the simulation was initially determined according to Equation 1.3, which gave the minimum time step to be equal or greater than 0.006 s. The convergence study was conducted for time step from 0.001 s to 0.04 s by comparing the time histories of displacement, which is shown in Figure 4.22. Mesh convergence was reached when the time step was less than 0.002 s. 0.001 s was then chosen as an appropriate time step for all of the subsequent simulations. It was noticed that there were some data left out for the output data with the chosen time step. However, the simulation with a smaller time step terminated without any error message.

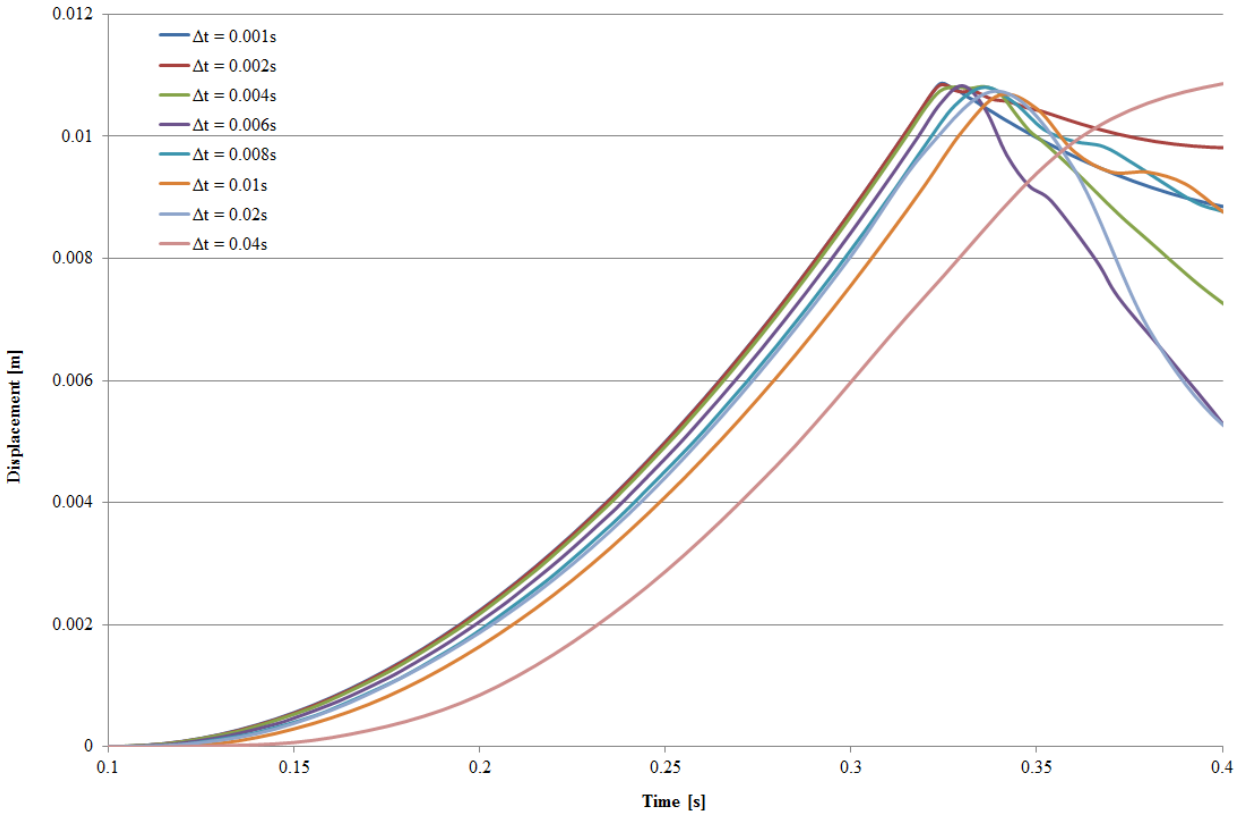

Figure 4.22: Convergence study for time step

4.3.7 Velocity and displacement

All simulations were run using 32 processors on the computer cluster. For all the simulation, the ice model was held still for 0.1 second for the hydrostatic pressure distribution to stabilize. The time cost for each simulation was in the range of 2 hours to 5 hours, which depends on the distance between the ice model and plate. The simulation results were all outputted in the data format. The moving trace and velocity of the ice model for each depth are shown through Figure 4.23 to Figure 4.32. The sphere accelerated when it was just released. Then it reached the maximum velocity and decelerated rapidly prior the impact. There are only two simulations which show different behavior, simulations with y = 0.192 m and y = 0.335 m. The ice model does not bounce downward after the impact. It is acting like the "sticky" interface exists, even with IGAP = 2. In addition, the velocity plots for most cases show that oscillations appeared when re-meshing occurred. Figure 4.33 shows the section view of the tank at initial, before and after re-meshing stages. It can be seen that the water mesh between the sphere and the bottom of the tank was stretched when the sphere is moving upward. LS-DYNA's automatic volume mesher re-meshed the water mesh in order to respect the Delaunay criterion. This occurrence of over-stretched mesh and re-meshing obviously affected the velocity of the sphere. After the re-meshing, the velocity oscillated a little and then settled with a lower velocity. As a result, re-meshing occurred more often for the further travel distance, and the difference of velocity between the numerical and physical tests were more obvious.

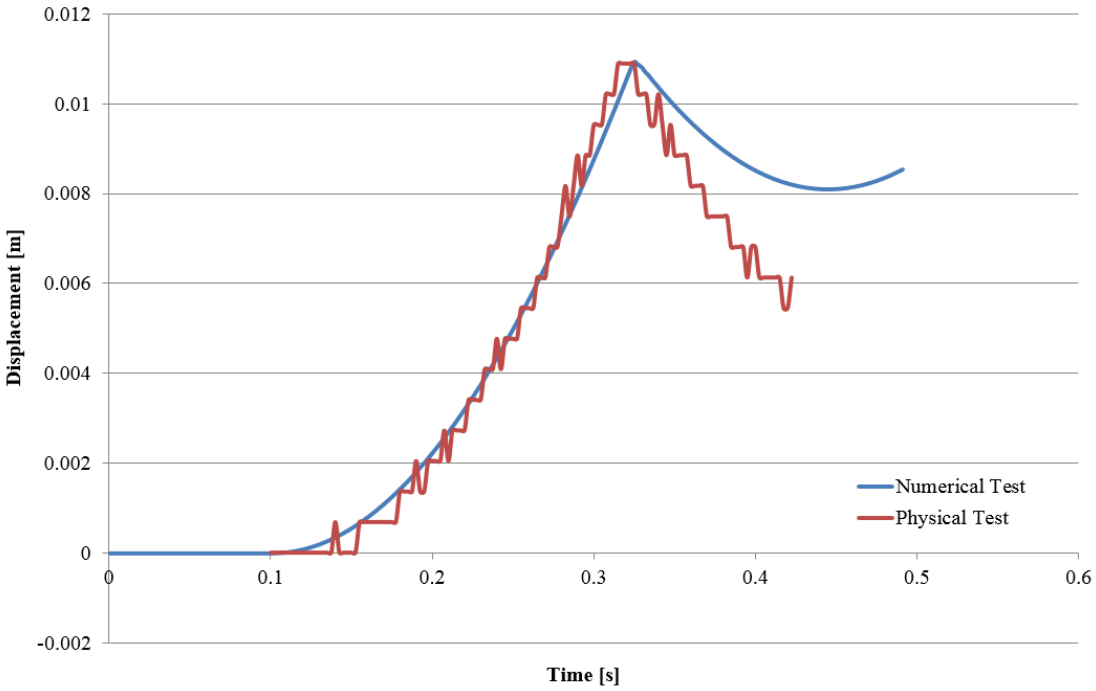

Figure 4.23: Comparison of displacement (y = 0.011m)

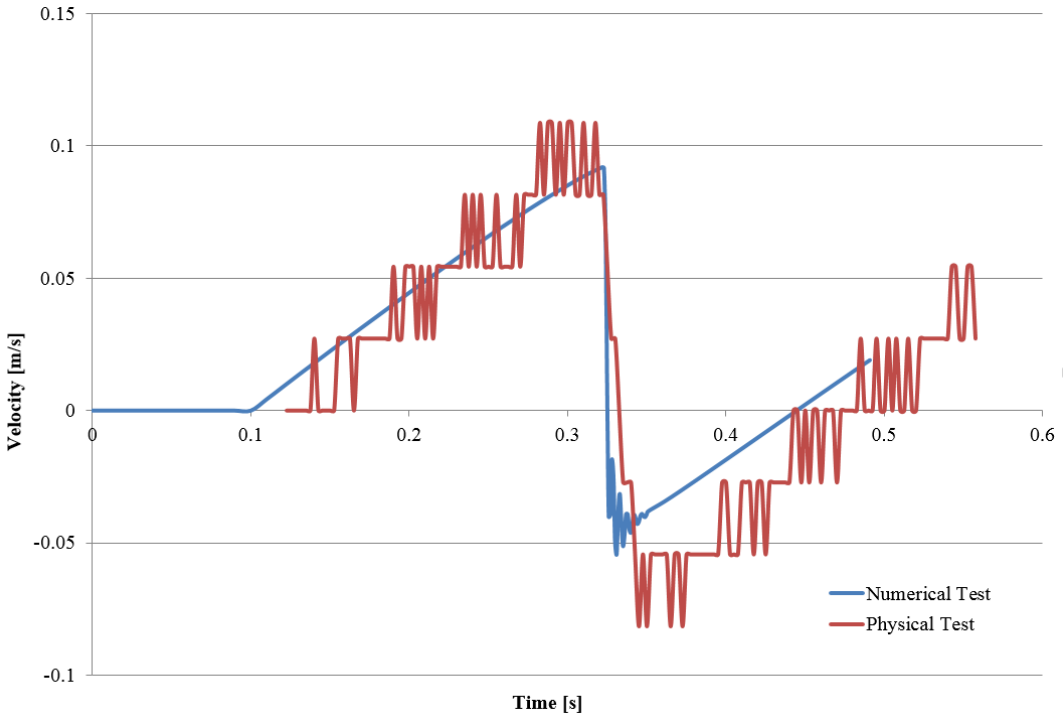

Figure 4.24: Comparison of velocity (y = 0.011m)

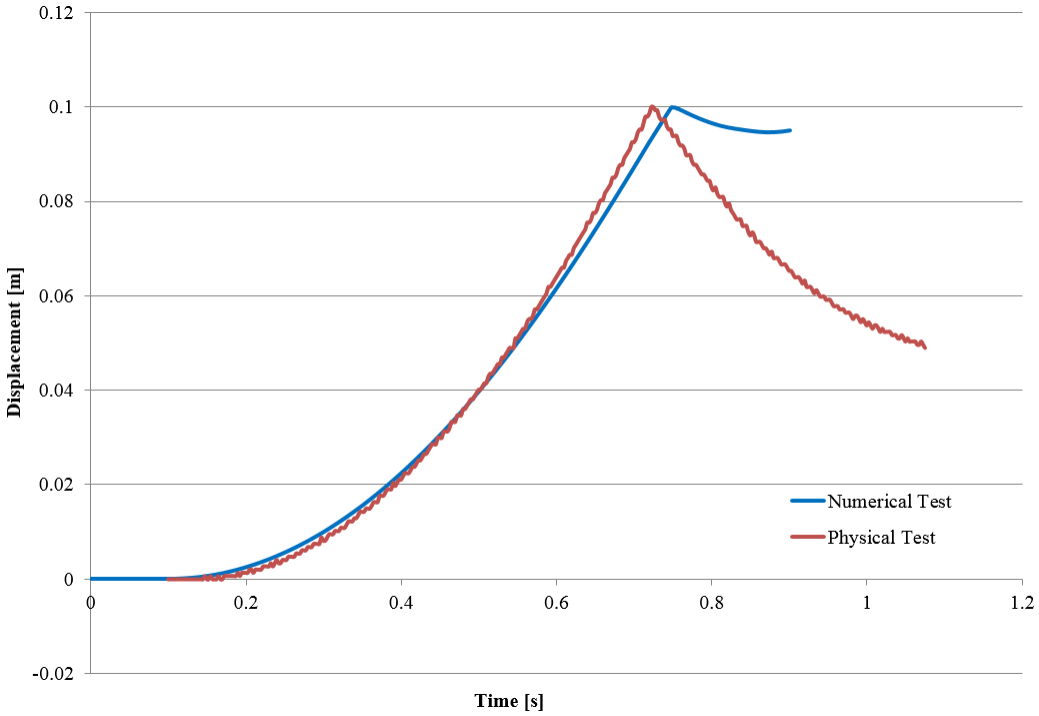

Figure 4.25: Comparison of displacement (y = 0.100m)

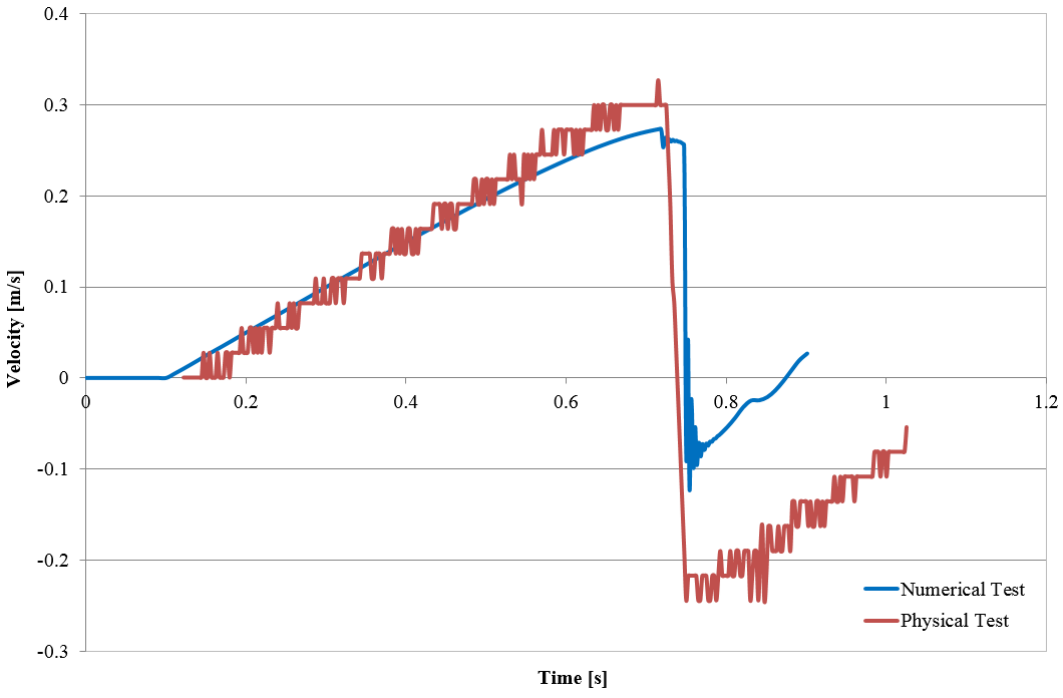

Figure 4.26: Comparison of velocity (y = 0.100m)

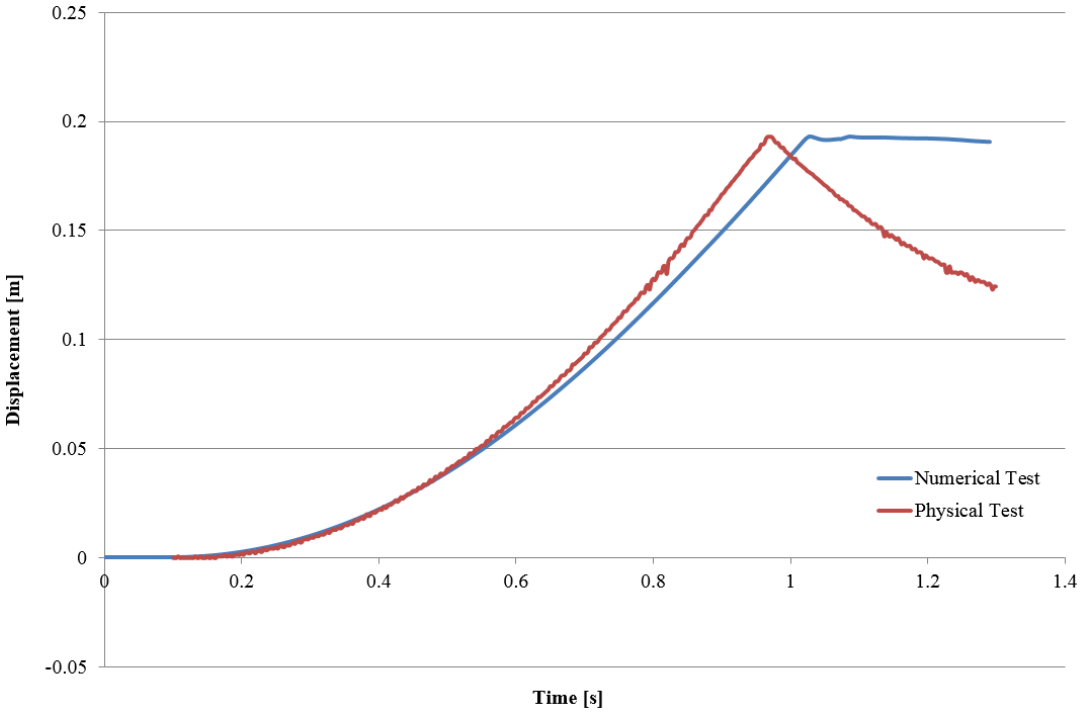

Figure 4.27: Comparison of displacement (y = 0.192m)

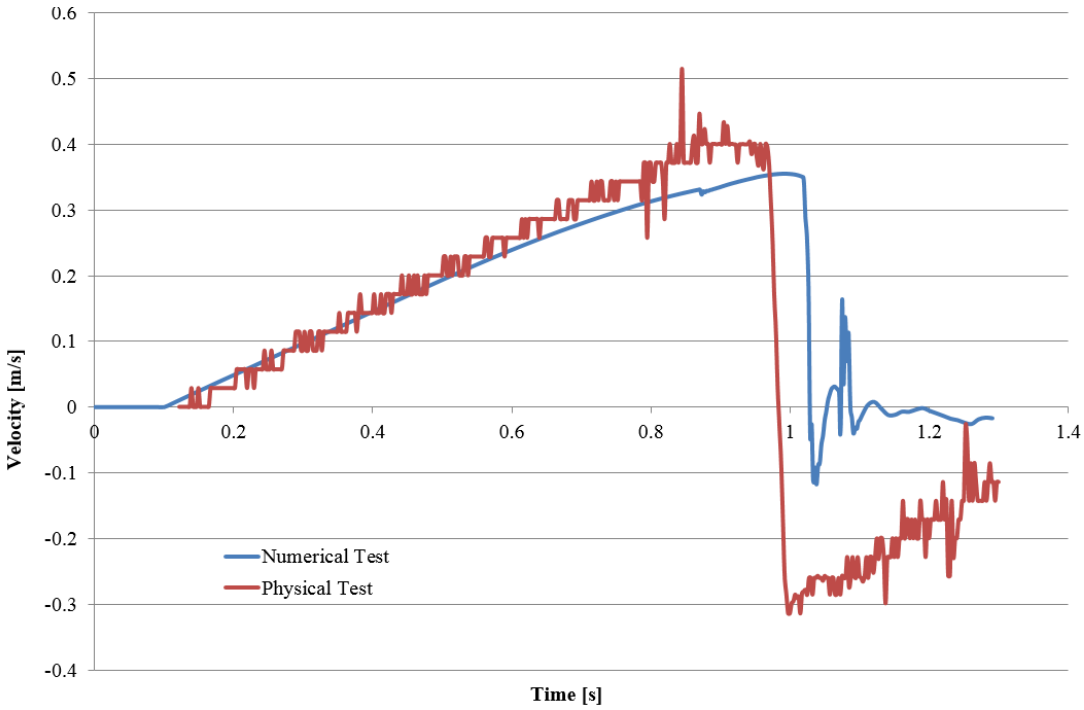

Figure 4.28: Comparison of velocity (y = 0.192m)

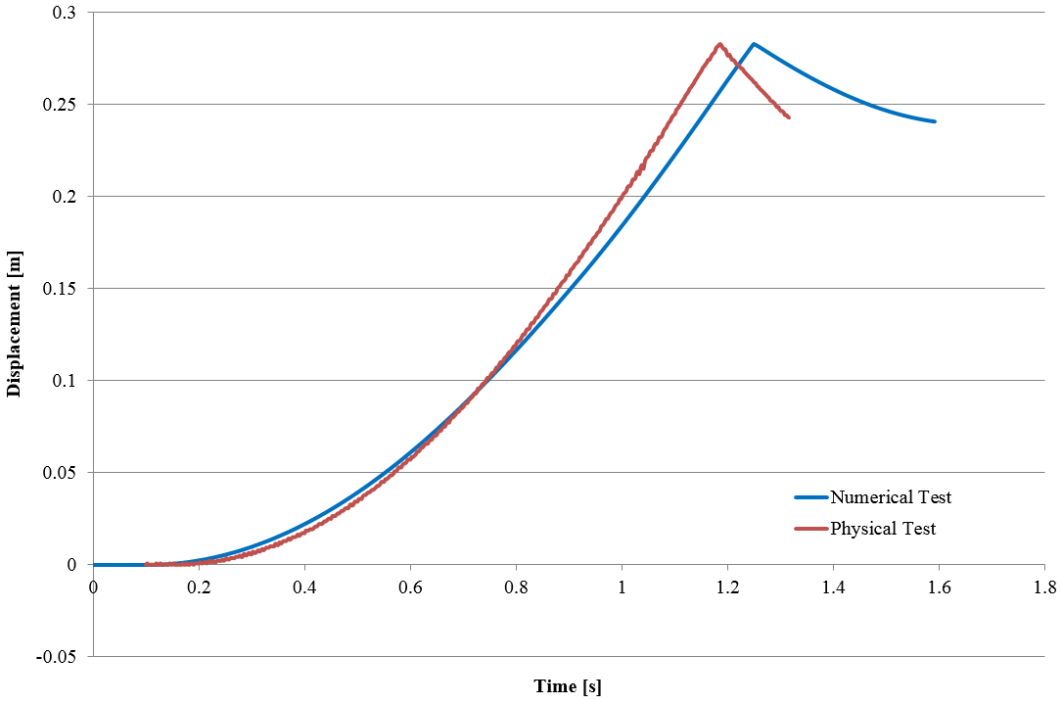

Figure 4.29: Comparison of displacement (y = 0.293m)

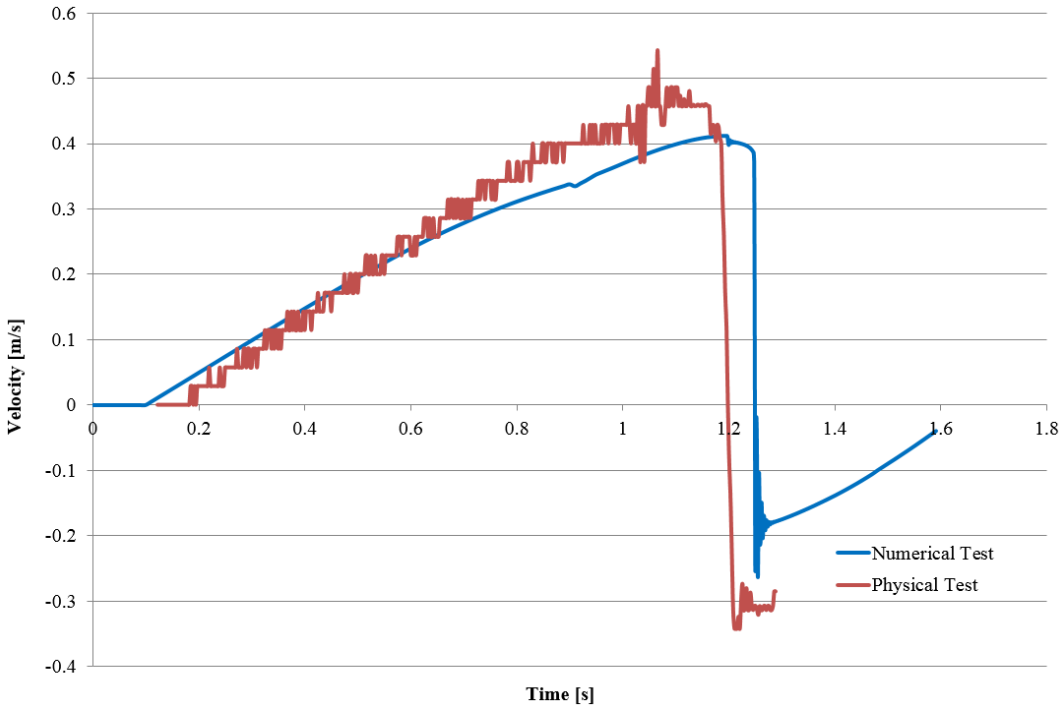

Figure 4.30: Comparison of velocity (y = 0.283m)

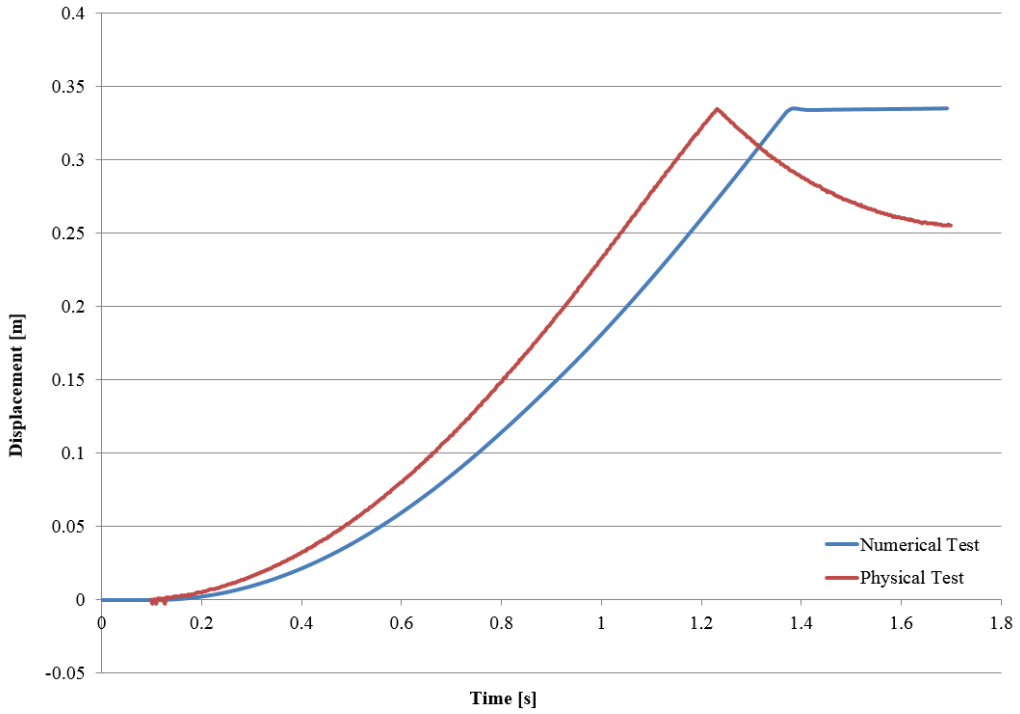

Figure 4.31: Comparison of displacement (y = 0.335m)

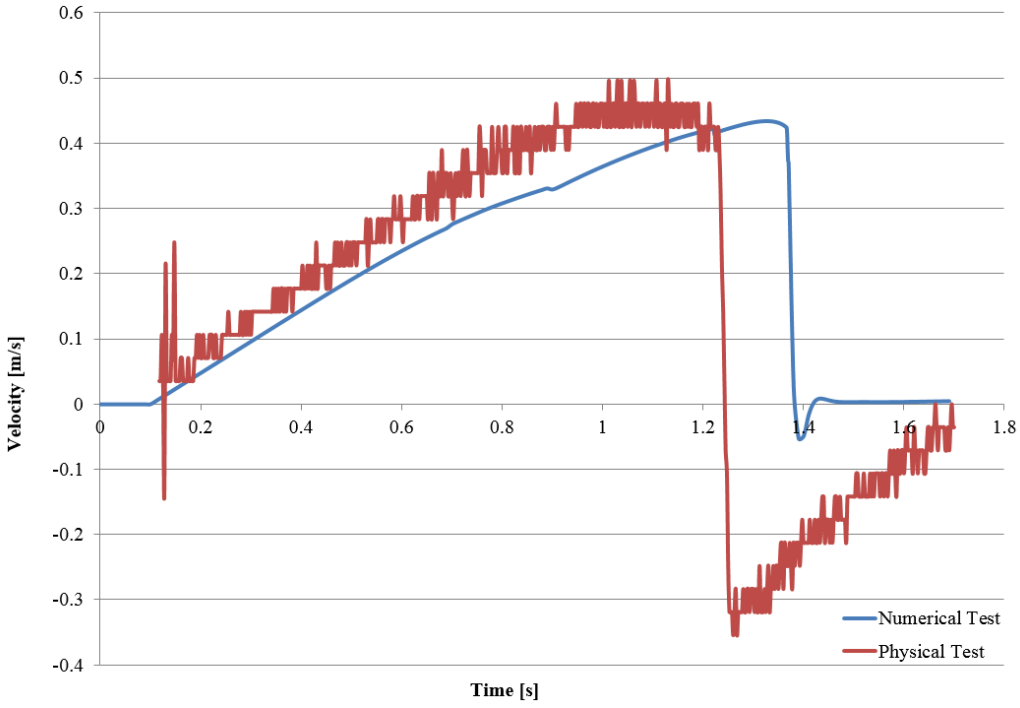

Figure 4.32: Comparison of velocity (y = 0.335m)

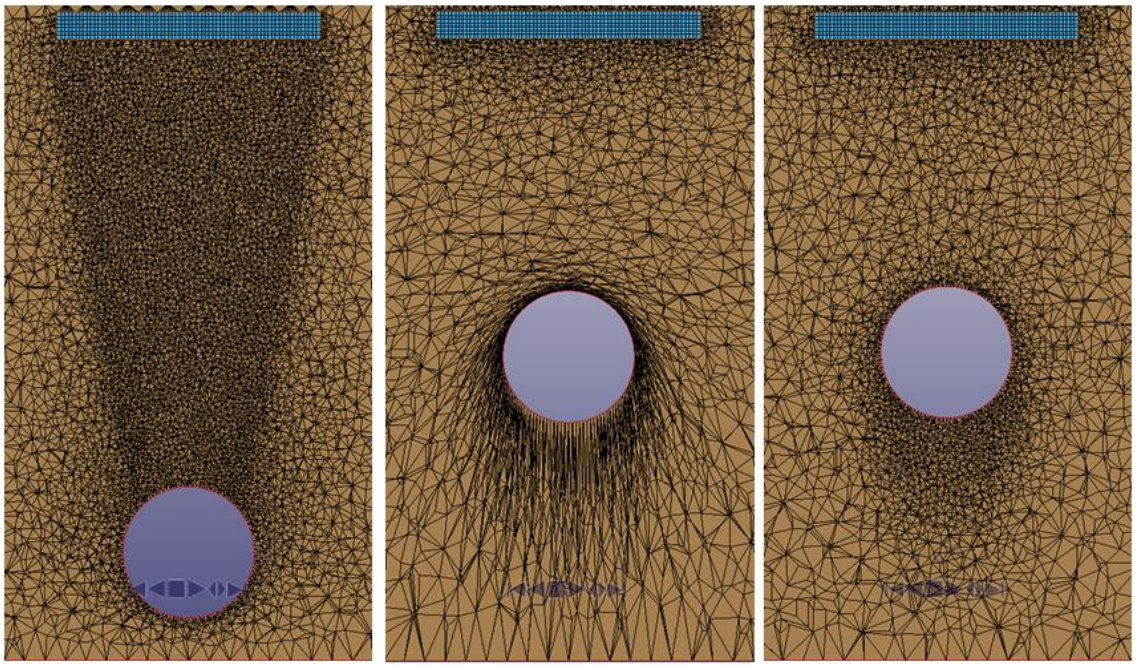

Figure 4.33: Section view at (a) Initial State, (b) Before re-meshing, (c) After re-meshing

4.3.8 Local impact force

The deeper the ice model was submerged, the higher velocity it would reach before the impact. However, it was investigated that the impact forces obtained from the simulation do not respect that, as listed in Table 4.11. It can be seem from Table 4.11, the maximum contact forces changing along the travel distance are irregular. It was found that there were still fluid elements between the ice model and the structure when the contact happened (Figure 4.34), which means that the pressure solved there did not correspond to the actual physical pressure. This is one of the reasons that caused the incorrect contact forces. The gap is artificial and any little change in the way the mesh movement and re-meshing is calculated would change the result. For example, the submerged depths of 0.3 m and 0.30001 m might result in completely different impact forces. This partly explains the abnormal behaviour of the ice model after impact. The other reason is

that the time step for the implicit solver is larger than the explicit solver and the implicit solver was used for this impact case. It causes the high level of overlap between the master and slave surfaces when contact happened.

Table 4.11: Contact forces simulated using LS-DYNA

Traveling Distance [m]	0.011	0.1	0.193	0.283	0.335
Maximum Impact Force [N]	64.1	181.4	70.2	472.7	0

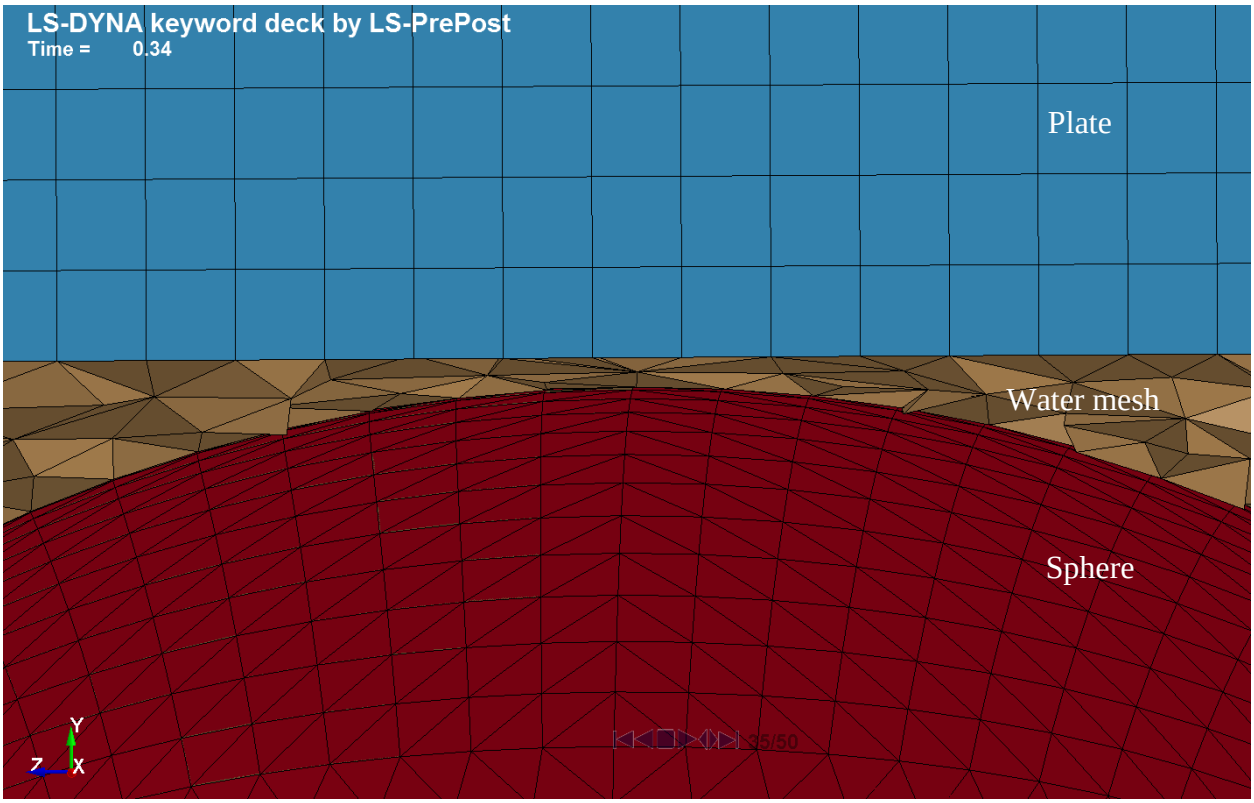

Figure 4.34: Section view of the artificial gap between the plate and sphere at contact

4.3.9 Some issues during the model development

Before discovery of the impracticality of modeling under water impact force using the ICFD solver, at the early stage of model development, there was not much information available about

the ICFD solver. A bug was uncovered and some other minor flaws significantly increased the difficulties of model development.

The most significant issue encountered at the early stage was a bug in the software. At the early stage of the model development, a 2D model was built instead of 3D model in order to save computation time. In other words, the impact of a cylinder and plate were simulated instead of a sphere and plate. Due to the similar density of ice and water, the numerical model includes the implicit method in order to trigger strong FSI strong coupling. The strong coupling requires simultaneous convergence of fluid and structure variables at the interface. At the convergence procedure of each time step, the normal of the solid interface elements should be updated so that the fluid knows what force to pass to each element during the FSI interaction. The bug was that the normals were not updated during the FSI interaction. As a result, although the structure had moved, since the normal was not updated, the fluid still carried on the old normal to communicate to the newly calculated force. In the case of the cylinder, a self-rotation was introduced by this error at each time step. Hence, at each new time step, some rotation forces were accumulated which made the cylinder spin and go out of control. Figure 4.35 is a screen shot of the simulation result when the bug had not been fixed. It can be seen that the cylinder was rotated counter-clockwise.

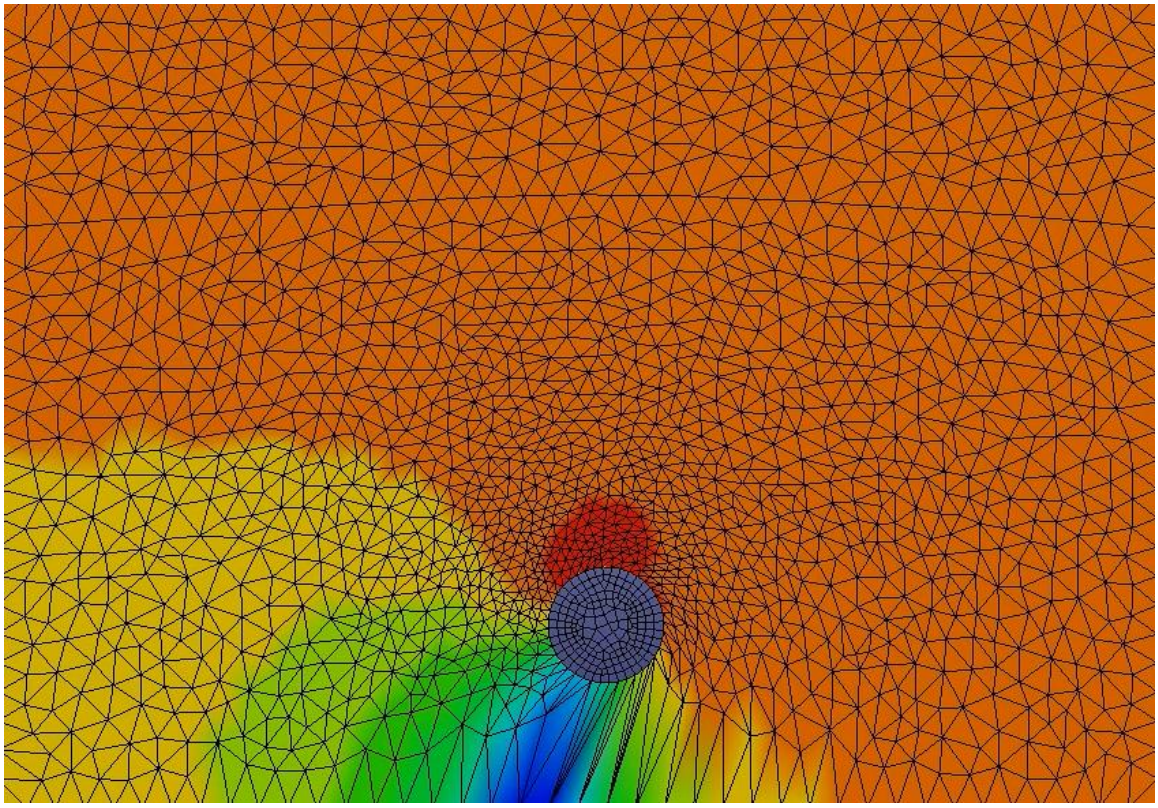

Figure 4.35: 2D Simulation result with a bug

With the great help from Dr. Inaki Caldichoury from LSTC, this bug had been solved. There was less rotation effect after that. With further mesh optimization, only some acceptable residual effect was left in the simulation.

There were some other minor flaws that with the gracious help of LSTC have also been fixed. For example, during the pre-processing stage, whenever an update has been made to the model, the Thermal Fluid Parameters card and Non-Newtonian Fluid Parameters card are automatically active, which introduced errors to and terminated the simulation. The deactivation could only be done manually in the code at that time. Another problem was regarding the mesh size of the ice sphere and plate. The mesh size of the ice sphere was not able to match to the mesh size of plate.

When their mesh sizes were similar, the simulation would terminate when contact happened. Hence the mesh size for the sphere and the plate are quite different for the model built at the early stage. This problem has been fixed now. For the final version of the numerical model, the mesh size for both objects is 2.8 mm. Another problem significantly hampered the simulation time at the early stage, which was the acceptable amount of processors to run the simulation. For the 2D model, when more than 8 processors were used, the simulation would terminate automatically without any error. For the 3D model, only 16 processors could be used to avoid the indescribable error. Fortunately, these problems have been solved when the new version solver was released in 2014. The last known problem that had been fixed is regarding the ICFD mesh card. The ICFD_CONTROL_ADAPT_SIZE card is for activation of the re-meshing feature while ICFD_CONTROL_ADAPT card is for the user to define the maximum and minimum mesh size allowed to the mesh generator. When the fluid or air mesh is distorted or beyond the defined range, the mesh can be automatically re-meshed in respect to the Delaunay Criterion. It worked perfectly in 2D model. However, for the 3D model, the simulation always terminated in the halfway with no specific error when ICFD_CONTROL_ADAPT card was included, even when the maximum and minimum mesh sizes were carefully determined. Therefore, the ICFD_CONTROL_ADAPT card has been excluded for all 3D models in this study initially.

There is another known problem which still exists in the pre-development stage of the numerical model. As mentioned before, the boundary shell needs to be converted to the multi-solver mesh in order for the automatic volume mesher to detect the nodes on the mesh. The initial volume mesh is then further developed in respect to the Delaunay criterion. This step is supposed be done through MSMesh from LS-PrePost, however, the simulation terminates and indicates that

no volume element had been generated. Consequently, the shell conversion can only be done by editing the keyword file directly instead of using MSMesh. The above issues show how new the ICFD is. Dr. Inaki Caldichoury from LSTC was very helpful in working to resolve the various issues. It has been very instructive to work closely with LSTC to test and help improve this new modelling capability of LS-DYNA.

4.4 Summary

This chapter presents the physical and numerical tests of underwater impact of an ice model and plate. The physical tests took place in the $1\times1\times0.5$ m clear tank. The ice model was released from five different submergences below the ship model. The displacement and velocity for each test were generated based on image analysis method. The numerical model was developed using coupled ICFD and implicit structural solvers of LS-DYNA. A mesh convergence study was performed and the time step was carefully selected. The test results from both experiments and the numerical models were compared. Oscillations appeared in the velocity plots when the re-meshing occurred. The movement of the ice model before the impact are very similar. However, the impact forces were not simulated correctly because of the artificial gap between the ice model and the plate and the great overlap of the master and slave surfaces when contact happened. In addition, this chapter includes the bug and flaws that had been fixed, as well as some flaws that hopefully would be fixed in the future.

Chapter 5 Added Mass Coefficient and the Proposed Method

Added mass is an important component that contributes to the local contact force on the structure in the water. When the ice model approaches the structure, the ice model, its added mass and the plate all influence each other. The ice model accelerates its ambient fluid when it is moving toward the plate. However, the ice model slows down due to resistance when it goes near the plate, while the added mass resist the change of movement of the ice model.

Kharlamov, Chára, and Vlasák generated hydraulic formulae for the added mass coefficient of a sphere moving toward to a plane wall (Equation 2.1). Their study validated that the added mass coefficient equals 0.803085 at contact (Kharlamov et al., 2007).

5.1 The Proposed Method

The proposed method of this study is to verify that the local impact force on the plate from the submerged ice model in the water equals the impact force from the same ice model with artificial hydrodynamic effect in the air. The artificial hydrodynamic effect in this study is prescribed added mass and velocity. For example, a hollow rigid ball with a mass of m kg travels upward due to buoyancy in the water and hits at a force sensor. At the point of contact, the velocity of the ball is v m/s and it causes a 100 N force at the sensor. The added mass of the ball at the contact point is $m + 0.8$ kg. According to the proposed method, a hollow rigid ball, with the same volume and a weight of $m + 0.8$ kg, would cause around a 100 N impact force at a constant velocity of v m/s.

The verification of the proposed method is explained in the next section (Section 5.2) and the calibration of the numerical model is described in Section 5.3.

5.2 Verification of the Method

A fellow researcher, Subodh Chander, studied the effects of added mass and kinematics during underwater ice and ship collisions (Chander, 2015). In his thesis, he compared the displacement and velocity of submerged ice collision with a stationary plate through physical experiments and a numerical model using Flow3d^{TM} for submerged depths of 2cm, 3.5cm, and 5cm. In his physical experiments, he measured the maximum velocity and force prior to the impact (Table 5.1).

Table 5.1: Peak velocity and force at contact (Chander, 2015)

Submergence [m]	V [m/s]	F [N]
0.02	0.1825	140
0.05	0.2740	270
0.08	0.3100	338
0.10	0.3990	394

To verify the proposed method, a numerical model was built to test the impact force with the prescribed impact velocities and artificial added mass based on Chander's experiments. The model simulated the ice model with defined added mass impacting with a steel plate with prescribed velocities in the air. The prescribed velocities were adopted from Chander's experiments results. The artificial added mass coefficient was 0.803085. The details of the numerical model are presented in the remaining sections of this chapter. The LS-DYNA k-file with main commands for the numerical model is included in Appendix C.

The maximum impact forces calculated using LS-DYNA were compared with Chander's experiment results which were measured by load cell. Figure 5.1 shows that the maximum impact forces from the ice model with artificial added mass at different velocities, which are very close to Chander's measurement.

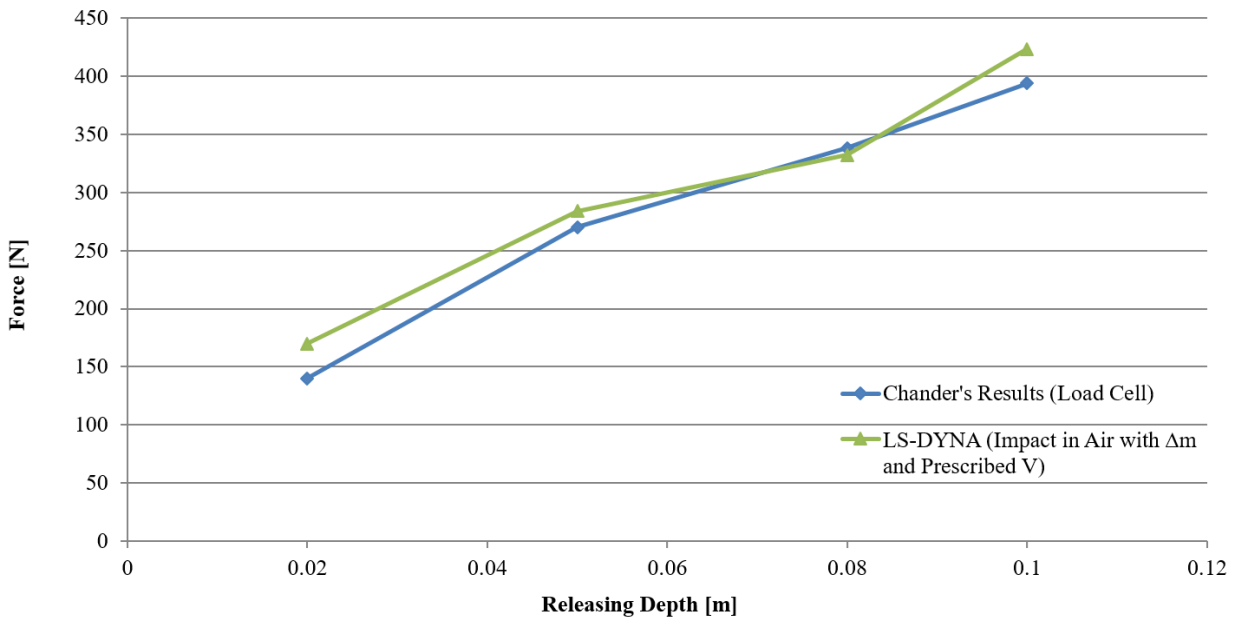

Figure 5.1: Peak impact forces

5.3 Calibration for the Numerical Model

5.3.1 Drop tests in air (Laboratory)

In order to verify the proposed method, a numerical model was needed to simulate impact in air. Prior to that, a series of drop tests were carried out physically and numerically for calibration purposes. An object free falling from a certain height in the air, *h*, is generally a process of momentum conservation, where the potential energy is mainly converted to kinetic energy and partially converted to heat due to air resistance. The object is subjected to two external forces: the gravitational force F_W and the drag force F_D. They are expressed as:

$$F_{net} = ma = F_W - F_D \qquad \text{Equation 5.1}$$

$$F_W = mg \qquad \text{Equation 5.2}$$

$$F_D = \frac{1}{2}\rho A C_D v^2 \qquad \text{Equation 5.3}$$

Where: F_{net} is the net force of the sphere model

m is the mass of the sphere

g is the acceleration of gravity

a is the acceleration

ρ is density of air, A is the projected area

C_D is the drag coefficient, v is the velocity

In Equation 5.3, the density, projected area, and drag coefficient are all constants. Velocity is the only time variable of drag force. Generally the whole process can be divided into three time stages. The first stage is when the falling object just leaves from rest. At this stage, the velocity is near zero and the kinetic energy is very low. Hence the drag force is very small and can be ignored at this stage. In the second stage, the velocity increases as the object falls further. The velocity keeps increasing until it reaches its maximum. The maximum velocity is also called the terminal velocity. The third stage is during the period from when the object reaches the terminal velocity until it hits the ground. At this stage, the drag force and the body weight balance out so that the net force is zero. The conducted drop tests for the calibration purpose for this study only reached the first stage due to the short drop height.

The ice model was employed in the process of the drop tests. The ice model was released from various heights (2 mm to 16 mm) and hit directly on the load cell (Omega's DLC 101) that was

mounted on a heavy steel plate on the ground. The load cell was made of 17-4 PH stainless steel with a frequency range of 0.08 Hz to 25 kHz and can measure the impact force up to 400 N.

All tests were recorded using a high speed camera for image analysis purposes. The recording frequency ranged from 2,000 Hz to 3,400 Hz. The recorded test videos were converted into picture frames using a software, AoaoPhoto Digital Studio. From each picture frame, the pixel coordinates for the movement of the sphere were recognized by a Matlab program. Hence, the displacement and the velocity of the sphere were obtained.

Since the drop heights were relatively small, the sphere only reached the first stage when the drag force was nearly zero before it hit the load cell. According to Equation 5.1 and 5.2, the acceleration of the sphere is approximately equal to gravity acceleration. Hence, the velocity can be determined as Equation 5.4 in this case.

$$v = \sqrt{2gh} \qquad \text{Equation 5.4}$$

Where: h is the drop height.

The impact velocities were based on calculations from Equation 5.4 and were compared with the data obtained from the image analysis, as tabulated in Table 5.2. The table shows that the impact force increases when the impact velocity rises as the drop height increases. The velocities obtained from the image analysis method and Equation 5.4 are very close, which shows the image analysis method for tracking the movement of the sphere is precise. The comparison is visually shown in Figure 5.2 and 5.3.

Table 5.2: Impact velocity and force for each height

Height [mm]	V_free fall (measured) [m/s]	V_free fall (Eq 5.4) [m/s]	F_load cell [N]	k_free fall
2.10	0.20	0.20	123.30	0.53
3.10	0.23	0.24	204.44	0.47
3.40	0.21	0.26	192.94	0.50
6.80	0.36	0.36	274.47	0.49
7.90	0.36	0.39	276.59	0.50
8.00	0.38	0.39	287.97	0.51
8.60	0.41	0.41	259.71	0.54
10.10	0.47	0.44	321.78	0.56
13.60	0.48	0.52	382.06	0.52
15.90	0.55	0.56	402.51	0.49

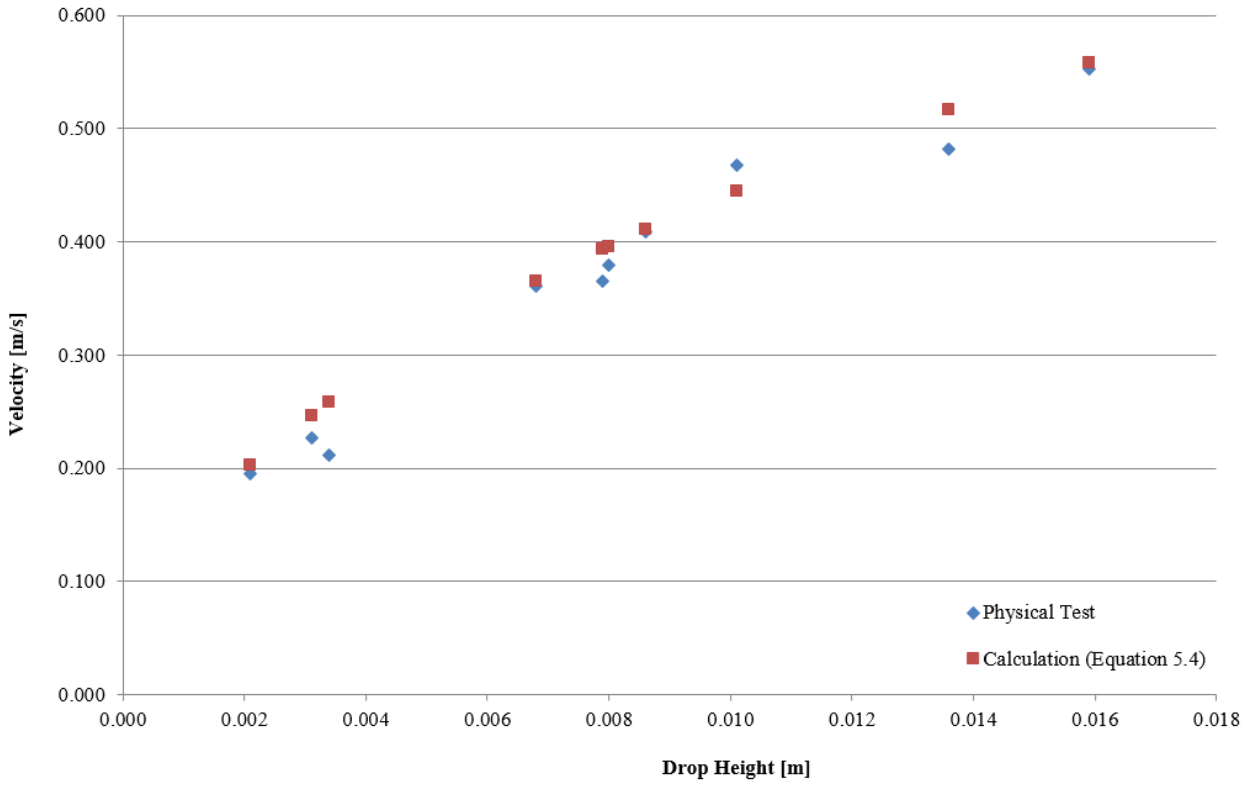

Figure 5.2: Comparisons of velocity for each test

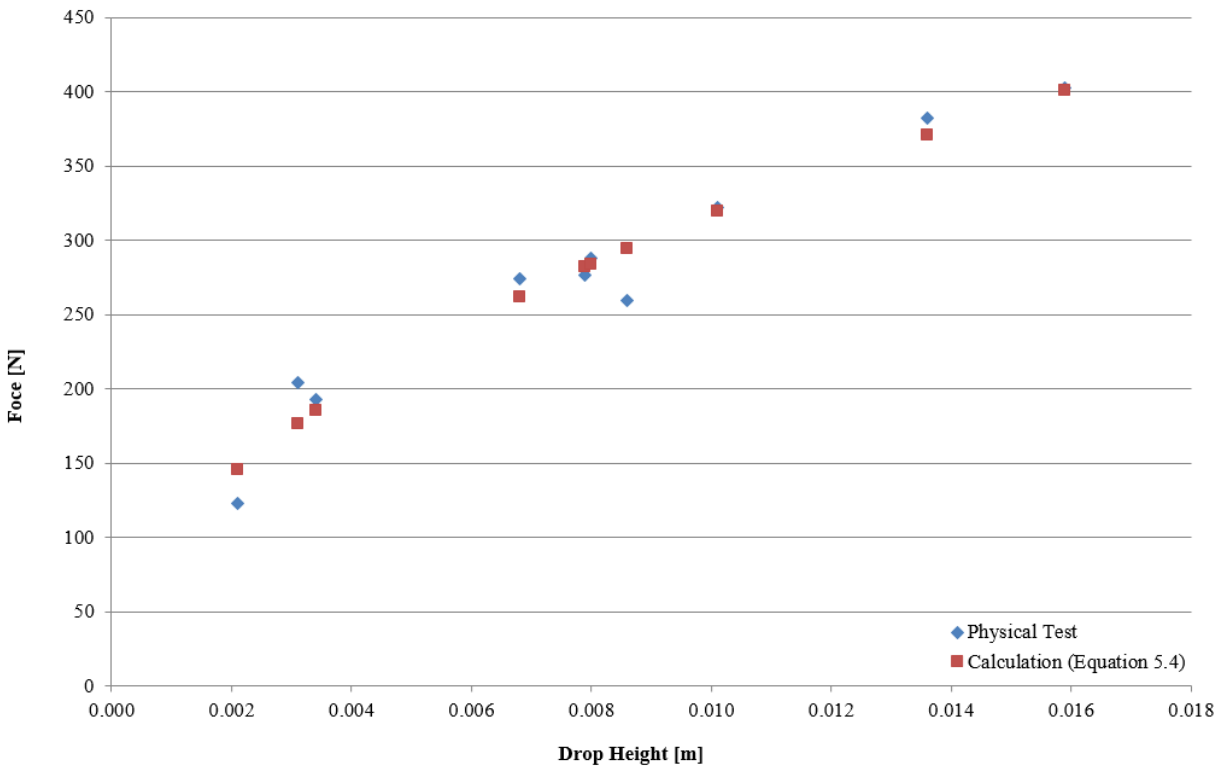

Figure 5.3: Comparisons of force for each test

The maximum impact forces were measured using the load cell and tabulated in Table 5.2. Figure 5.4 shows a typical force history of impact for one of the drop tests. The area under the curve is the change in momentum of the sphere, which can be described as the Equations 5.5 and 5.6. *k* is the ratio of the change in momentum over the maximum force multiplied by time. The *k* for the ten physical tests are tabulated in Table 5.2 and will be compared with *k* calculated based on the numerical tests.

$$\Delta Momentum = \text{area under the curve} = \int F dt \qquad \text{Equation 5.5}$$

$$k = \frac{\int F dt}{F_{\max} dt} \qquad \text{Equation 5.6}$$

Where F_{max} is the maximum impact force

k is a constant

5.3.2 Drop tests in air (Numerical)

5.3.2.1 Material Model

The laboratory tests were simulated using the explicit structural solver of LS-DYNA (the keyword file is giving in Appendix D). The sphere model was considered as a simple elastic material model while the plate model was a rigid material model. The inputs for both material models are listed in Tables 5.3 and 5.4.

Table 5.3: Material property for the sphere

Card ID	*MAT_ELASTIC (001)	
Density	Young's Modulus	Poisson's Ratio
930 kg/m^3	0.17 GPa	0.40

Table 5.4: Material property for the plate

Card ID	*MAT_RIGID (020)	
Density	Young's Modulus	Poisson's Ratio
7780 kg/m^3	197 GPa	0.272

5.3.2.2 SOFT options

The two-way contact card *CONTACT_AUTOMATIC_SINGLE_SURFACE was chosen for the drop tests. It gives the option to choose different ways to calculate the contact spring stiffness. For the explicit simulation, SOFT = 1 option is recommended, especially as the contact parts have dissimilar material properties. SOFT = 0 option is more suitable for contact surfaces with similar material properties. For a better comparison, the simulations were run with all three options and are shown in Figure 5.4. SOFT = 0 option gave less contact force when

compared to SOFT = 1 and SOFT = 2 options, and the peak contact force happened later than in the other two options. The load curves for SOFT = 1 and SOFT = 2 are very similar. SOFT = 1 was chosen for this model as it is more suitable for this test scenario.

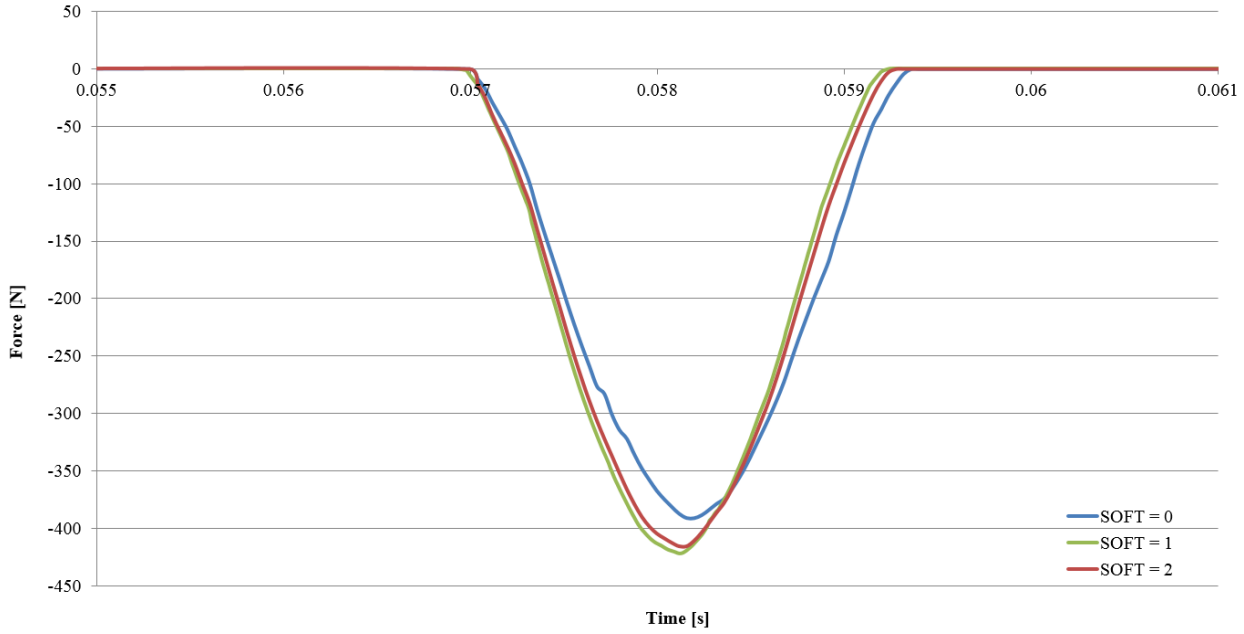

Figure 5.4: SOFT options

5.3.2.3 Mesh Convergence Study

Both the sphere and plate model consist of hexahedral solid elements, which have a higher computational cost compared with the tetrahedral element, but are more accurate for this case. A mesh convergence study was conducted where mesh sizes ranged from 1.00 mm to 5.48 mm. The time histories of the impact force for different mesh sizes were compared. Figure 5.5 shows that convergence is reached when the mesh size is 1.83 mm. This mesh size was chosen for the subsequent simulations of the drop tests. The screenshot of the mid-section of the model with selected mesh size is shown in Figure 5.6.

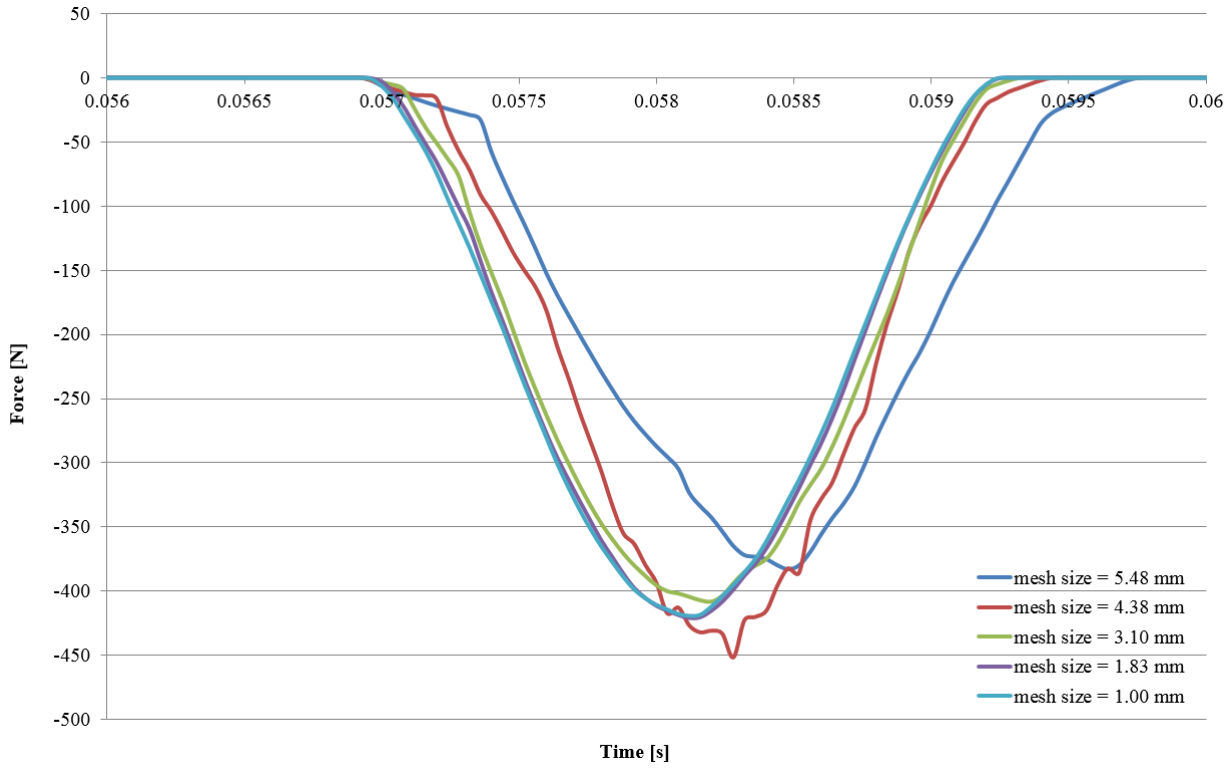

Figure 5.5: Mesh convergence

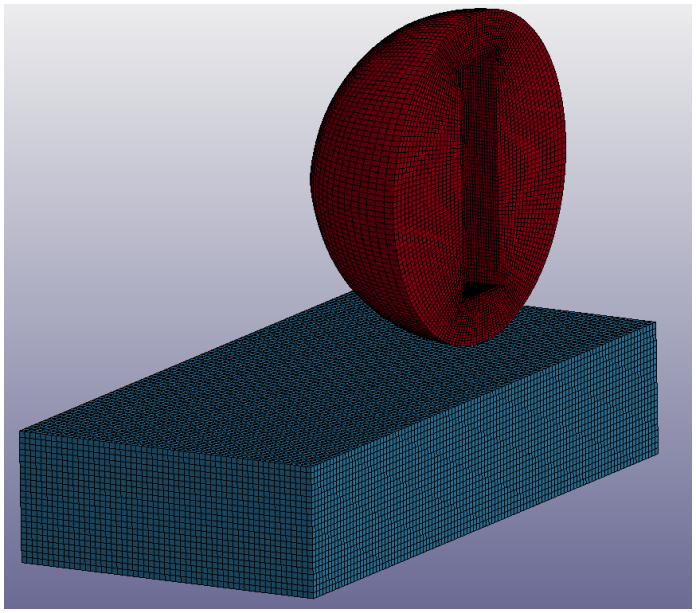

Figure 5.6: Mid-Section view of the model

The ice model with the selected mesh size and the defined density gave the mass of the sphere, which was slightly less than 0.459 kg. In order to match the mass of the sphere tested in the lab, the difference was added evenly to every node of the sphere using the Mass_Trimming function in the pre-processing stage. The model with added weight is shown in Figure 5.7.

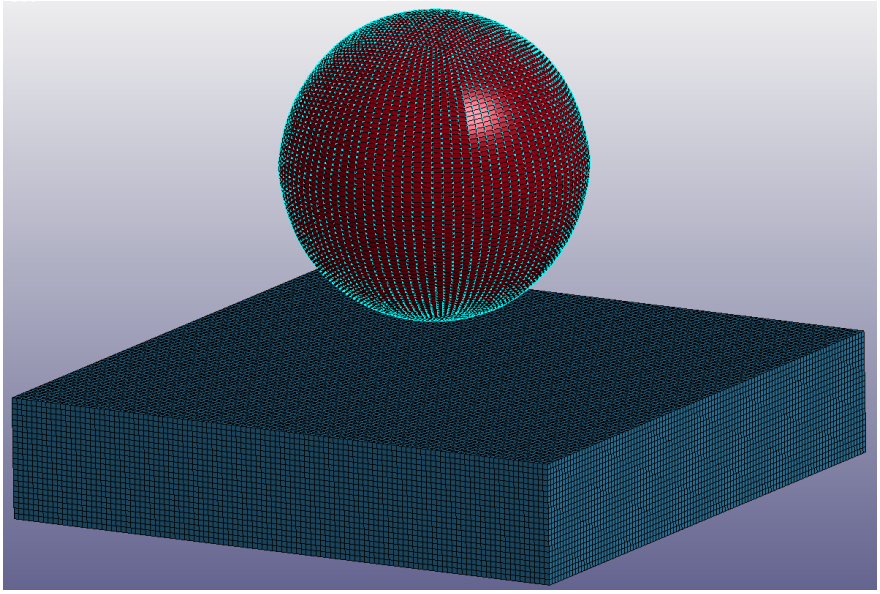

Figure 5.7: Model with added weight

5.3.2.4 Time step and other input

The dimension of the plate was $0.2 \times 0.2 \times 0.04$ m. In each simulation, gravity force was the only force that was applied to the sphere in the –y direction. Constraints were applied to the lower four corners of the plate during the whole process of the simulations. The ice model was released at 0 seconds and fell toward the load cell due to gravity force.

With the selected mesh size, LS-DYNA initially recommended the time step should be equal or less than 3.34e-7 s to avoid numerical instabilities. After initialization was completed, the model ran with the time step of 6.11e-7s automatically. On the other hand, from the force data which

was obtained from the load cell, the average time for the force to ramp up from zero to maximum contact force varied. The shortest time was 0.00064 s. Hence the data output time step for the simulation should be smaller than 0.00064 s in order to capture the maximum contact force. The data output time step study included the time steps from 3.0e-7 s to 1.0e-4 s (Figure 5.8). It shows that the maximum forces were not completed shown until the data output time step is equal or less than 0.00001 s. Hence, the data output time step 0.00001 s was chosen for all subsequent simulations.

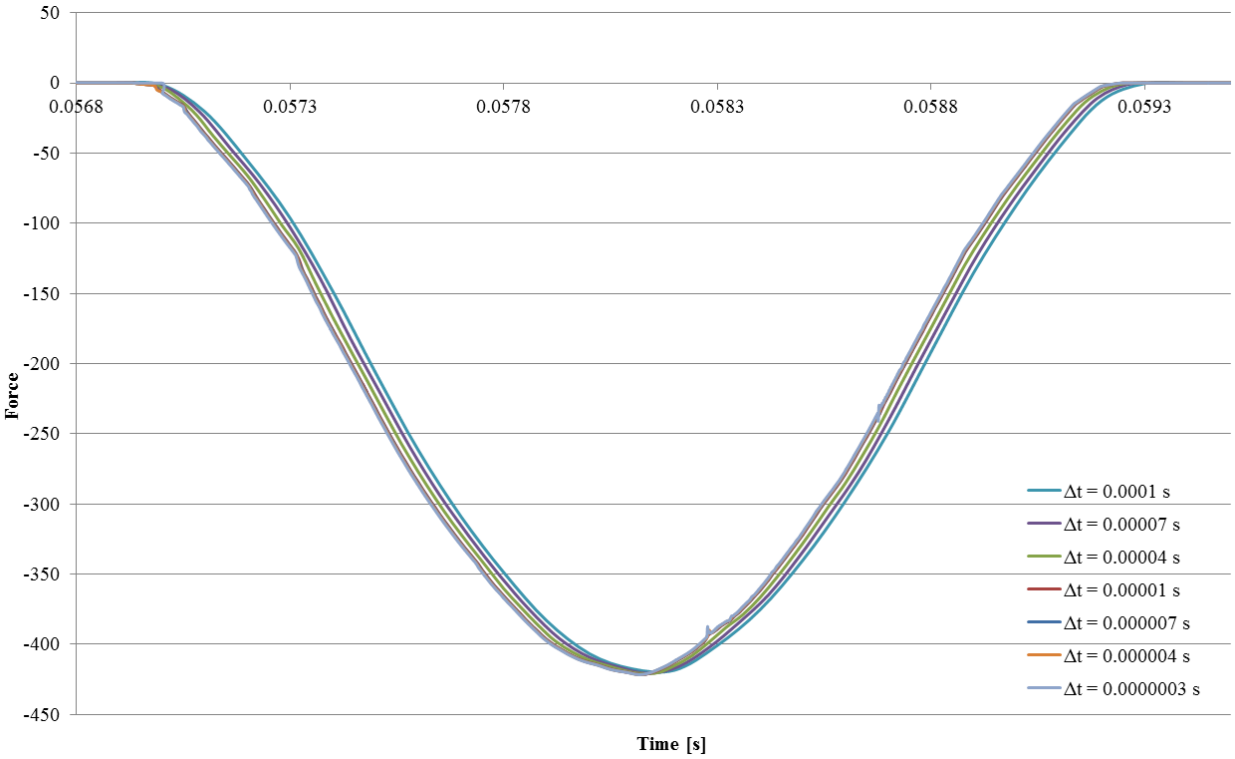

Figure 5.8: Data output time step study

5.3.3 Result comparisons

For each simulation, the displacement, impact velocity, and force were acquired from the DATABASE card of LS-DYNA. They were compared with the results obtained from physical

tests. The displacements of the sphere generated from numerical and physical tests were closely matched except for drop height of 0.0159 m. Figure 5.9 shows the comparison of displacement with a drop height of 2 mm, 8 mm, and 16 mm. The comparison of impact velocities and force are shown in Figure 5.10 and 5.11 respectively. All three methods agree with each other. It is believed that this model can correctly simulate the impact force from the free falling object. Figure 5.12 is the comparison of *k*, which shows that the *k* value is around 0.5 for both physical and numerical tests.

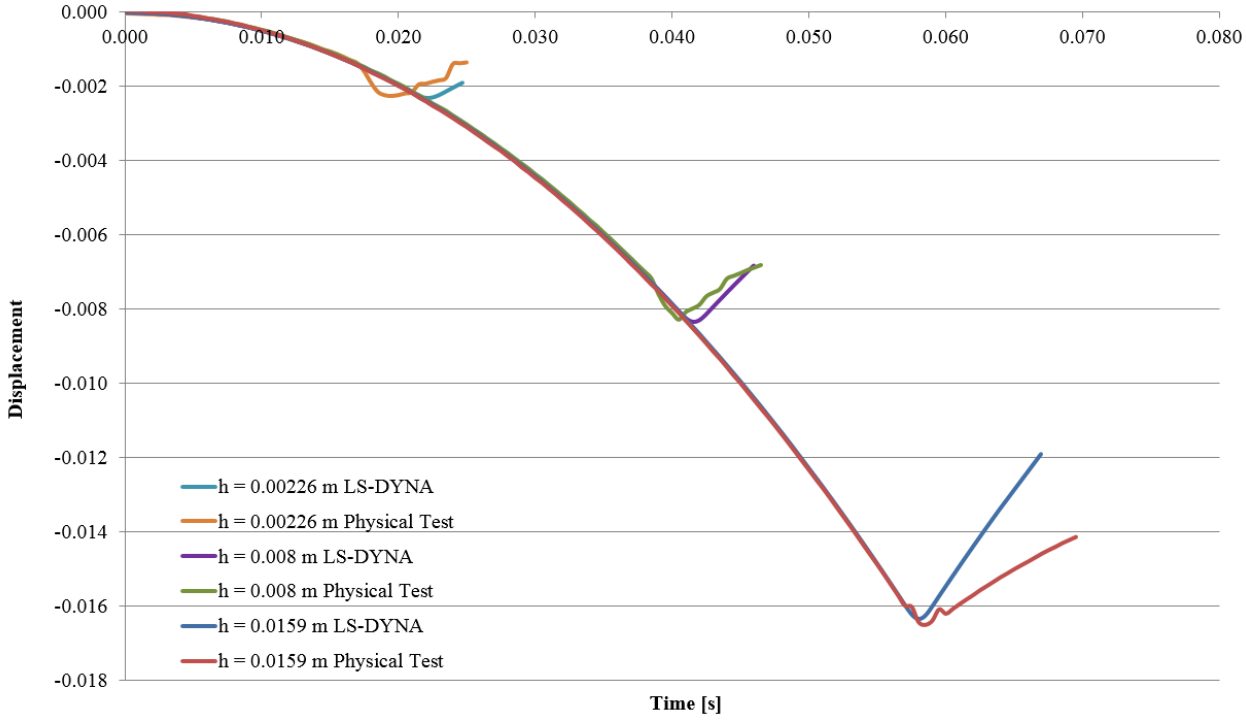

Figure 5.9: Comparisons of displacements for minimum, medium and maximum drop height for numerical and physical tests

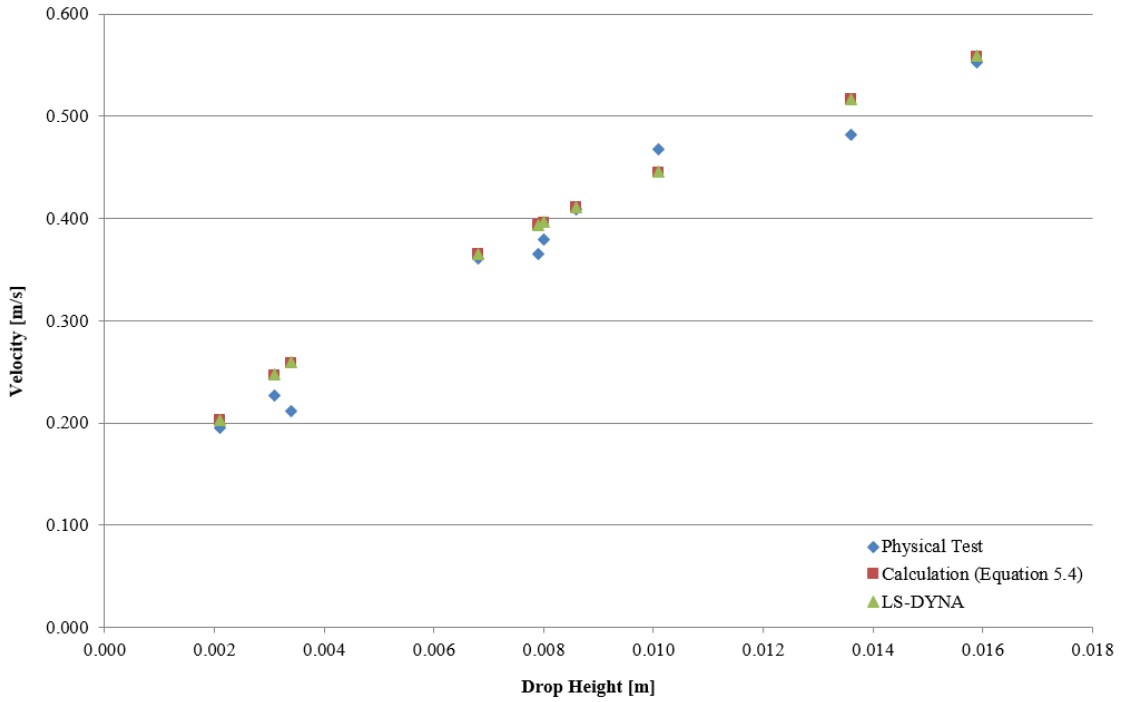

Figure 10: Comparisons of velocity for each test

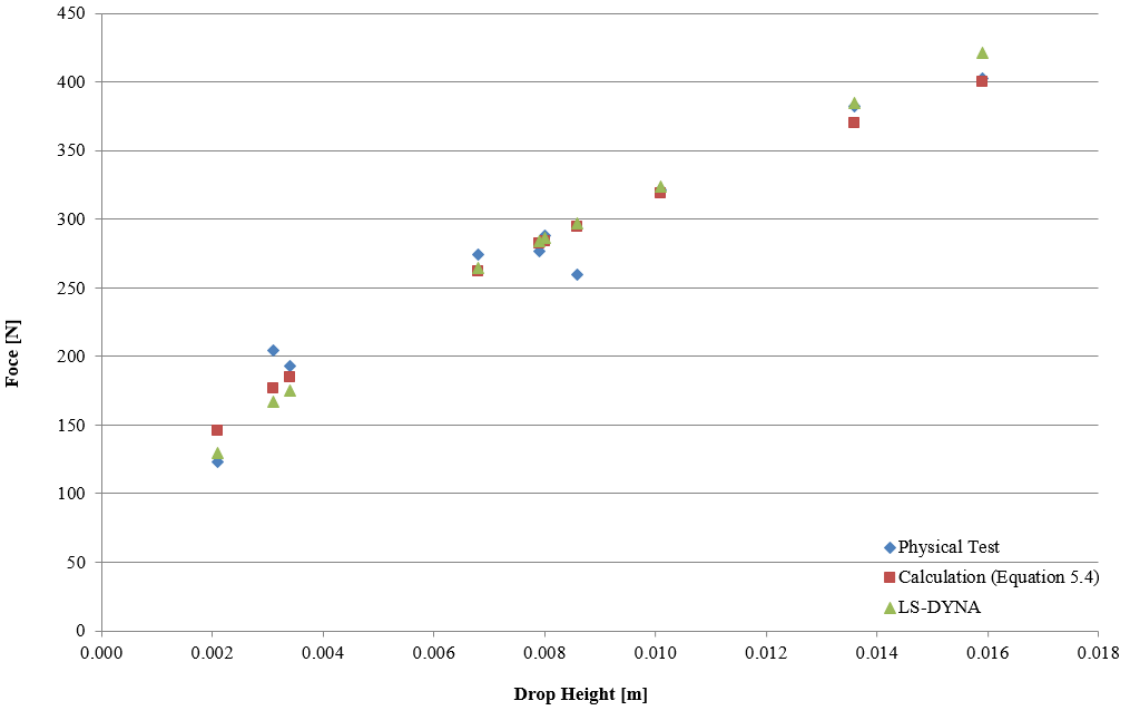

Figure 11: Comparisons of impact force for each test

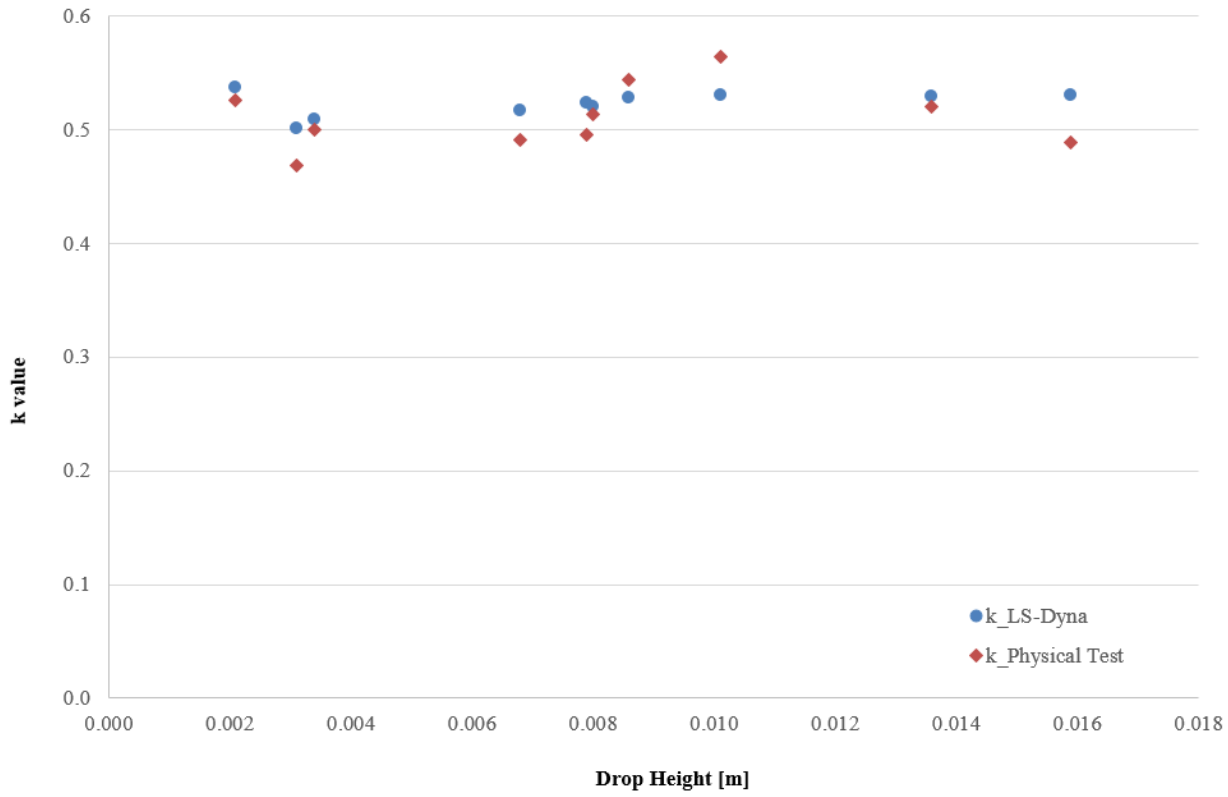

Figure 12: k values

The numerical model tested with the artificial added mass and prescribed velocity was based on this model with three main modifications. First, the gravity force was removed. Second, the prescribed velocity (Table 5.1) were applied to the ice model. Third, the added mass coefficient for each test was 0.803085.

5.4 Summary

This chapter presents the proposed method that assuming the underwater impact force on the structure from the submerged ice model equals to the impact force from the ice model with artificial added mass and prescribed velocity. A LS-DYNA model has been developed to verify

the proposed method. The simulation results show that the impact forces from the ice model with prescribed velocity and the added mass coefficient of 0.803085 on a steel plate were close to Chander's measurements in his physical experiments.

Chapter 6 Conclusion and Recommendations

6.1 Conclusion

The goal of this study is to verify the capability of modeling underwater impact of ice and structure using the ICFD solver of the commercial FEA software LS-DYNA.

Due to lack of suitable load cell for underwater impact tests, a couple of pre-tests were performed to check the potential ability of modeling underwater impact. Firstly, this thesis presents the physical and numerical impact tests due to the gravity in the air. With the selected numerical material, the numerical model successfully modeled the impact test by matching the velocities, displacements and impact forces. Secondly, the 2D numerical model of steady fluid flowing past a stationary cylinder for the Reynolds number range up to 50,000 was conducted. The drag coefficients calculated based on the simulation results were similar to the available literature. Especially for the tests where $\mathrm{Re} \le 160$ and $\mathrm{Re} > 10,000$. The fluid stream for different Reynolds numbers also coincide with the available literature. These imply that ICFD is able to model the dynamic interaction of fluid and structure in the defined range.

Initially, it was believed that ICFD of LS-DYNA had the potential ability to model underwater impact. The underwater impact tests were designed and performed in the fluid lab of Memorial University's S. J. Carew Building. In the process of the tests, the ice model was released from 5 different depths below the bottom of the ship model. The submergence range was from 0.011m to 0.335 m. The test results were recorded using a high speed camera. The image analysis method was used to analyze the test result. The numerical model was developed using ICFD solver of LS-DYNA. A number of bugs had been encountered during the numerical model developing process. With generous help from LS-DYNA, these bugs were fixed. Comparing

the results from physical and numerical respects, the travel displacements and velocities before contact were similar. However, the contact forces generated from LS-DYNA were not reasonable. That was due to the artificial gap between the ice model and the structure when contact happened, as well as the larger time step for the implicit solver. The artificial gap caused the wrong pressure to be calculated at the contact point, while the larger time step resulted in the great overlap of the master and slave surfaces when contact happened. Overall, the ICFD solver is not yet capable of modeling underwater impact in an incompressible fluid, however, it is a practical tool that can precisely simulate the fluid and structure interaction.

A method was proposed that the peak impact force under the water surface equals to the peak impact force in the air where the impact velocity is the same and the added mass is included in the total impacting weight. A series of numerical tests were performed and compared with other literature to verify the proposed method. In the process of validation, the numerical model was calibrated and simulated the ice model with the certain added mass impacting a piece of steel plate with prescribed velocities. The velocities were adopted from the underwater impact tests by Chander. The simulation results were similar to Chander's study.

6.2 Recommendation

Several thoughts have occurred to the author but as with most research, the work leads to many questions, as well as answers, and are beyond the scope of this research. When underwater impact happens in reality, the impacted structure does not necessarily stay still and the ice does not always strike the hull at a right angle. In other words, when better tools are available, more realistic situations can be modeled. For example, the impacted structures can be moving with different speeds when the impact happens. Also, ice can impact the hull at different locations, or the impact can be angled. In addition, the fluid flow could be taken into concern as well.

The method proposed in this study has only been verified for submergences up to 0.1 m due to limited data available in the literature. Future studies with deeper submergences should be carried out. The calibration of the numerical model for the proposed method was carried by comparing a series of drop tests in air, numerically and physically. However, the impact velocities for the underwater impact tests were varied from 0.1825 m/s to 0.3990 m/s, while the test velocities for the calibration were varied from 0.20 m/s to 0.55 m/s – a small gap that was not covered in the lower range of velocities. Also, the mass of the ice model in the calibration was 0.459 kg, while the mass of the ice model impact for the underwater tests included the original weight (0.459 kg) and its "added mass". Therefore, a more rigorous calibration should be carried with the same effective mass and proper velocity range.

Base on this study, the author believes that LS-DYNA is capable of simulating the hydrodynamics behaviours of an ice model traveling toward a plate. The only major defect is the existing water mesh at contact. If the water mesh cannot be eliminated during the impact under the water, a further study could simplify the proposed method, combine the simulations of an ice model moving under the water, and the impact in the air into one simulation. The integrated model could turn off the ICFD cards and turn on the pre-defined added mass card at the same time upon the impact. This would reduce the computing time and the results would be more precise.

References

Akinturk, A, 2013, Matlab Code for the Detecting the Boundary of Sphere

Bathe, K., 1996, Finite Element Procedures, Prentice Hall, Upper Saddle River, New Jersey 07458.

Benra, F.K., Dohmen, H. J., Pei, J., Schuster, S., and Wan, B., 2011, A Comparison of One-Way and Two-Way Coupling Methods for Numerical Analysis of Fluid-Structure Interactions, University of Duisburg-Essen, Germany.

Chander S., 2015, Experimental and Numerical Hydrodynamics Study of Submerged Ice Collision, Master's thesis, Memorial University, Canada.

Clift R., Grace J. R., and Weber M. E., 1978, Bubbles, Drops, and Particles, Academic Press, Unite State.

Dennis, S.C.R., Chang, G., 1970, Numerical Solutions for Steady Flow Past a Crcular at Reynolds Number up to 100, J. Fluid Mech., Vol. 42.

Föppl, L, 1913, Vortex Motion behind a Circular Cylinder, NASA.

Fornberg, B., 1979, a Numerical Study of Steady Viscous Flow Past a Circular Cylinder, J. Fluid Mech., Vol. 98.

Fornberg, B., 1985, Steady Viscous Flow Past a Circular Cylinder up to Reynolds Number 600, Journal of Computational Physics.

Hicks, W. M., 1880, On the Motion of Two Spheres in a Fluid, Philosophical Transactions.

Kharlamov, A. A., Chára, Z., and Vlasák, P., 2007, Hydraulic Formulae for the Added Masses of an Impermeable Sphere Moving Near a Plane Wall, Journal of Engineering Mathematics

Lienhard, J.H., 1966, Synopsis of Lift, Drag, and Vortex Frequency Data for Rigid Circular Cylinders, Washington, Washington State University.

LSTC, 2011, LS-DYNA Support, 2011, Livermore Software Technology Corporation.

LSTC, 2012, Test Case Documentation and Testing Results – Flow Around a Two Dimensional Cylinder, Livermore Software Technology Corporation.

LSTC, 2013, ICFD Theory Manual, Incompressible Fluid Solver in LS-DYNA, 2013, Livermore Software Technology Corporation.

LSTC, 2013, LS-DYNA Class Notes, Incompressible CFD Slover (ICFD) and FSI in LS-DYNA, 2013, Livermore Software Technology Corporation.

LSTC, 2014, Some Guidelines for Implicit Analyses Using LS-DYNA, Livermore Software Technology Corporation.

Martin, P.A., Farina, L., 1996, Radiation of Water Waves by a Heaving Submerged Horizontal Disc, J. Fluid Mech., Vol. 337.

Massey, B., 2006, Mechanics of Fluids, 8th edition, London, Taylor & Francis.

Involving Submerged Oscillating Bodies. Journal of Engineering Mathematics 18, England.

Michler, C., Hulshoff, S. J., Van Brummelen, E. H., de Borst, R., A, 2003, Monolithic Approach to Fluid-structure Interaction, Faculty of Aerospace Engineering, Delft University of Technology, The Netherlands.

Pantaleone, J., Messer, J., 2011, The Added Mass of a Spherical Projectile, American Journal of Physics, Alaska.

Park, J., Kwon, K., Choi, H., 1998, Numerical Solutions of Flow Past a Circular Cylinder at Reynolds Numbers up to 160, KSME International Journal, Vol. 12.

Pin, F. Del, Çaldichoury, I., 2012, Recent Developments, Application Areas and Validation Process of the Incompressible Fluid Solver (ICFD) in LS-DYNA, 12th International LS-DYNA Users Conference, Livermore, CA

Popov, Yu., Faddeyev, O., Kheisin, D., and Yalovlev, A., 1967, Strength of Ships Sailing in Ice, U.S. Army Foreign Science and Technology Center

Schlichting, H., 1979, Boundary Layer Theory, 7th edition, McGraw-Hill, Inc., New York.

Subramanian R. S., 2010, Drag on Spherical Particles and Steady Settling Velocities, Notes of Fluid Mechanics, Clarkson University.

Quinton, W.T., B, Kearsey, A., 2011, Benchmarking of Three Parallelized Implementations of LS-Dyna on a HPC Server Cluster, Canada

Stokes, G.G., 1880, Mathematical and Physical Papers, Vol. 1, Cambridge.

Wang, S., Wahab, R., 1971, Heaving oscillations of twin cylinders in a free surface, Journal of Ship Research, N1.

Zdravkovich, 1997, M. M., Flow around Circular Cylinder, vol. 1, Oxford Science Publication.

List of Appendixes

Appendix A: Main K-file of Fluid with Cylinder Interaction Using Incompressible CFD solver

```
*KEYWORD
*TITLE
$# title
LS-DYNA keyword deck by LS-PrePost
*DATABASE_BINARY_D3PLOT
$#      dt      lcdt      beam     npltc    psetid
  0.100000         0         0         0         0
$#   ioopt
         0
*DEFINE_CURVE_TITLE
constant 1
$#    lcid      sidr       sfa       sfo      offa      offo    dattyp
       1         0  1.000000  1.000000     0.000     0.000         0
$#              a1                o1
            0.000          1.000000
         10000.000          1.000000
*DEFINE_CURVE_TITLE
constant 0
$#    lcid      sidr       sfa       sfo      offa      offo    dattyp
       2         0  1.000000  1.000000     0.000     0.000         0
$#              a1                o1
            0.000             0.000
         10000.000             0.000
*INCLUDE
geo.k
*ICFD_BOUNDARY_FREESLIP
$#     pid
         3
*ICFD_BOUNDARY_NONSLIP
$#     pid
         4
*ICFD_BOUNDARY_PRESCRIBED_VEL
$#     pid       dof       vad      lcid        sf       vid     death     birth
         1         1         1         1  1.000000         01.0000E+28     0.000
*ICFD_BOUNDARY_PRESCRIBED_VEL
$#     pid       dof       vad      lcid        sf       vid     death     birth
         1         2         1         2  1.000000         01.0000E+28     0.000
*ICFD_BOUNDARY_PRESCRIBED_PRE
$#     pid      lcid        sf     death     birth
         2         2  1.0000001.0000E+28     0.000
```

```
*ICFD_CONTROL_TIME
$#     ttm        dt       cfl
 200.00000     0.004         1
*ICFD_DATABASE_DRAG
$#     pid
       4
*ICFD_MAT
$#     mid       flg        ro       vis        st       thd
       1         1  1.0000000.00714285     0.000     0.000
*ICFD_PART
$#     pid     secid       mid
       1         1         1
*ICFD_PART
$#     pid     secid       mid
       2         1         1
*ICFD_PART
$#     pid     secid       mid
       3         1         1
*ICFD_PART
$#     pid     secid       mid
       4         1         1
*ICFD_PART_VOL
$#     pid     secid       mid
       5         1         1
$#   spid1     spid2     spid3     spid4     spid5     spid6     spid7     spid8
       1         2         3         4         0         0         0         0
*ICFD_SECTION
$#     sid
       1
*MESH_BL
$#     pid    nelth
       4         3
*MESH_SIZE_SHAPE
$#   sname
      box
$#   msize     pminx     pminy     pminz     pmaxx     pmaxy     pmaxz
      0.1        14        17         0        36        23         0
*MESH_SIZE_SHAPE
$#   sname
      box
$#   msize     pminx     pminy     pminz     pmaxx     pmaxy     pmaxz
    0.025      14.5        19         0        26        21         0
*MESH_VOLUME
$#   volid
       1
$#    pid1      pid2      pid3      pid4      pid5      pid6      pid7      pid8
```

```
      1       2       3       4       0       0       0       0
*END
```

Appendix B: Main K-file of Underwater Impact of the Ice Model and Plate

```
*KEYWORD
*TITLE
$#                                                                         title
LS-DYNA keyword deck by LS-PrePost
*CONTROL_IMPLICIT_AUTO
$#  iauto    iteopt    itewin     dtmin     dtmax     dtexp     kfail    kcycle
       0         0         0     0.000     0.000     0.000         0         0
*CONTROL_IMPLICIT_DYNAMICS
$#  imass     gamma      beta    tdybir    tdydth    tdybur     irate
       1  0.500000  0.250000  0.1000001.0000E+281.0000E+28         0
*CONTROL_IMPLICIT_GENERAL
$# imflag      dt0    imform      nsbs       igs     cnstn      form    zero_v
       1 1.0000E-3         2         0         2         0         0         1
*CONTROL_IMPLICIT_SOLUTION
$# nsolvr    ilimit    maxref     dctol     ectol     rctol     lstol    abstol
       2       100       100  2.000000     0.000     0.000  0.9000001.0000E-10
$#  dnorm    diverg     istif   nlprint    nlnorm   d3itctl     cpchk
       2         1         1         0         2         0         0
$# arcctl    arcdir    arclen    arcmth    arcdmp
       0         0     0.000         1         2
$#  lsmtd     lsdir      irad      srad      awgt      sred
       1         2     0.000     0.000     0.000     0.000
*CONTROL_TERMINATION
$# endtim    endcyc     dtmin    endeng    endmas
 1.700000         0     0.000     0.000     0.000
*DATABASE_MATSUM
$#      dt    binary      lcur     ioopt
   0.001         0         0         1
*DATABASE_RBDOUT
$#      dt    binary      lcur     ioopt
       0         1         2         1
*DATABASE_RCFORC
$#      dt    binary      lcur     ioopt
       0         1         2         1
*DATABASE_SPCFORC
$#      dt    binary      lcur     ioopt
       0         0         2         1
*DATABASE_BINARY_D3PLOT
$#      dt      lcdt      beam     npltc    psetid
   0.000         2         0         0         0
$#  ioopt
       0
*DATABASE_BINARY_INTFOR
$#      dt      lcdt      beam     npltc    psetid
```

```
   0.000       2       0       0       0
*BOUNDARY_SPC_SET
$#   nsid      cid     dofx     dofy     dofz    dofrx    dofry    dofrz
       1        0        1        1        1        1        1        1
*LOAD_BODY_Y
$#   lcid      sf    lciddr       xc       yc       zc      cid
       1 9.810000        0    0.000    0.000    0.000        0
*CONTACT_AUTOMATIC_SINGLE_SURFACE_ID
$#     cid                                                title
       1
$#    ssid     msid    sstyp    mstyp   sboxid   mboxid      spr      mpr
       1        0        2        0        0        0        1        1
$#      fs       fd       dc       vc      vdc   penchk       bt       dt
   0.000    0.000    0.000    0.000    0.000        0    0.0001.0000E+20
$#     sfs      sfm      sst      mst     sfst     sfmt      fsf      vsf
 1.000000 1.000000    0.000    0.000 1.000000 1.000000 1.000000 1.000000
$#    soft   sofscl   lcidab   maxpar    sbopt    depth    bsort   frcfrq
       0 0.100000        0 1.025000 2.000000        2        0        1
$# penmax   thkopt   shlthk    snlog     isym    i2d3d   sldthk   sldstf
   0.000        0        0        0        0        0    0.000    0.000
$#    igap   ignodprfac/mpadtstif/mpar2   unused    unused   flangl   cid_rcf
       2        0    0.000    0.000                0.000        0
*SET_PART_LIST
$#     sid      da1      da2      da3      da4    solver
       1    0.000    0.000    0.000    0.000MECH
$#    pid1     pid2     pid3     pid4     pid5     pid6     pid7     pid8
       1        2        0        0        0        0        0        0
*CONTACT_FORCE_TRANSDUCER_PENALTY_ID
$#     cid                                                title
       2
$#    ssid     msid    sstyp    mstyp   sboxid   mboxid      spr      mpr
       2        1        3        3        0        0        1        1
$#      fs       fd       dc       vc      vdc   penchk       bt       dt
   0.000    0.000    0.000    0.000    0.000        0    0.0001.0000E+20
$#     sfs      sfm      sst      mst     sfst     sfmt      fsf      vsf
 1.000000 1.000000    0.000    0.000 1.000000 1.000000 1.000000 1.000000
$#    soft   sofscl   lcidab   maxpar    sbopt    depth    bsort   frcfrq
       0 0.100000        0 1.025000 2.000000        2        0        1
$# penmax   thkopt   shlthk    snlog     isym    i2d3d   sldthk   sldstf
   0.000        0        0        0        0        0    0.000    0.000
$#    igap   ignodprfac/mpadtstif/mpar2   unused    unused   flangl   cid_rcf
       2        0    0.000    0.000                0.000        0
*PART_CONTACT
$#                                                     title

$#     pid    secid      mid    eosid     hgid     grav   adpopt     tmid
```

```
       1       1       1       0       0       0       0       0
$#     fs      fd      dc      vc    optt     sft     ssf
   0.000   0.000   0.000   0.000 1.0000E-3   0.000   0.000
*SECTION_SHELL
$#   secid  elform    shrf     nip   propt  qr/irid   icomp   setyp
       1       2 1.000000       2       1       0       0       1
$#     t1      t2      t3      t4    nloc   marea    idof  edgset
5.0000E-3 5.0000E-3 5.0000E-3 5.0000E-3   0.000   0.000   0.000       0
*MAT_RIGID
$#     mid      ro       e      pr       n  couple       m   alias
       1 920.00000 5.0000E+9 0.300000   0.000   0.000   0.000
$#     cmo    con1    con2
       0       0       0
$#lco or a1       a2       a3       v1       v2       v3
   0.000   0.000   0.000   0.000   0.000   0.000
*PART
$#                                                  title
steel
$#     pid   secid     mid   eosid    hgid    grav  adpopt    tmid
       2       2       2       0       0       0       0       0
*SECTION_SOLID_TITLE
solid plate
$#   secid  elform     aet
       2       1       0
*MAT_ELASTIC
$#     mid      ro       e      pr      da      db  not used
       2 7850.00002.0700E+11 0.300000   0.000   0.000       0
*DEFINE_CURVE_TITLE
constant 1
$#    lcid    sidr     sfa     sfo    offa    offo   dattyp
       1       0 1.000000 1.000000   0.000   0.000       0
$#              a1              o1
          0.000          1.000000
    1.000000e+005          1.000000
*DEFINE_CURVE_TITLE
data output
$#    lcid    sidr     sfa     sfo    offa    offo   dattyp
       2       0 1.000000 1.000000   0.000   0.000       0
$#              a1              o1
          0.000      1.000000e-002
        1.280000      1.000000e-002
        1.280001      1.000000e-003
        1.390000      1.000000e-003
        1.390001      1.000000e-002
        2.000000      1.000000e-002
*INCLUDE
```

```
ball.k
*INCLUDE
tank_shell.k
*ICFD_BOUNDARY_FREESLIP
$#     pid
       1
*ICFD_BOUNDARY_NONSLIP
$#     pid
       3
*ICFD_BOUNDARY_NONSLIP
$#     pid
       4
*ICFD_BOUNDARY_FSI
$#     pid
       4
*ICFD_BOUNDARY_FSI
$#     pid
       5
*ICFD_BOUNDARY_NONSLIP
$#     pid
       5
*ICFD_CONTROL_FSI
$#     owc        bt        dt       idc
       0     0.0001.0000E+20  0.250000
*ICFD_CONTROL_TIME
$#     ttm        dt       cfl
  1.700000 1.0000E-3  1.000000
$  0.003500  0.005000
$         1
*ICFD_CONTROL_ADAPT_SIZE
$#   asize      freq
       1         0
*ICFD_DATABASE_DRAG
$#     pid      cpid
       4         0
*ICFD_MAT
$#     mid       flg        ro       vis        st       thd
       1         1 1000.0000 8.9400E-4     0.000     0.000
$     0.000     0.000     0.000
$     0.000     0.000     0.000     0.0001.0000E+30
$     0.000     0.000     0.000
$     0.000     0.000     0.000     0.0001.0000E+30
*ICFD_MAT
$#     mid       flg        ro       vis        st       thd
       2         0  1.225000 1.8100E-5     0.000     0.000
$     0.000     0.000     0.000
```

```
$    0.000    0.000    0.000    0.0001.0000E+30
$    0.000    0.000    0.000
$    0.000    0.000    0.000    0.0001.0000E+30
*ICFD_PART
$#    pid    secid      mid
       1        1        1
*ICFD_PART
$#    pid    secid      mid
       2        1        1
*ICFD_PART
$#    pid    secid      mid
       3        1        2
*ICFD_PART
$#    pid    secid      mid
       4        1        1
*ICFD_PART
$#    pid    secid      mid
       5        1        1
*ICFD_PART_VOL
$#    pid    secid      mid
       6        1        1
$#  spid1    spid2    spid3    spid4    spid5    spid6    spid7    spid8
       1        2        4        5        0        0        0        0
*ICFD_PART_VOL
$#    pid    secid      mid
       7        1        2
$#  spid1    spid2    spid3    spid4    spid5    spid6    spid7    spid8
       2        3        0        0        0        0        0        0
*ICFD_SECTION
$#    sid
       1
*MESH_INTERF
$#  volid
      10
$#   pid1     pid2     pid3     pid4     pid5     pid6     pid7     pid8
       2        0        0        0        0        0        0        0
*MESH_VOLUME
$#  volid
      10
$#   pid1     pid2     pid3     pid4     pid5     pid6     pid7     pid8
       1        3        4        5        0        0        0        0
*END
```

Appendix C: Main K-file of Impact Test in Air with Artificial Added Mass

```
*KEYWORD MEMORY=30000000
*TITLE
$#                                                         title
LS-DYNA keyword deck by LS-PrePost
*CONTROL_TERMINATION
$# endtim    endcyc     dtmin    endeng    endmas
 3.0000E-2         0     0.000     0.000     0.000
*DATABASE_MATSUM
$#      dt    binary      lcur     ioopt
    0.000         0         2         1
*DATABASE_RBDOUT
$#      dt    binary      lcur     ioopt
    0.000         1         2         1
*DATABASE_RCFORC
$#      dt    binary      lcur     ioopt
    0.000         1         2         1
*DATABASE_SPCFORC
$#      dt    binary      lcur     ioopt
    0.000         0         2         1
*DATABASE_BINARY_D3PLOT
$#      dt      lcdt      beam     npltc    psetid
    0.000         2         0         0         0
$#   ioopt
         0
*DATABASE_BINARY_INTFOR
$#      dt      lcdt      beam     npltc    psetid
    0.000         2         0         0         0
*BOUNDARY_SPC_SET
$#    nsid       cid      dofx      dofy      dofz     dofrx     dofry     dofrz
         1         0         1         1         1         1         1         1
*SET_NODE_LIST_TITLE
NODESET(SPC) 1
$#     sid       da1       da2       da3       da4    solver
         1     0.000     0.000     0.000     0.000MECH
$#    nid1      nid2      nid3      nid4      nid5      nid6      nid7      nid8
   444835    164005    164115    444945         0         0         0         0
*CONTACT_AUTOMATIC_SINGLE_SURFACE_ID
$#     cid                                                    title
         1
$#    ssid      msid     sstyp     mstyp    sboxid    mboxid       spr       mpr
         1         0         2         0         0         0         1         1
$#      fs        fd        dc        vc       vdc    penchk        bt        dt
    0.000     0.000     0.000     0.000     0.000         0     0.0001.0000E+20
$#     sfs       sfm       sst       mst      sfst      sfmt       fsf       vsf
```

```
 1.000000  1.000000     0.000     0.000  1.000000  1.000000  1.000000  1.000000
$#    soft    sofscl    lcidab    maxpar     sbopt     depth     bsort    frcfrq
       1  0.100000         0  1.025000  2.000000         2         0         1
*SET_PART_LIST
$#     sid       da1       da2       da3       da4    solver
       1     0.000     0.000     0.000     0.000MECH
$#    pid1      pid2      pid3      pid4      pid5      pid6      pid7      pid8
       1         2         0         0         0         0         0         0
*CONTACT_FORCE_TRANSDUCER_PENALTY_ID
$#     cid                                                   title
       2
$#    ssid      msid     sstyp     mstyp    sboxid    mboxid       spr       mpr
       2         1         3         3         0         0         1         1
$#      fs        fd        dc        vc       vdc    penchk        bt        dt
    0.000     0.000     0.000     0.000     0.000         0     0.0001.0000E+20
$#     sfs       sfm       sst       mst      sfst      sfmt       fsf       vsf
 1.000000  1.000000     0.000     0.000  1.000000  1.000000  1.000000  1.000000
$#    soft    sofscl    lcidab    maxpar     sbopt     depth     bsort    frcfrq
       1  0.100000         0  1.025000  2.000000         2         0         1
*PART
$#                                                    title
ice
$#     pid     secid       mid     eosid      hgid      grav    adpopt      tmid
       1         2         1         0         0         0         0         0
*SECTION_SOLID_TITLE
solid plate
$#   secid    elform       aet
       2         1         0
*MAT_ELASTIC
$#     mid        ro         e        pr        da        db  not used
       1 930.00000 1.7000E+8  0.400000     0.000     0.000         0
*PART
$#                                                    title
steel
$#     pid     secid       mid     eosid      hgid      grav    adpopt      tmid
       2         2         2         0         0         0         0         0
*MAT_RIGID
$#     mid        ro         e        pr         n    couple         m     alias
       2 7780.00001.9700E+11  0.272000     0.000     0.000     0.000
$#     cmo      con1      con2
    0.000         0.        0.
$#lco or a1        a2        a3        v1        v2        v3
    0.000     0.000     0.000     0.000     0.000     0.000
*INITIAL_VELOCITY_NODE
$#     nid        vx        vy        vz       vxr       vyr       vzr      icid
*DEFINE_CURVE_TITLE
```

```
constant 1
$#    lcid      sidr       sfa       sfo      offa      offo    dattyp
       1         0  1.000000  1.000000     0.000     0.000         0
$#              a1                o1
             0.000          1.000000
      1.000000e+005          1.000000
*DEFINE_CURVE
$#    lcid      sidr       sfa       sfo      offa      offo    dattyp
       2         0  1.000000  1.000000     0.000     0.000         0
$#              a1                o1
             0.000       1.000000e-005
       2.200000e-002       1.000000e-005
       2.200100e-002       3.000000e-003
       3.500000e-002       3.000000e-003
*ELEMENT_MASS
$#   eid     nid           mass     pid
*INCLUDE
ball.k
*END
```

Appendix D: Main K-file of Drop Test in the Air

```
*KEYWORD
*TITLE
$#                                                                title
LS-DYNA keyword deck by LS-PrePost
*CONTROL_TERMINATION
$# endtim    endcyc     dtmin    endeng    endmas
 7.0000E-2         0     0.000     0.000     0.000
*DATABASE_MATSUM
$#      dt    binary      lcur     ioopt
    0.000         0         2         1
*DATABASE_RBDOUT
$#      dt    binary      lcur     ioopt
    0.000         1         2         1
*DATABASE_RCFORC
$#      dt    binary      lcur     ioopt
    0.000         1         2         1
*DATABASE_SPCFORC
$#      dt    binary      lcur     ioopt
    0.000         0         2         1
*DATABASE_BINARY_D3PLOT
$#      dt      lcdt      beam     npltc    psetid
    0.000         2         0         0         0
$#   ioopt
         0
*DATABASE_BINARY_INTFOR
$#      dt      lcdt      beam     npltc    psetid
    0.000         2         0         0         0
*BOUNDARY_SPC_SET
$#    nsid       cid      dofx      dofy      dofz     dofrx     dofry     dofrz
       1         0         1         1         1         1         1         1
*SET_NODE_LIST_TITLE
NODESET(SPC) 1
$#     sid       da1       da2       da3       da4    solver
       1     0.000     0.000     0.000     0.000MECH
$#    nid1      nid2      nid3      nid4      nid5      nid6      nid7      nid8
   444835    164005    164115    444945         0         0         0         0
*LOAD_BODY_Y
$#    lcid        sf    lciddr        xc        yc        zc       cid
       1  9.810000         0     0.000     0.000     0.000         0
*CONTACT_AUTOMATIC_SINGLE_SURFACE_ID
$#     cid                                                           title
       1
$#    ssid      msid     sstyp     mstyp    sboxid    mboxid       spr       mpr
       1         0         2         0         0         0         1         1
```

```
$#     fs       fd       dc       vc       vdc    penchk       bt       dt
   0.000    0.000    0.000    0.000    0.000        0    0.0001.0000E+20
$#    sfs      sfm      sst      mst     sfst     sfmt      fsf      vsf
 1.000000 1.000000    0.000    0.000 1.000000 1.000000 1.000000 1.000000
$#   soft   sofscl   lcidab   maxpar    sbopt    depth    bsort   frcfrq
      1 0.100000        0 1.025000 2.000000        2        0        1
*SET_PART_LIST
$#    sid      da1      da2      da3      da4    solver
      1    0.000    0.000    0.000    0.000MECH
$#   pid1     pid2     pid3     pid4     pid5     pid6     pid7     pid8
      1        2        0        0        0        0        0        0
*CONTACT_FORCE_TRANSDUCER_PENALTY_ID
$#    cid                                                   title
      2
$#   ssid     msid    sstyp    mstyp   sboxid   mboxid      spr      mpr
      2        1        3        3        0        0        1        1
$#     fs       fd       dc       vc       vdc    penchk       bt       dt
   0.000    0.000    0.000    0.000    0.000        0    0.0001.0000E+20
$#    sfs      sfm      sst      mst     sfst     sfmt      fsf      vsf
 1.000000 1.000000    0.000    0.000 1.000000 1.000000 1.000000 1.000000
$#   soft   sofscl   lcidab   maxpar    sbopt    depth    bsort   frcfrq
      1 0.100000        0 1.025000 2.000000        2        0        1
*PART
$#                                                    title
ice
$#    pid    secid      mid    eosid     hgid     grav   adpopt     tmid
      1        2        1        0        0        0        0        0
*SECTION_SOLID_TITLE
solid plate
$#  secid   elform      aet
      2        1        0
*MAT_ELASTIC
$#    mid       ro        e       pr       da       db  not used
      1 930.00000 1.7000E+8  0.400000    0.000    0.000        0
*PART
$#                                                    title
steel
$#    pid    secid      mid    eosid     hgid     grav   adpopt     tmid
      2        2        2        0        0        0        0        0
*MAT_RIGID
$#    mid       ro        e       pr        n   couple        m    alias
      2 7780.00001.9700E+11  0.272000    0.000    0.000    0.000
$#    cmo     con1     con2
   0.000       0.       0.
$#lco or a1       a2       a3       v1       v2       v3
   0.000    0.000    0.000    0.000    0.000    0.000
```

```
*DEFINE_CURVE_TITLE
constant 1
$#    lcid      sidr       sfa       sfo      offa      offo    dattyp
         1         0  1.000000  1.000000     0.000     0.000         0
$#              a1                o1
             0.000          1.000000
       1.000000e+005          1.000000
*DEFINE_CURVE
$#    lcid      sidr       sfa       sfo      offa      offo    dattyp
         2         0  1.000000  1.000000     0.000     0.000         0
$#              a1                o1
             0.000       3.000000e-003
       5.000000e-002       3.000000e-003
       5.000100e-002       1.000000e-005
       6.400000e-002       1.000000e-005
       6.400100e-002       3.000000e-003
          0.200000       3.000000e-003
*INCLUDE
ball.k
*END
```